INVESTIGATION OF THE IMMUNOPHILIN INTERACTOME OF MALARIAL PARASITES

DARREN LENEGHAN

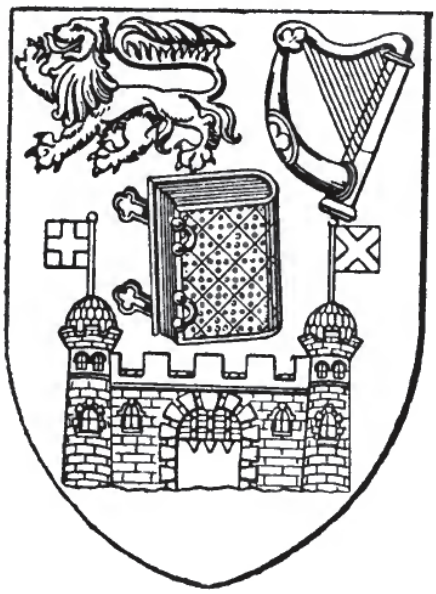

A thesis submitted for the degree of Doctor of Philosophy

Moyne Institute of Preventive Medicine
School of Genetics and Microbiology
Trinity College Dublin
October 2013

DECLARATION

This is to certify that the experimentation recorded herein represents my own work, unless otherwise stated, and has not been submitted for a higher degree at this or any other university. This thesis may be lent at the discretion of the librarian, Trinity College Dublin.

Dublin, October 2013

Darren Leneghan

SUMMARY

Malaria presents a significant global challenge in both human and economic terms. Approximately 40% of the population of the planet are at risk of contracting malaria, leading to an estimated 225 million cases and approximately 781,000 deaths anually. Emerging resistance to front-line antimalarial drugs means that the search for new drugs and drug targets continues to be a high priority in the fight against this disease. The immunophilin-binding drugs FK506, cyclosporin A, and rapamycin as well as some non-immunosuppressive derivatives of these drugs have all been shown to have strong inhibitory effects on malarial culture in culture and, in the case of cyclosporin A, in animal models. The antimalarial activity of the non-immunosuppressive derivatives indicates that a target exists in malarial parasites which is distinct from the immunosuppressive target in human T-lymphocytes. In an effort to elucidate this target or targets we have attempted to identify and characterise the interacting protien partners (interactome) of the two major cytosolic cyclosporin receptors (cyclophilins), PfCYP19A and PfCYP19B and the FK506-binding protein (FKBP), PfFKBP35, of the most prevalent and deadly malaria parasite *Plasmodium falciparum*.

One whole-cell method, co-immunoprecipitation (co-IP), and one whole-genome method, yeast-2-hybrid screening, have been used to identify possible novel interactions for these immunophilins. Co-IP and subsequent mass-spectrometric analysis of the co-immunoprecipitates identified a number of novel immunophilin–protein interactions for both of the cyclophilins and the FKBP. Yeast-2-hybrid screening was used to identify a number of novel protein–protein interactions for PfFKBP35, some of which tallied with results seen in the co-IP screen. Some of these interactions were predicted, based on data from other organisms, such as the identification of Hsp70 and Hsp90 as putative partners and a putative interaction between histones and PfFKBP35. Others, such as the identification of immunophilins interacting with RAP1, and possibly other rhoptry proteins, were completely novel and may provide starting points for new investigations into functional roles of immunophilins and potential protein–protein interaction modulating drugs. Further investigation confirmed *in vitro* an interaction between PfCYP19B and Hsp70, a possible role for cyclophilins in RAP1 chaperoning with implications for host cell invasion, and an interaction between PfFKBP35 and histones with a

potential significance for histone modification and epigenetic gene regulation.

In parallel to these efforts we also investigated the molecular basis of a novel interaction between PfFKBP35 and calcineurin that takes place in the absence of FK506. Using *in silico*, genetic, *in vitro* assays with recombinant protein, and *in vivo* methodologies we identified a 15 amino acid N-terminal extension which may play a role in this interaction.

The work presented in this thesis has encompassed studies with intact parasites, parasite extracts and recombinant parasite proteins and has added to the understanding of the biological roles of immunophilins during the parasite erythrocytic life cycle.

Some humans would do anything to see if it was possible to do it. If you put a large switch in some cave somewhere, with a sign on it saying 'End-of-the-World Switch. PLEASE DO NOT TOUCH', the paint wouldn't even have time to dry.

—Terry Pratchett

Among competing hypotheses, the hypothesis with the fewest assumptions should be selected.

—Ockham's Razor

What cannot be settled by experiment is not worth debating.

—Newton's Flaming Laser Sword

ACKNOWLEDGMENTS

The work presented in this document would not have been possible without the help of a number of fantastic people. Firstly I'd like to thank my supervisor Prof. Gus Bell for all the help, support and guidance he's given me for the last 4 years. I apologise for the many mis-uses of hyphens, dashes and gross Americanisms that you've had to correct, but most importantly thank you for teaching me what scientific research is all about.

Next I'd like to thank the members of my postgraduate committee, Prof. Alistair Fleming, Prof. Tim Foster and Prof. Ursula Bond, for their helpful guidance over the course of my work. I'd like to thank the other members of the Bell lab that I've had the pleasure to work with during my time in the Moyne, Dr. Alejandro Marin-Menendez for all his help, particularly showing me the ropes of malaria culture and Dr. Daniela Boehm for leading by her hardworking example in the last few years, as well as the undergraduate students that I've had the pleasure of supervising and who generated useful results for my work. I'd also like to thank Deirdre Muldowney for her help and the many reagents she's lent me over the years as well as Jayne Vance for her immeasurable assistance in every way during my time in the Moyne.

I would like to thank my girlfriend Karen Howe and my parents, Damian and Karen Leneghan, for all their support and encouragement during the last four years. Without their support, both financially and emotionally, the successful conclusion of the work in this thesis would not have been possible.

Finally I would like to acknowledge SFI for providing funding to enable this work and the Trinity Trust for providing funding which allowed me to attend the molecular parasitology conference in Woods Hole and the Catalysts2013 conference in Halle both of which aided my scientific career and development greatly.

CONTENTS

LIST OF FIGURES

LIST OF TABLES

1

INTRODUCTION

1.1 MALARIA

1.1.1 *Historical Outline*

The earliest known evidence of malaria comes from mosquitoes preserved in amber from the Palaogene period, approximately 30 million years ago [129]: oocysts, sporozoites, possible microgametes and an ookinete were isolated from the body cavity of a female *Culex* mosquito. This particular malaria parasite's primary host was likely a member of the order Galliformes and aligns this ancient malaria with extant avian malarial parasite species. Humans are believed to have initially caught malaria from gorrillas [101], and the disease has affected us for the entire history of our species [79], co-evolving along with its mosquito and human hosts.

The modern name malaria comes from the association of the disease with the "bad air" in marshy areas – "mal aria" in mediaeval Italian, but the earliest written report of malaria comes from a book written sometime around the late second century BCE. Known as the Huangdi Neijing, it is a compiled canon of internal medicine ordered by the Chinese emperor Huang Di, and refers to repeated paroxysmal fevers associated with enlarged spleens and a tendency to epidemic occurrence. Indeed, there is a large body of evidence that suggests that malaria was endemic accross the ancient world, from

sub-Saharan africa [94] to China [42] to Europe [48] and North America [54]. Even Shakespeare wrote about malaria, or "marsh–fever" in eight of his plays.

It wasn't until 1880 that the causative agent of malaria was revealed. French physician Charles Louis Alphonse Laveran observed pigmented parasites in the red blood cells of patients suffering from malaria. He determined that these parasites were cleared from the blood by quinine and after noting exflagellation events named the parasite *Oscillaria malariae* [43]. The advent of improved microscopy allowed elucidation of the reproductive cycle of the parasite in human blood a short time later as well as the observation that division cycles coincided with febrile episodes [149] and the organism was renamed *Plasmodium*. Seventeen years after Laveran's discovery British army surgeon Sir Ronald Ross showed that mosquitoes were the transmission vector of malaria and a short while later other researchers demonstrated that only *Anopheles* mosquitoes were capable of transmitting human malaria [31].

Successful early control measures included the use of quinine (discussed in section 1.1.6) and vector control by eradicating mosquitoes. But it wasn't until around the 1930s that vector control was adopted on a large scale. In 1938 *Anopheles gambiae* appeared in South America. This species of mosquito is native to Africa and is a particularly effective vector for human malaria. This very quickly lead to the largest epidemic of malaria ever seen in the Americas, but vector eradication by chemical agents such as Paris Green and pyrethium lead to eradication of *A. gambiae* from Brazil by 1940 and eventually from the continent [124]. During World War II, the insecticide dichlorodiphenyltrichloroethane (DTT) was used to combat insect borne diseases, particularly malaria. Cheap, highly potent against mosquitoes and with

low toxicity to man it seemed like just the "silver bullet" needed to combat malaria and lead to the introduction of a worldwide malaria eradication programme by the World Health Organisation (WHO) during the 1950s. Spraying of mosquito breeding grounds and indoor residual spraying were wildly successful, with malaria eradicated from Europe, North America and Russia by the mid-1960s. The incidence of the disease was also dramatically reduced in many parts of the tropics, South America, India and Sri Lanka. However in 1962 American biologist Rachel Carson published a book called *Silent Spring* which brought to light the environmental side effects of synthetic pesticides and sparked the global environmental movement. Environmental and public health concerns along with the emergence of mosquitoes resistant to DTT lead to a decrease in its use, eventually being banned for the US in 1972 and worldwide by the Stockholm Convention in 2001. As a result the incidence of malaria increased from the 1970s until recently in many areas in which the mosquito vector hadn't been completely eradicated [139].

After the apparent failure of this method of malaria control the WHO moved its focus to the use of antimalarial drugs. Antimalarial herbs had been used for centuries in the treatment of malaria and since its discovery in 1820 quinine had been the gold standard (see section 1.1.6). During World War II the Americans, Germans and French produced synthetic derivatives of quinine, of which the most important was chloroquine. Chloroquine became widely used throughout the middle of the 20th century but unfortunately resistant parasites were discovered in Columbia and Thailand. Chloroquine resistance has since spread globally.

Plasmodium was first successfully continuously cultured in the lab by Trager and Jensen in 1976 [165] and this allowed researchers to

investigate more easily the molecular biology of the parasite and increased the rate of development of new drugs hugely. Even still, there was no drug or vaccine which proved wholly effective and the despondency caused by the failure of both malaria control strategies lead to malaria research falling into the background of scientific importance around the 1990s.

1.1.2 *Malaria today*

In the last decade there has been a renewed effort to eradicate malaria on a global scale, thanks largely to initiatives by organisations such as the Bill and Melinda Gates Foundation and Roll Back Malaria. Even still, malarial disease presents a significant global challenge both in human and economic terms. The World Health Organisation classified 104 countries around the world as endemic for the disease in 2010 (http://www.who.int/malaria/). Among the approximately 3.3 billion people who were at risk of contracting malaria in 2009 there were an estimated 219 million cases leading to approximately 660,000 deaths. The rate of malaria mortality has fallen by 26% around the world between 2000 and 2010. This decrease was higher in the area where the WHO is focusing most, the African Region, decreasing by 33%. The WHO estimated that an estimated 1.1 million malaria deaths were averted globally during this period, primarily as a result of a scale-up of intervention strategies.

Despite these recent improvements, particularly in the African Region, malarial disease remains inextricably linked with poverty. Countries with the highest burden of extreme poverty (proportion of the people living below US$1.25 per day) also shoulder the highest bur-

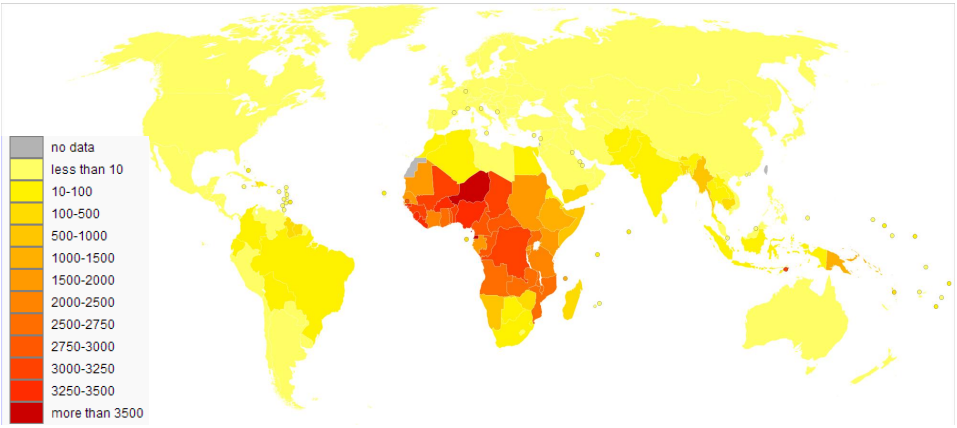

Figure 1: Disability-adjusted life year for malaria per 100,000 population in 2004. (Open Commons image, no citation needed)

den of malaria mortality. The six African countries with the highest burden of malaria, Nigeria, Democratic Republic of the Congo, Tanzania, Uganda, Mozambique and Cote d'Ivoire account for approximately 103 million (47% of all) malaria cases. The top 17 most affected countries worldwide account for an estimated 80% of yearly malaria cases. Three per cent of the total estimated cases are accounted for by 50 countries and these countries are on track to reduce their malaria case incidence rates by 75%, in line with targets set by the World Health Assembly.

Unfortunately surveillance of malaria is particularly weak across the world and published case and mortality figures are estimates rather than hard data. In the 2012 World Malaria Report, the WHO estimated that it was able to detect only around 10% of the estimated global number of cases and that it was not possible to make a reliable estimate of malaria trends in 41 countries WHO [173].

1.1.3 *Plasmodium species*

Transmissible malaria in humans is caused by five species of the parasitic protozoa *Plasmodium* and is spread by females of the *Anopheles* mosquito. These are *P. falciparum, P. vivax*, *P. ovale*, *P. malariae* and *P. knowlsei. P. knowlsei* is originally a parasite of monkeys but monkey to human transmission has been observed [168]. *Plasmodium* species also infect other vertebrates: for example, *P. chaubaudi* and *P. yoelii* and *P. berghei* infect rodents, *P. lophurae* and *P. fallax* infect birds and *P. knowlsei* infects monkeys. Of the species that make humans their host, *P. falciparum* causes the most severe and more frequently fatal disease while *P. vivax*, *P. ovale, P. knowlsei* and *P. malariae* cause a more mild disease that is only rarely fatal. *P. vivax* and *P. ovale* can persist for many years as hypnozoites in the liver, that can cause recurring blood infection and clinical relapses. *P. falciparum, P. knowlsei* and *P. malariae* do not cause a relapse of disease symptoms in this way. *P. ovale* now consists of two subspecies, *P. ovale curtisi* and *P. ovale wallikeri* [156].

1.1.4 *Life cycle*

The malaria parasite has a very complex life cycle (Figure 2) involving both insect and mammalian hosts and is essentially the same for all species which cause malaria in humans. Female malaria-infected mosquitoes inoculate sporozoites into the human host during a blood meal. It had long been thought that mosquitoes inject sporozoites directly into the bloodstream but recent experimental work has demonstrated that the majority of sporozoites are injected into the extra-

cellular matrix of the skin and leave the bite site by blood or lymphatic vessels [111]. Within half an hour sporozoites move through the blood stream and infect hepatocytes in the liver. Exo-erythrocytic schizogony (figure 2, A), a developmental process within these cells, then occurs, leading to production of merozoites and release of merozoites into the bloodstream. During this stage parasites multiply by approximately 10,000-fold.

After this initial replication in the liver, the parasites undergo asexual multiplication in the erythrocytes, a process known as erythrocytic schizogony (figure 2, B). Erythrocytes are infected by merozoites, with the life cycle progressing through the ring stage trophozoites, mature trophozoite stage and eventual maturation into schizonts, which rupture releasing the next round of merozoites. Parasites in this erythrocytic cycle are responsible for the clinical manifestations of the disease.

Also during erythrocytic cycle, a percentage of parasites differentiate into sexual erythrocytic stages (gametocytes). When an infected individual is fed upon by an *Anopheles* mosquito, it ingests gametocytes (male microgametocytes, and female macrogametocytes). Parasites then develop in the mosquito: this is known as the sporogonic cycle (figure 2, C). Microgametes exflagellate and penetrate macrogametes while in the mosquito's midgut and generate zygotes. Zygotes undergo differentiation into motile and elongated ookinetes, which are able to invade the midgut wall of the mosquito and develop into oocysts. Oocysts contain thousands of sporozoites which are produced by asexual multiplication. These oocysts then rupture, and release the sporozoites. Sporozoites make their way to the mosquito's salivary glands from where they are injected into a new human host during a blood meal and perpetuate the malaria life cycle.

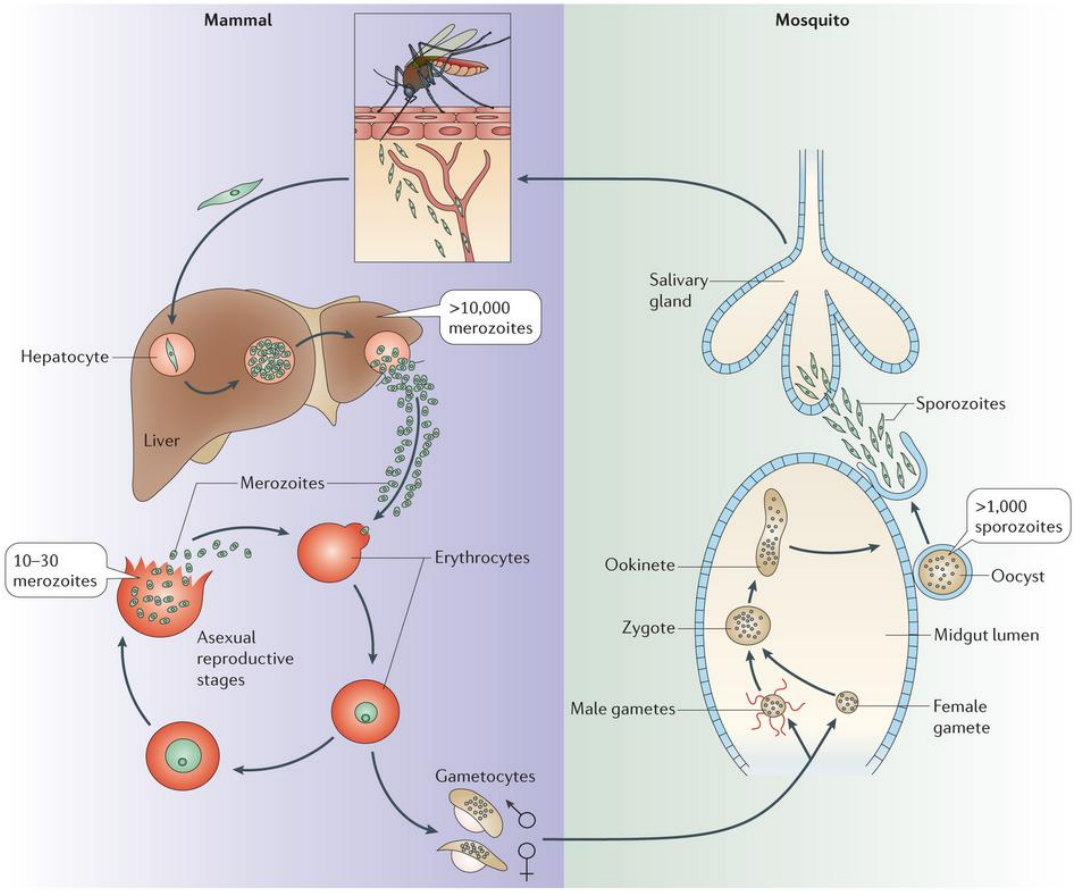

Figure 2: Life cycle of the malaria parasite in human and mosquito hosts. (Reproduced from Menard *et al.* (2013) [111])

1.1.5 *Intra-erythrocytic stages*

The intra-erythrocytic cycle of the life cycle is initiated when parasite merozoites invade host erythrocytes. The smallest stage in the life cycle of *Plasmodium* and one of the smallest known eukaryotic cells, at ~1–2 µm the blood stage merozoite is the erythrocyte-invasive stage and is excellently adapted for this job [15]. The overall architecture of the merozoite is that of an apicomplexan cell, which is characterised by an apical complex of secretory organelles (micronemes, rhoptries and dense granules) [14, 109, 141]. Figure 3 illustrates the spatial arrangement of organelles within the merozoite.

The process whereby a merozoite invades a host erythrocyte is a complex one, which is relatively well characterised on a cellular level but not very well understood on a molecular level. After merozoites are propelled into the bloodstream by bursting schizonts, they associate rapidly with red cells. This association is followed by the parasite cell reorientating itself so that the apical surface contacts the erythrocyte cell membrane, followed by release of proteins into the erythrocyte by the apical organelles. An electron dense structure known as the tight junction or moving junction complex then forms [95]. There is then a brief pause during which the parasite appears to induce reorganisation of the erythrocyte cytoskeleton [180] after which the parasite enters the erythrocyte through the action of an actin-myosin motor complex. The parasite then seals itself into a vacuole derived from the host cell membrane, known as the parasitophorous vacuole.

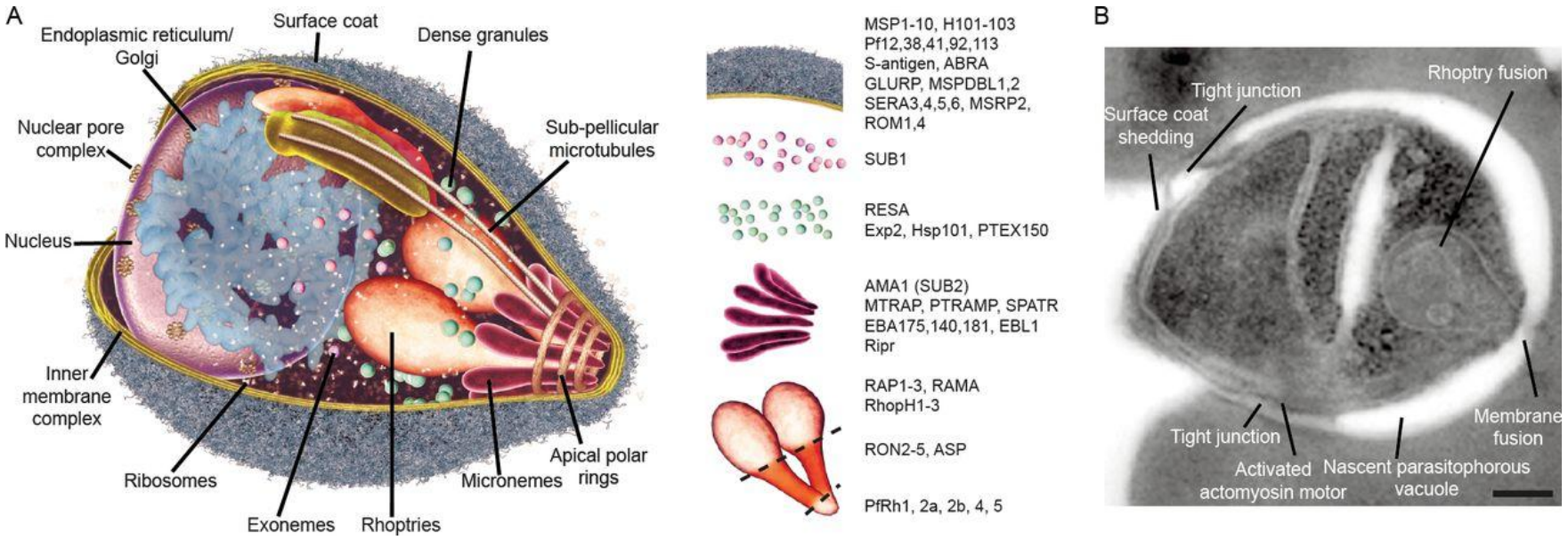

Cowman A F et al. J Cell Biol 2012;198:961-971

Figure 3: Three-dimensional diagram of a merozoite and its core secretory organelles. (A) The sectioned cell highlights the major cellular architecture and organelle repertoire of the invasive merozoite, with dissected organelles listing core molecular constituents of these key invasion-related compartments. (B) A *P. falciparum* merozoite in the process of invading a human red blood cell. Bar, 200 nm. Reproduced from Cowman *et al.* (2012) [41]

On the molecular level, we understand a large number of parasite proteins to be involved in the process of invasion. Merozoite surface proteins are directly exposed to the immune response of the host and are considered excellent vaccine candidates [53]. The first merozoite surface protein (MSP-1) was identified in 1988 [81] and since then researchers have elucidated a greatly expanded repertoire of surface proteins [41]. MSP-1 is the most abundant and functionally conserved protein on the merozoite but the family of merozoite surface proteins continues all the way up to MSP-11 with at least 14 other proteins (such as SERA proteins and S-antigen) thought to be involved in invasion [41]. In spite of our knowledge of the abundance of proteins on the merozoite surface, we are still not sure of their full functions. Some are are required for the survival of the parasite, since the genes coding for certain proteins cannot be disrupted, and by using antibodies specific for some proteins, invasion is inhibited [21, 120]. It is also thought that the parasite uses some of its repertoire of surface proteins to modulate host responses to assist in merozoite survival after release from the infected erythrocyte [121].

Merozoite proteins acting directly in invasion are involved in a finely coordinated series of events which depend on step-by-step processing and release of proteins just prior to and during invasion [146]. These proteins are divided loosely into adhesins and invasins. Adhesins, such as reticulocyte binding-like homologues (PfRh's), are generally located in the micronemes and rhoptries [41]. Invasins, so far as we know, appear to all be essential for merozoite invasion and are therefore considered excellent vaccine candidates. Apical membrane antigen-1 (AMA1) is in clinical trials as a vaccine candidate and has recently progressed from phase 1 to phase 2 [159].

After this exceptionally complex process of invasion, the parasite loses the organelles required for invasion and differentiates into a immature trophozoite form known as a ring because of its appearance in stained blood smears. During the ring stage, the parasite grows in size to approximately 50% of the uninfected erythrocyte volume by pinocytosing erythrocyte cytoplasm and ingesting and digesting haemoglobin in its digestive vacuole (DV) [163], though the total volume of the infected erythrocyte remains relatively constant [75]. The major by-product of this digestive process is haemozoin, a crystallised form of haem which accumulates in the DV throughout the erythrocytic stage of the life cycle, and is the parasite's way of detoxifying potentially lethal haem [154]. This digestive process requires the action of various aspartic acid, cysteine and metallo-proteases which degrade haemoglobin. Approximately 70–80% of the host cell's haemoglobin [61] is digested by the parasite but it uses only ~15% in de novo synthesis of its own proteins [89], with excess amino acids apparently exported from the erythrocyte by new transport pathways which the parasite creates [68]. After a period of growth, the parasite initiates DNA synthesis, late in the trophozoite stage, and then begins shizogony. This process first involves the division of the parasite nucleus by mitosis (during this time the parasite is known as a schizont), followed by rapid partitioning of the cytoplasm and organelles (when it is known as a segmenter). After segmentation of the schizont nuclei and cytoplasm, a number of merozoites are produced from one schizont. Up to 32 merozoites can be produced in this way (on average 20 daughter cells are produced), and after being expelled into the bloodstream by the schizont bursting they are free to re-invade fresh erythrocytes and begin the erythrocytic cycle over again.

The parasite induces a number of changes in the properties of the host cell. As the parasite matures it stiffens the erythrocyte membrane, decreasing the relative membrane deformability by over 90% compared to uninfected erythrocytes [55]. Infected erythrocytes often become sequestered in a number of tissues and organs, such as the heart, liver and brain. Sequestration is caused by the export of parasite proteins to the erythrocyte surface where they can bind to host receptors. Sequestration in the brain causes cerebral malaria, a serious complication of malaria infection, associated with a coma, encephalopathy and a high mortality rate [110].

Synchronised release of merozoites into the bloodstream, followed by a huge loss of erythrocytes by both diserythropoea and lysis cause the disease's main symptoms, and in this way the erythrocytic stage of the parasite life cycle can be held responsible for the characteristic paroxysm, a cyclical occurrence of sudden coldness followed by rigor and then fever and sweating.

1.1.6 *Chemotherapy and prophylaxis*

Antimalarial drugs are used in a number of ways, to guard against disease (prophylaxis), to treat an established infection, or to prevent transmission of the parasite. Drugs used as antimalarials can be categorised broadly depending on their mechanism of action, or according to their action on particular stages of the life cycle of the parasite. Causal prophylactic drugs generally act on pre-erythrocytic stages of the parasite preventing establishment of infection in the liver and blood: for example primaquine. Blood schizonticidal drugs act on the asexual stages of the parasite during the erythrocytic cycle, chloro-

quine (CQ) being an example of a blood schizonticide. Gametocytocidal drugs are those which destroy the sexual forms of the parasite, while sporonticidal drugs such as pyrimethamine would target the sporogonic stage of development in the mosquito vector. Anti-relapse, or secondary tissue schizonticides act on exoerythrocytic forms of the parasite and are used for *P. vivax* and *P. malariae* infections [28].

1.1.6.1 *History of antimalarial therapy*

Traditional herbal remedies have been used to treat malaria for thousands of years [174]. *Qing-hao,* first referred to in around the second century BCE, is a traditional chinese remedy made by soaking fresh plants of the *Artemisia* herb in cold water, wringing it out and ingesting the bitter juice in its raw state [175]. In the western world, quinine has been used for centuries as an antimalarial, originally discovered as a muscle relaxant by native peoples in what is now Peru it was imported into Europe and was first used as a malaria treatment in 1631 [164]. Quinine is isolated from the bark of the *Cinchona* tree: originally the bark was dried, ground into a powder and mixed into a liquid such as wine which was then drunk [144].

Control of the supply of *Cinchona* bark has, historically, been of major importance. In the early 19th century, Peru and nearby countries forbade the export of *Cinchona* seeds and strictly controlled export of the bark, but their monopoly was broken when in 1865, agents of the Dutch government smuggled a number of seeds out of Peru and began successful cultivation of the tree in Java. Eventually the Dutch came to monopolise over 97% of the world's supply of quinine [71]. Allied powers were isolated from their supply of quinine by the German occupation of the Netherlands and the Japanese control of the Philippines and Indonesia during World War II. The resulting short-

supply is thought to have led to the deaths of tens of thousands of US troops in Africa and the South Pacific by the end of the war.

Research by both Axis and Allied powers during the war eventually led to synthesis of a number of quinine derivatives, the most effective of which was chloroquine. CQ became the most widely used antimalarial throughout the late 1940s, 1950s and early 1960s until the emergence of resistance in the late 1950s and the subsequent spread of resistance across the globe. In the late 1960s a team of Chinese scientists re-discovered the antimalarial properties of *Qinghao*, in a screen of over 2,000 traditional herbal remedies. The active compound was eventually isolated and named artemisinin [98]. Artemisinin has high efficacy, and it and its derivatives in combination with other drugs are currently the treatment of choice for uncomplicated malaria.

1.1.6.2 *Current antimalarial therapy*

At present there is no "silver bullet" for malaria, and current antimalarial therapies act differently against the different species of human malaria and can even vary in efficacy against different strains of the same species. Host factors such as immune status can also alter the way in which antimalarial drugs act. The WHO currently recommends "Artemisinin Combination Therapy" (ACT) as the frontline treatment for *P. falciparum* malaria. These are combinations in which one of the components is an artemisinin derivative (artesunate, artemether or dihydroartemisinin), and the other is lumefantrine, amodiaquine, mefloquine, sulfadoxine–pyrimethamine or piperaquine. The artemisinins produce rapid clearance of parasitaemia and rapid resolution of symptoms, by reducing parasite numbers 100- to 1000-fold per asexual cycle of the parasite, which is more than the other cur-

rently available antimalarials achieve, but is also cleared rapidly from the body. The other component of the ACT is generally a longer life antimalarial which may also act on liver or gametocyte stages.

1.1.7 *Drug targets and drug resistance*

The growing problem of drug resistance presents a significant challenge to the successful eradication of malaria. Resistance to all known classes of antimalarial drugs is now common, with the exception of the artemisinins, though decreased susceptibility to even these drugs has been recorded in Vietnam, Thailand, Cambodia and Burma [172]. This raises the worrying possibility that strains of malaria may emerge that are untreateable with the drugs we have currently available. The search for new antimalarials is therefore of the highest priority in the fight against this disease.

The emergence and spread of antimalarial resistance parallels antibiotic resistance, particularly antituberculous drug resistance, where, as for malaria, transferable resistance genes are not involved in the emergence of resistance [172]. The spread of antimalarial resistance occurs primarily because it confers a particular advantage to survival in the presence of an antimalarial, and increases the chance of transmission of resistant over sensitive parasites. Recrudescence is also more likely in resistant parasites and as resistance worsens, infections with resistant parasites respond more slowly to treatment. Both increased rates of recrudescence and slow initial responses to treatment increase the likelihood of generating sufficient gametocyte densities to transmit, compared with drug-sensitive infections. It is this

ratio of transmission probabilities in drug-resistant compared with drug-sensitive infections that drives the spread of resistance.

Genetically, the events which culminate in antimalarial drug resistance (while retaining parasite viability) are thought to be spontaneous, rare and independent of the drug used [172]. Sometimes mutations occur in the genes encoding or relating to the influx/efflux pumps that affect concentrations of the drug in the parasite. Resistance to CQ for example is caused by mutations initially in the CQ resistance transporter (PfCRT). These mutations confer the ability to efflux CQ from the digestive vacuole, resulting in significantly reduced concentrations of CQ in the DV in CQ resistant parasites compared to CQ sensitive ones. CQ resistance can be further modulated by secondary mutations in another transporter (PfMDR-1) [52]. Other examples include resistance to antifols (pyrimethamine and cycloguanil) resulting from the sequential acquisition of mutations in the gene encoding dihydrofolate reductase (DHFR) [128] and resistance to the sulphonamides and sulphones, resulting from sequential acquisition of mutations in the gene encoding dihydropteroate synthase (DHPS) [6].

Recently the search for chemotherapeutic targets in malaria has been significantly aided by the introduction of new tools and technologies that allow a greater understanding of the genetic, molecular and biochemical basis of drug resistance. The genomic sequence of all three organisms involved in malaria are now available: *P. falciparum*, *Anopheles gambiae* and *Homo sapiens* [167, 11, 64]. It is expected that this will lead to advances in the understanding of interactions between the parasite and its hosts. Rational drug design too shows promise, and recent advances in studying the 3D structure of proteins

have allowed scientists to design inhibitors *in silico* that target particular proteins very specifically and have antimalarial effects [118].

Ideal antimalarial drug targets should possess a number of attributes: they should perform essential functions for growth, survival, or propogation of disease in the host, and should have low potential for resistance, and parasite-specificity (that is the target exists only in the parasite, such as rhoptry proteins, digestive vacuole proteins etc., or if the host possesses an analagous target, inhibitors of the target should be selective for the parasite over the host). With luck, identification of new targets that fit these criteria should continue to accelerate thanks to the cutting edge tools which are now available to researchers.

1.2 IMMUNOPHILINS

1.2.1 *History*

German researchers in the 1980s originally isolated a ~17 kDa protein from pig kidney which they determined to possess peptidyl-prolyl *cis-trans* isomerase (PPIase) activity (see below), and the ability to accelerate *in vitro* protein folding [58, 57]. At the same time, researchers in the USA purified a protein of a similar size and demonstrated that it bound with high affinity to the immunosuppressive compound cyclosporin A (CsA) [74]. The American researchers named their protein cyclophilin-A (CyP-A), a protein which still represents the archetype of the cyclophilin family of proteins. Shortly later, in the late 1980s, it was discovered that these two proteins were the same [60, 157].

Around the same time that Fischer, Takahashi and co-workers demonstrated that PPIase and cyclophilin were the same protein, two re-

search groups discovered a PPIase distinct from cyclophilin that was the major intracellular target of the newly introduced immunosuppressive drug FK506 [76, 145]. This new receptor was, rather unimaginatively, named FK506-binding protein or FKBP, the archetype of which is considered to be human FKBP12.

In the interceding two decades immunophilins have been discovered as ubiquitous accross nearly all forms of bacteria & archaea and eukaryotic organisms, often with organisms encoding multiple cyclophilins and FKBPs in their genomes [63]. Quite some time after the initial discovery of cyclophilins and FKBPs, in 2005, researchers identified a novel class of dual family immunophilins which contain both an FK506-binding and a cyclophilin domain [2]. These dual family immunophilins were identified in *Toxoplasma*, *Flavobacteria* and *Treponema*.

1.2.2 *PPIases*

Correct protein folding is limited by the *cis-trans* isomerisation of X-Pro bonds, where X is any other amino acid [25]. Uniquely among naturally occuring amino acids, proline has a relatively low difference in free energy between the *cis-* and *trans*-conformations of the peptide bond preceding it. The energy needed for catalysis of *cis–trans* isomerisation is relatively high: ~20 kcal/mol compared to ~0 kcal/mol for other peptide bonds. This means that X-Pro bonds do not spontaneously adopt their indended conformation, and this effectively limits the rate of protein folding [59]. Figure 4 illustrates a schematic of *cis-trans* isomerisation about a peptidyl-prolyl bond.

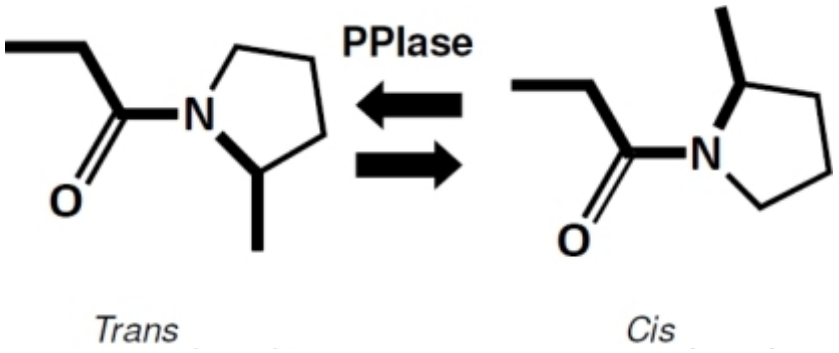

Figure 4: A schematic presentation of *cis-trans* isomerization about a peptidylprolyl bond catalyzed by one of the multiple members of the four dissimilar families of PPIases.

Catalysis of *cis-trans* isomerisation can be mediated by four classes of proteins which possess PPIase activity [63]. These four groups comprise the cyclophilins (CYPs), FK506-binding proteins (FKBPs), Pin1/parvulins and trigger factors. There is no significant sequence homology between the four groups, but they do exhibit some overlap in sequence-specificity for X-Pro epitopes in peptide substrates. Their active sites are also dissimilar, possessing different architectures and binding to small molecules with totally dissimilar structures [63] (Figure 5).

1.2.3 *The immunophilin family*

Immunophilins are a subset of this PPIase family, whose members bind to specific immunosuppressant molecules, originally isolated from fungi and *Streptomyces*. Members of the immunophilin superfamily are the cyclophilins, most of which bind to cyclosporin A (Fig. 5) and the FKBPs, most of which bind to macrolactides (FK506 [tacrolimus] and rapamycin [sirolimus], Fig 5) [17]. The immunosuppressive actions of CsA, FK506 and rapamycin (Rap) are mediated by drug–immunophilin complexes. CsA–CYP and FK506–FKBP bind to

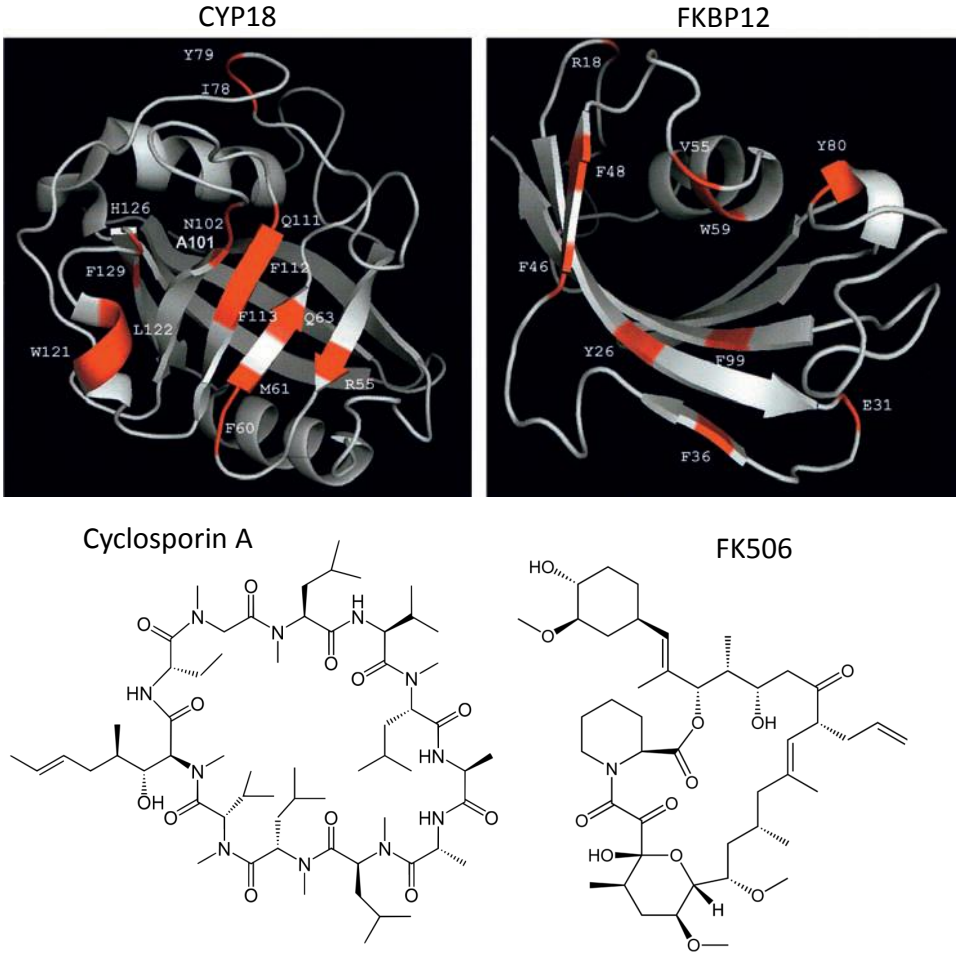

Figure 5: 3D comparison of the polypeptide backbones of human CYP18 and FKBP12. Structures drawn from the 2CPL and 1FKK entries in PDB.org respectively. The conserved amino acids of the PPIase domains involved in substrate–binding are coloured red and labeled. Also shown are the structures of cyclosporin A and FK506.

the protein phosphatase 2B (PP2B or calcineurin), inhibiting its phosphatase activity, resulting in the elevated phosphorylation of several PP2B substrates. One of these substrates is a subunit of nuclear factor of activated T-cells (NF-AT), the phosphorylated form of which is unable to translocate from the cytosol to the nucleus, where it would normally activate transcription of genes important in the T-cell activation pathway in response to immune stimulus. As a result these genes remain silent and the T-cell activation pathway is inhibited [80]. Rapamycin has a different effect, in that the Rap–FKBP complex inhibits a protein called mTOR (mammalian or mechanistic target of rapamycin) and results in inhibition of T- and B- cell proliferation by inhibiting their responses to interleukin 2 (IL-2) (Figure 6 is a schematic representation of the mechanism of these immunosuppressive activities). CsA, FK506 and Rap are used clinically as immunosuppressants to prevent rejection of transplanted organs.

Immunophilins have been discovered in nearly all higher eukaryotes [63, 169]. In humans for example, the genome appears to encode approximately 15 FKBPs and 16 CYPs. In terms of their architecture these proteins are quite diverse: CYP18 for example comprises only a PPIase domain whereas HsFKBP52 comprises two PPIase domains and three tetratricopeptide (TPR) repeat domains. Larger immunophilins often carry accessory domains such as TPR, RNA-binding, WD-repeat and signalling domains [63], and the largest known immunophilin is HsCYP324 (also kown as Nup 358 or RanBP2). The overall domain archetecture of a number of immunophilins is illustrated in figure 7.

Aside from their activity as PPIases, at least some immunophilins are also known to function as molecular chaperones in a manner comparable to certain members of stress-response protein families

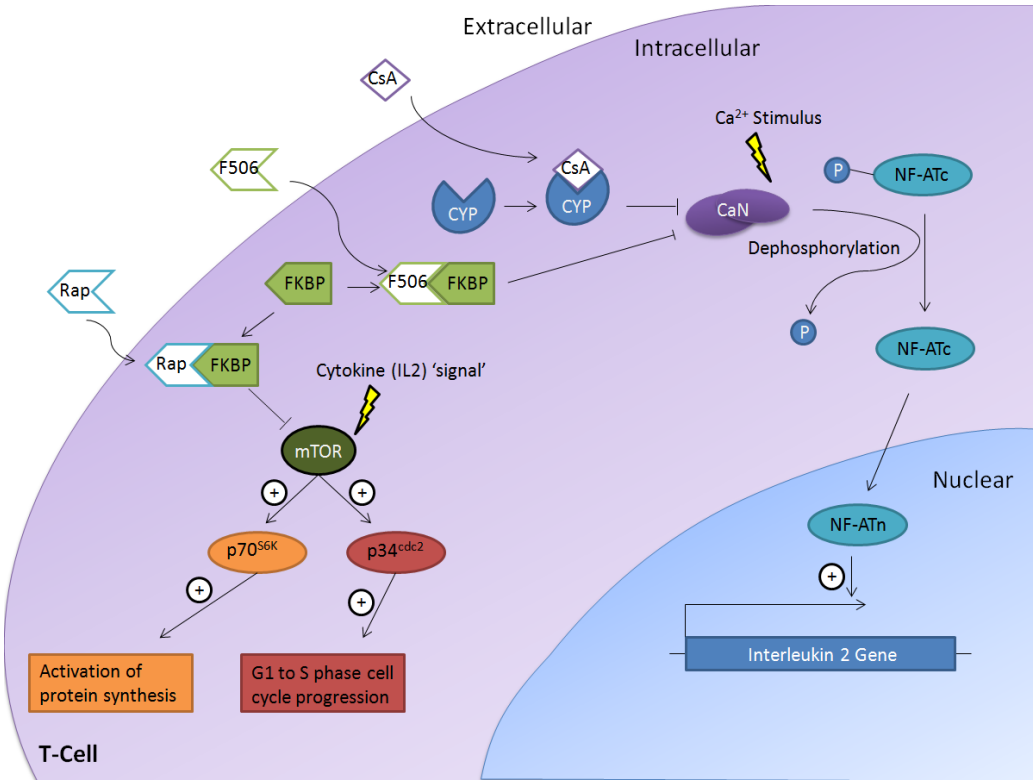

Figure 6: Schematic of the immunosuppressive action of CsA, FK506 and Rap. Cyclosporin A and FK506 bind to cyclophilin (CYP) and FK506-binding protein (FKBP) respectively. These complexes inhibit the dephosphorylation activity of calcineurin (CaN). CaN is unable to dephosphorylate the cytosolic form of nuclear factor of activated T-cells (NF-ATc), in this form NF-ATc is unable to translocate to the nucleus (NF-ATn) where it would normally activate important genes in T-cell proliferation. Rapamycin binds FK506 and this complex inhibits mechanistic target of rapamycin (mTOR) which results in inhibition of T- and B- cell proliferation by inhibiting their response to interleukin 2 (IL-2).

Figure 7: Representative domain arrangements of immunophilins: FKBPs, CYPs and dual family immunophilins. CYP = cyclophilin domain, FKBD = FK506-binding domain, CaM = putative calmodulin binding domain, WD40 = 40aa Trp/Asp containing β-propellor repeat domain, TPR = tetratricopeptide repeat domain, Hs = *Homo Sapiens*, Pf = *Plasmodium falciparum*, Dm = *Drosophila melanogaster*, Tg = *Toxoplasma gondii*, Fj = *Flavobacterium johnsonii*, Td = *Treponema denticola*

[63, 19]. The chaperone activity of immunophilins can be measured *in vitro*, for example via aggregation assays using model substrates, and may or may not be dependent on the presence of a functioning PPIase domain; indeed in many cases inhibition of the PPIase activity of the immunophilin has no effect on the chaperone activity [19, 107, 62]. How immunophilins act as molecular chaperones is unclear, but there is some evidence for a role of novel hydrophobic grooves outside the PPIase active site in chaperone activity. Studies in human FKBPs demonstrated that the majority of the chaperone activity of HsFKBP51/52 resided mainly in the C-terminal domain, which contained the TPR motifs [127]. Similarly analysis of Cyp40 deletion mutations demonstrated that the chaperone activity was primarily located within a linker region between the PPIase and TPR domains [112]. Smaller immunophilins, that possess limited extra sequence apart from the PPIase domain, also possess chaperone activity that is distinct from their PPIase activity [107, 132].

The structure of CypA contains 8 antiparallel β–strands forming a right handed β–barrel with an α–helix at each end. The core of the β-barrel is closed meaning that neither CsA or the X-Pro substrates can bind to the hydrophobic core; they instead bind to the outer surface of CypA via a number of critical hydrophobic residues (illustrated in figure 5). By contrast, FKBP12 is composed of 5 β–strands wrapped around a short α–helix forming a conical shape with a hydrophobic groove to which FK506 and X-Pro substrates can bind (illustrated in figure 5).

1.2.4 *Physiological roles of immunophilins*

It is currently unknown whether immunophilins are generally required for survival in biological systems; certainly they are not required for growth of *Saccharomyces cerevisiae* in culture. Dolinski *et al.* [50] demonstrated that deleting all twelve immunophilin genes in *S. cerevisiae,* both individually and together, had no effect on a number physiological paramaters, including temperature viability, arrest and recovery from pheromones or glycogen stress, mating or sporulation. This is often used as an example of how immunophilins are entirely dispensible, but a more likely explanation is that they are only required in response to certain stress conditions or environmental cues. For example researchers have demonstrated that the *E. coli* PPIase SurA is dispensible for growth in culture but required for biogenesis of the pilus which is required for urinary tract invasion [85], and that mutants of *Bacillus subtilis* with both of the organism's PPIases deleted had strongly reduced growth under near–starvation conditions [70].

Studies in mice have demonstrated some physiological roles for immunophilins. CYP18 knockout mice are viable but develop an allergic disease, caused by derepression of the Tec family tyrosine kinase ITK which is responsible for repressing the T helper 2 (Th2) response [39]. Research on FKBP12 knockout mice demonstrated that these mice were deficient in trabeculation and compaction of the embryonic myocardium, morphogenetic events crucial for the formation and function of the ventricular walls. These researchers identified that FKBP12 is a novel negative modulator of activated Notch1, suggesting that Fkbp1a-mediated regulation of Notch1 plays an important role in intercellular communication between endocardium and my-

ocardium, which is crucial in controlling the formation of the ventricular walls [36]. FKBPs have enriched expression in the human nervous system and participate in neuronal differentiation and neuritic outgrowth [131]. CYP18 and CYPB have also been demonstrated to act extracellularly as potent lymphotactic agents by their interaction with CD147 on immune cells [10]. But by far most of the information we have on immunophilin function is derived from work on steroid receptors, which require ordered assembly of chaperone proteins to mature into functional conformations [134, 137]. This receptor complex machinery consists of Hsp90, CYP40, FKBP52 (or FKBP51), and an additional p23 protein component, assembly of which is mediated by Hsp70 in association with accessory chaperones Hsp40, Hip and Hop [133, 32, 123]. Figure 8 is a schematic representation of what we understand of the glucocorticoid receptor assembly process. Interaction of these immunophilins is mediated by TPR domains interacting with a C-terminal peptide (MEEVD) in Hsp90.

1.2.5 *Immunophilins as drug targets*

Recently immunophilins have garnered a lot of attention as potential druggable targets in a number of diseases that affect humans. Detailed below are some examples of the roles immunophilins have in human disease and infection and what therapeutic potential immunophilin ligands offer.

1.2.5.1 *Immunophilins in human disease*

FKBPs are particularly highly expressed in the nervous system and as such are associated with a number of neurodegenerative diseases

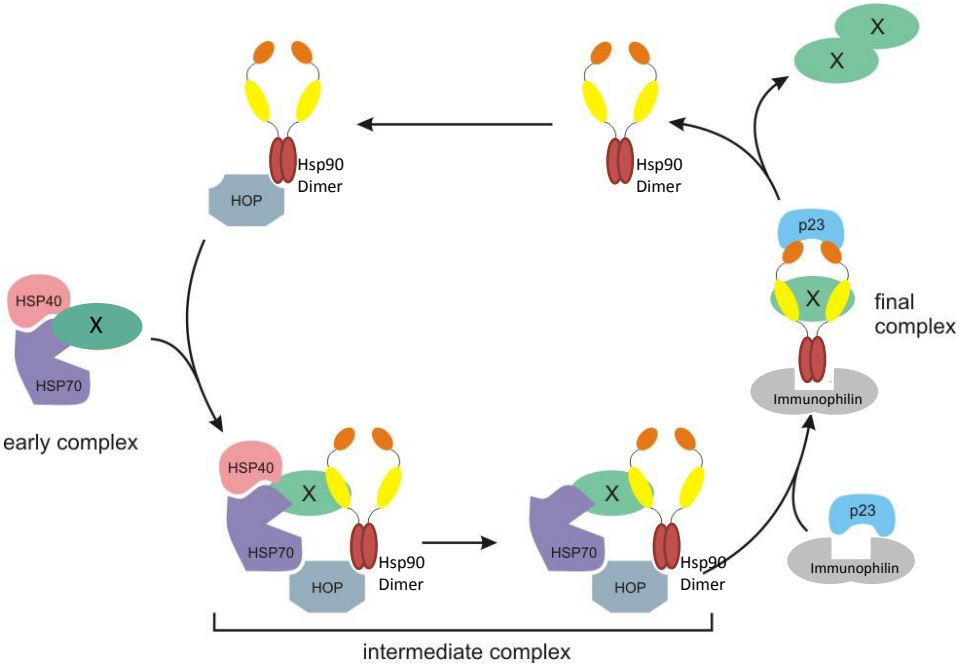

Figure 8: Steroid receptor assembly by the Hsp/immunophilin machinery. Four proteins, Hsp90, p60/Hop, Hsp70 and Hsp40, form a foldosome complex that associates with the stripped, non-steroid-binding state of the glucocorticoid receptor (X) in an ATP/Mg^{2+}-dependent and K^{+}-dependent manner to assemble a X–Hsp90–p60–Hsp70–Hsp40 heterocomplex with a steroid-binding site (intermediate complex). p23 is not a component of the native foldosome, but it associates with the assembly intermediate formed with purified proteins as well as with native glucocorticoid receptor–Hsp90 heterocomplexes isolated from cells. In both cases, p23 binding is reversible, does not require ATP and stabilises the complex. Immunophilins such as FKBP52, CyP-40 or the immunophilin-like PP5 bind to Hsp90 via tetratricopeptide repeat (TPR) domains. Because Hop and immunophilins bind to the same TPR acceptor site on Hsp90, immunophilins cannot bind until Hop has dissociated from this site. Immunophilins and p23 binding result in formation of the final complex, whereupon the glucocorticoid receptor is correctly folded and p23, immunophilins and the folded receptor disassociate from the Hsp90 dimer.

[151]. In Alzheimer's disease FKBPs have been shown to associate with tau, a microtubule-binding protein that has been associated with a number of neurodegenerative diseases (tauopathies). Researchers have reported that FKBP12 co-locates with neurofibrillary tangles in Alzheimer patients, and Alzheimer's disease brains contain much lower levels of FKBP12 than age-matched controls [153]. The larger immunophilins FKBP51 and FKBP52 have also been shown to have a role in tau turnover. FKBP51 overexpression in HeLa cells confers increased tau levels [84], but conversely FKBP52 overexpression in PC12 cells decreased the levels of tau detected [34]. FKBP12 and FKBP52 are also known to associate with Alzheimer's amyloid precursor protein and beta-amyloid peptides [30].

Parkinson's disease is characterised by the formation of Lewy bodies; alpha-synuclein (α–SYN) is the primary structural component of Lewy bodies where it aggregates to form insoluble fibrils. Reduction of FKBP12 and FKBP52 by knockdown in a neuronal cell culture model reduced the number of α-SYN fibrils observed and this effect was also observed after inhibition with FK506 [66]. Subsequent studies on the effect of several physiologically relevant PPIases, namely FKBP12, FKBP38, FKBP52, FKBP65, Pin1, and CYP18, on α-SYN aggregation *in vitro* and in neuronal cell culture, demonstrated that FKBP12 was the most potent enhancer of α–SYN aggregation [47].

FKBP52 and FKBP12 are upregulated in regenerating neurons, suggesting that it may play a protective or regenerative role following injury [104]. Indeed FK506 was known to have neuroregenerative action for some time, and recently this action was elucidated as a process imitating the early steps of neuronal differentiation, by FK506-induced regeneration of an Hsp90–FKBP52–p23 chaperone complex in damaged neurons [130].

Immunophilins are also involved in several types of cancer. FKBP51 is upregulated in prostatic hyperplasia [122], and levels of FKBP51 and FKBP52 are increased in prostate cancer cell lines, and FK506 has an inhibitory effect on growth of these cells [125]. FKBP51 is also involved in colorectal adenocarcinoma [117], where it suppresses proliferation. Inhibition of FKBP51 in leukaemia cells by Rap induced apoptosis [12], and this protein is a marker of melanocyte malignancy [140]. Less is known about the role of FKBP52 in cancer but some studies have demonstrated that it is upregulated in breast tumours [148].

1.2.5.2 *Immunophilins in viral infection*

Recently a number of obligate parasites have been shown to co–opt host immunophilins for infection and growth. In human immunodeficiency virus (HIV), CYP18 is thought to play a number of roles. Studies have shown that mutations in the promoter region of CYP18 promote disease progression from HIV–positive status to acquired immunodeficiency syndrome (AIDS) [7]. CYP18 knockouts [24] and regulatory mutations [138] have a protective effect from HIV–1 infection. CYP18 is packaged into mature HIV virions [22] and disruption of this packaging attenuates the infectivity of progeny virions [158]. A number of HIV accessory proteins are thought to interact with CYP18, such as viral protein R (Vpr) [179] and Nef [3]. An FKBP is also stolen by HIV, where it appears to package an average of 25 molecules of FKBP12 into each HIV-1 virion [29].

Cyclophilins are also involved in hepatitis B (HBV) and C (HCV) infection. There is evidence for increased extracellular export of CYP18 in HBV [162]. The active site of CYP18 appears to be critical for HCV replication and knockdown of endogenous CYP18 significantly ham-

pers HCV RNA replication and viral protein expression [35]. CYPB appears to interact with HCV RNA-dependent RNA polymerase NS5, and this interaction is critical for viral genome replication [170].

Influenza virus too, is known to co–opt host immunophilins. CYP18 has been discovered in the core of the influenza virion [143], and is up–regulated in certain cell lines upon infection with influenza virus [100]. Interestingly, overexpression or depletion of CYP18 had an inhibitory effect on, or enhanced viral replication respectively. Other viral infections also appear to interact with CYP18 in some way. Vaccinia virus (VV), infection leads to an increase in CYP18 stability and colocation with the sites of viral production, the protein then being incorporated into the virus particle [33]. CYP18 has been found associated to be with vesicular stomatitis virus (VSV) and severe acute respiratory syndrome coronavirus (SARS-CoV), where in both cases it interacts with the nucleocapsid protein and is incorporated into viral particles [23, 103].

1.2.6 *Immunophilins in malaria*

P. falciparum possesses thirteen immunophilin genes, eleven cyclophilin or cyclophilin-like and two FKBP or FKBP-like [107, 65, 113]. These will be discussed with relation to their genetic location, sequence similarities of their PPIase domains relative to archetypal immunophilins, stage specificity, properties and functions. Figure 9 is a brief schematic of some of these properties.

1.2.6.1 *Location, expression and similarity of P. falciparum immunophilins*

PfFKBP35 was the first FKBP identified in apicomplexan parasites [26]. It is thought to be the only true FKBP that *P. falciparum* possesses and is encoded by a 915-bp gene located on chromosome 12. Expression data indicate that PfFKBP35 begins expression during the late ring stage, peaking during the late trophozoite stage before falling off during the schizont stages [96]. During the ring stage, PfFKBP35 is predominantly cytosolic, but as the parasites mature into trophozoites and schizonts, the protein appears to undergo nucleocytoplasmic shuttling, with the majority of the protein becoming located in the nucleus, as shown by immunofluorescent microscopy [90].

InterPro (http://www.ebi.ac.uk/interpro/) prediction based on domain and functional site analysis has annotated four additional *P. falciparum* proteins as containing FKBP or FKBP-like domains: these are PF3D7_1111800, PF3D7_1313300, PF3D7_1303700 and PF3D7_1212400. All four of these additional proteins appear to be expressed at the mRNA level at some point in the parasite life cycle, though only very weak data exist that indicate the proteins were detected by mass spectrometry at any stage and only PF3D7_1111800 possesses any significant sequence similarity to other FKBPs when analysed by basic local sequence alignment (BLAST) searching (data not shown). No investigation on whether these proteins possess any of the typical functional characteristics of FKBPs has been performed to date.

Of the eleven cyclophilin or cyclophilin-like genes, all are expressed in at least one stage of the life cycle [88]. PfCYP19A and PfCYP19B appear to the most abundant of the *P. falciparum* cyclophilins (making up ~1.2% and ~0.5% of total cellular protein respectively) and

are located predominantly in the cytosol of the erythrocytic stage of the parasite [65]. Additionaly they are the only two cyclophilins pulled down by CsA-coupled affinity columns from these stages [65]. PfCYP19B has been detected at the surface of infected erythrocytes [176], and PfCYP32 is predicted to be in to the mitochondrion [88]. In increasing order of size the cyclophilins are located on chromosomes 11, 3, 11, 5, 8, 12, 12, 14, 9, 8 and 5 respectively. An inferred phylogenetic study grouped PfCYP81CLD and PfCYP72CLD as the most distantly related from all of the other proteins and grouped PfCYPs 19B, 26, 19A, 32CLD & 25 and 19C, 23, 52CLD & 87CLD into two closely related groups (CLD = cyclophilin–like domain)[107].

1.2.6.2 *Protein properties and functions*

PfFKBP35 possesses a multi-domain architecture, comprised of an N-terminal FK506-binding domain (FKBD), followed by a TPR domain, and a putative calmodulin binding site as shown in figure 9. PPIase activity of the protein is conferred by the FKBD and both the TPR domain and FKBD demonstrate chaperone activity [113]. The domain architecture is remarkably similar to HsFKBP51 and HsFKBP52, apart from the second FKBD in these proteins, that are known to interact with HSP90 via their TPR domain. Indeed PfFKBP35 has been demonstrated to interact with PfHsp90 via its TPR domain [90] indicating a possible role for PfFKBP35 in chaperone machinery analogous to that seen in humans. Among FKBPs with PPIase activity there is exceptional conservation in 14 amino acids that are known to interact with FK506, and interestingly PfFKBP35 only conserves 12 of these residues and has substituted a hydrophobic doublet (Gly89/Ile90) from hFKBP12 to a hydrophilic doublet (Glu108/Ser109) [113]. PfFKBP35 (recombinant full–length, and FKBD) has also been found to

interact with calcineurin (from bovine and recombinant *Plasmodium* sources) in a manner independent of the presence of FK506 [113, 90]. This may represent a point of difference between the parasite and host and a potentially druggable target. This observation is however debated in the literature, with one group of researchers claiming that the calcineurin–FKBP interaction using recombinant FKBP is dependent on the addition of FK506 [178].

The architecture of the malarial parasite cyclophilins is moderately varied. Most contain a cyclophilin or cyclophilin like domain (CLD) ranging in size from 160–219 amino acids. Only PfCYP19A and PfCYP19B are known to possess PPIase activity and the ability to bind the classic cyclophilin ligand CsA, while PfCYP19A, 19B, 19C, 23, 25, 26, 32CLD & 52CLD all possess chaperone activity *in vitro* on at least one model substrate [107]. Aside from these data, little else is known about the subcellular location of the remaining cyclophilins, and it is thought that the parasite requires such a large cohort of cyclophilins perhaps for different stages of the life cycle, different subcellular compartments, or that some are specialised for folding of specific protein substrates [107].

PlasmoDB Identifier	Chaperone Activity	PPIase activity	Ligand Binding	Domain Architecture
PF3D7_1116300	R + CS -	No	No	PfCYP19C
PF3D7_0322000	R + CS +	Yes*	CsA	PfCYP19A
PF3D7_1115600	R + CS+	Yes*	CsA	PfCYP19B
PF3D7_0528700	R + CS -	No	No	PfCYP23
PF3D7_0804800	R + CS +	No†	No	PfCYP25
PF3D7_1202400	R + CS +	No	No	PfCYP26
PF3D7_1215200	R + CS +	No	No	PfCYP32
PF3D7_1423200	R + CS +	No	No	PfCYP52
PF3D7_0930600	ND	ND	ND	PfCYP72
PF3D7_0803000	ND	ND	ND	PfCYP81
PF3D7_0510200	ND	ND	ND	PfCYP87
PF3D7_1247400	R + * CS +*	Yes*	FK506, Rap	PfFKBP35

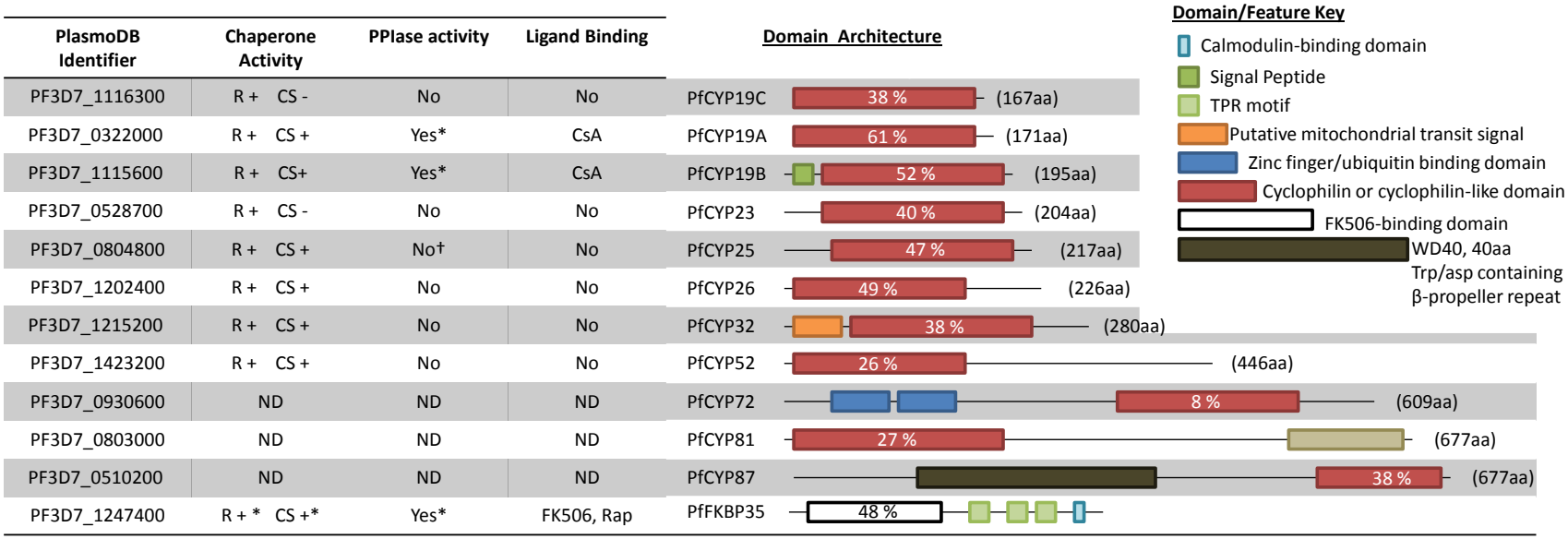

Figure 9: Schematic of the properties and domain architectures of 12 *P. falciparum* immunophilins. Activities were determined by the performance of recombinant proteins in a number of assays. Chaperone activity was assayed by rhodanese (R) and citrate synthase (CS), PPIase activity was assessed by the *cis-trans* isomerisation of a synthetic xaa-Pro peptide, and ligand binding was assessed by thermal stability shift assay. * Indicates that the activity indicated is inhibited by addition of relevant ligands (CsA for CYPs and FK506 for FKBP). † Indicates that there are conflicting reports in the literature. + Indicates detectable activity, - indicates no detectable activity. Numbers in the CYP18 and FKBP domains indicate sequence identity to the archetypal proteins HsCypA and HsFKBP12 respectively [107, 113].

1.2.6.3 *Antimalarial effects of immunophilin ligands*

The antimalarial activity of CsA was first observed in mouse models [161], and follow up investigations revealed activity against *P. berghei* and *P. yoelii* in rodents and on cultured *P. falciparum*, *P. berghei* and *P. vivax* [18]. The most susceptible form of the parasite appears to be during the asexual erythrocytic cycle, though the data on which particular stage during the cycle are the most susceptible are inconsistent [20, 18]. Gametocyte stages appeared somewhat susceptible and the liver stages are largely resistant to CsA treatment [18].

The PPIase activity of whole parasite extracts on synthetic Xaa-Pro peptides is wholly inhibited by CsA concentrations above 0.1 µM but this effect is not seen with FK506 or rapamycin [20]. This suggests that the majority of the PPIase activity in erythrocytic parasites is attributable to the parasite's cyclophilins 19A and 19B. CsA, Rap and FK506 all demonstrate antimalarial activity in culture with 50% inhibitory concentrations (IC50) of ~300 nM, 1.9 µM and 2.6 µM respectively [20]. These drugs don't represent potential antimalarial therapies because of their immunosuppressive effects; however, non-immunosuppressive derivatives of these drugs also demonstrate antimalarial activity. The cyclosporin derivative 3'-keto cyclosporin D had a similar IC50 (~320 nM) to CsA but has negligible immunosuppressive activity, though it appears to be a poor inhibitor of PPIase activity. The derivative [MeVal]^4-Cs also had similar activity to CsA and does appear to inhibit PPIase action in whole parasite extracts [20]. Non-immunosuppressive FK506 derivatives also have antimalarial activity against parasite culture [114].

1.3 PROJECT OBJECTIVES

Understanding the nature of protein–protein interactions is predicted to lead to novel small-molecule inhibitors, but unfortunately often protein–protein interfaces are flat, lacking the grooves typical of proteins that interact with ligands [171]. Recent work has identified several novel small–molecule inhibitors of protein–protein interfaces, including molecules that inhibit interleukin-2 (IL-2)'s interaction with the alpha-chain of its receptor IL-2Rα, and inhibitors of the B-cell lymphoma 2 (BCL-2) family's interaction with BCL-2-antagonist/killer and BCL-2 antagonist of cell death [171]. Small molecules are also known to stabilise protein–protein interactions. Paclitaxel is a compound isolated from the bark of *Taxus brevifolia* which allosterically stabilises polymerised microtubule structures by binding to the β-tubulin subunit [160]. CsA, FK506 and Rap also stabilise protein–protein interactions as discussed in section 1.2. Other examples include molecules such as brefeldin A, forskolin and auxin [160].

Since it is probable that immunophilins in *P. falciparum* interact with many proteins in the parasite due to their nature as chaperones and PPIases and that many of these interactions are probably independent of PPIase activity, the aims of this PhD project were as follows:

1. To investigate the protein–interaction repertoire of the two major cytosolic cyclophilins PfCYP19A and PfCYP19B, and the FKBP, PfFKBP35 by whole cell (co-immunoprecipitation [co-IP]) and whole genome (yeast-2-hybrid [Y2H]) methods. From this work, to identify novel interactions as well as interactions indicated by immunophilin–protein interactions in other organisms.

2. To follow up any interactions discovered by co-IP and Y2H using *in vitro* and *in vivo* methods such as far Western blotting, immunofluorescent microscopy, protein based assays etc. In particular this research would focus on any interactions discovered which we deemed to be interesting because of particular importance of the interacting partner in parasite biology, or because of indicated importance of similar interactions in other organisms in the available literature.

3. To attempt to characterise the molecular basis of an unusual interaction between PfFKBP35 and calcineurin which appears to take place in the absence of FK506 (usually this compound is required for the interaction to take place). In this investigation we would first attempt to model the interaction *in silico*, and follow up with *in vitro* and *in vivo* methodologies.

2

MATERIALS AND METHODS

2.1 CHEMICALS AND REAGENTS

All chemicals and reagents used in this study were purchased from Sigma Aldrich Ireland Ltd. unless otherwise stated. All general chemicals were of analytical grade. All reagents used during electrophoresis were of electrophoresis grade. All chemicals used for cell culture were cell culture tested. [MeVal]^4-Cs was a gift from Sandoz AG, Basle, and BC556 from Biotica, Cambridge.

2.2 CULTURE OF PARASITES

2.2.1 *Routine culture*

Plasmodium falciparum line 3D7, adapted to grow in Albumax®, was maintained in continuous culture in human erythrocytes (obtained from the National Blood Transfusion Service Board, Dublin every three weeks or as necessary and prepared as in section 2.2.2) according to the method of Trager and Jensen [166]. Parasites were routinely cultured at 2.5 % (v/v) hematocrit in complete medium (RPMI 1640 supplemented with 25 mM 4-(2-hydroxyethyl)-1-piperazineethanesulphonic acid (HEPES), 0.18% w/v sodium bicarbonate, hypoxanthine (50 µg/ml), 0.4% w/v Albumax® II [BioSciences, Dun Laoghaire, Ire-

land], 0.16% w/v glucose), maintained in tissue culture dishes (Sarstedt Ltd., Drinagh, Co. Wexford) at 37 ºC in a candle jar. Parasitaemia was monitored by microscopic examination of Giemsa-stained smears and routine cultures were fed depending on the parasitaemia and diluted with fresh erythrocytes twice a week or as necessary.

2.2.2 *Treatment of whole human blood*

Erythrocytes for parasite culture were prepared as follows from whole human blood: 10 parts whole blood were mixed with 1 part PIGPA solution (50 mM sodium pyruvate, 50 mM inosine, 100 mM glucose, 500 mM disodium hydrogen phosphate, 5 mM adenine made up in 0.9% [w/v] NaCl and pH adjusted to 7.2) and incubated at 37 °C for 1 h with periodic agitation. The mixture was centrifuged at 500 x *g* for 10 min at 4 °C in a Sorvall RT6000D benchtop centrifuge. The supernatant and buffy coat were removed by aspiration. The pellet was washed twice by resuspension in cold sterile PBS and centrifuged for 500 x *g* 10 min at 4 °C, and once with culture medium. Packed erythrocytes were resuspended in an equal volume of culture medium to give a final hematocrit of 50%. Prepared erythrocytes were stored at 4 °C for up to 1 week.

2.2.3 *Harvesting of cultures*

Free parasites were generated from infected erythrocytes as follows: parasite cultures with high parasitaemia (generally >10%) were collected by centrifugation at 2000 rpm (650 x *g*) at 4 ºC for 10 min and washed twice in ice-cold PBS. The pelleted erythrocytes were in-

cubated with 0.05% (w/v) saponin in ice cold saline sodium citrate (SSC) [150 mM NaCl, 15 mM tri-sodium citrate] for 20 min with vigorous shaking every 5 min to lyse erythrocyte membranes and release intracellular parasites [181]. Freed parasites were pelleted for 15 min at 3000 rpm (975 x *g*) at 4 ºC and washed twice with SSC. Parasite pellets were resuspended in freezing solution (PBS containing 10% w/v glycerol and 1 x Complete mini protease inhibitor [Roche Diagnostics, Mannheim, Germany]) and snap frozen in liquid nitrogen for storage at -80 ºC until needed.

2.2.4 *Synchronization of cultures*

Routine erythrocytic *P. falciparum* cultures are an asynchronous culture consisting of rings, trophozoites, schizonts and merozoites. To enrich for the late stages of erythrocytic development, parasites at high parasitaemia (>15%) were subjected to magnetic selection essentially as described by Staalsoe *et al.* [150] before use in experiments. Briefly, parasitised erythrocytes are passed over a CS column (Miltenyi Biotec, Surrey, UK) which is mounted on a VarioMacs magnet (Miltenyi Biotec). When mounted in the magnet the steel-wool packed in the column becomes magnetic, this allows selection of late stages of erythrocytic develepment by virtue of the high content of paramagnetic haem in these stages. The column is then washed with incomplete medium to remove unparasitised erythrocytes and is then removed from the magnet, whereupon a further wash with incomplete medium elutes parasitised erythrocytes.

2.2.5 *Invasion assay*

Parasites synchronised to late stages (trophozoite/schizont) by magnetic selection (section 2.2.4), were incubated with either the compound being tested or vehicle only control (e.g. DMSO) in complete medium for 2 h. Treated schizonts were washed with complete medium by centrifugation at 350 x *g* for 10 min. Washing was repeated twice. Treated schizonts were then introduced to fresh erythrocytes at 2.5% hematocrit and incubated overnight (14–16 h) with shaking. Parasitaemia was assessed by counting the number of ring stages in parasitised erythrocytes in giemsa stained blood smears by light microscopy.

2.2.6 *Preparation of whole cell parasite extracts*

Parasites harvested as described in section 2.2.3 were thawed on ice to minimise protease activity. Pellets were lysed by incubation with one of two buffers: parasite lysis buffer (PLB) (0.5% (v/v) Triton X-100 in freezing solution) or native PAGE age lysis buffer (NPLB) (0.5% (v/v) Triton X-100 in 20 mM Bis-tris, 500 mM ε-aminocaproic acid, 20 mM NaCl, 2 mM EDTA, 10% (v/v) glycerol, 1 x Complete mini protease inhibitor) on ice for 30 min with agitation every 5 min to enhance lysis. The lysate was then clarified by centrifugation at 18,000 x *g* for 10 min at 4 °C, the supernatant was carefully removed to a fresh microfuge tube, leaving behind the unwanted cellular debris, and this process was repeated twice more to ensure removal of cellular debris and insoluble material.

2.3 GENERATION OF RECOMBINANT PLASMIDS.

Table 1: Names and sequences of primers used to generate recombinant plasmids

Primer	Sequence
PfFKBP35fw	5′-GACGAATTCATGACTACCGAACAAG-3′
PfFKBP35rev	5′- TACCTGCAGTTAATTTGCACTATTTTTTTTTTC-3′
PfFKBDrev	5′- GTCCTGCAGTCATCTAAAGCTTAATAATTC-3′
PfΔNFKBDfw	5′-GATGGATCCGGAGTTATCAAAACTATATTAAAAAAAG-3′
PfΔNFKBDrev	5′-GTCTCTAGATTAGTGATGGTGATGGTGATGAC-3′
PlugOligo-1	5′-AAGCAGTGGTATCAACGCAGAGTACGGGGG-PHOS*-3′
PlugOligo-3M	5′-AAGCAGTGGTATCAACGCAGAGTGGCCATTACGGCCGGGGG-PHOS*-3′

PHOS* indicates that the primer is phosphorylated in this position.

2.3.1 *Amplification of full length PfFKBP35 and its FKBD by PCR*

Primers (PfFKBP35fw and PfFKBP35rev [Table 1]) were used to amplify the coding sequence for the full length PfFKBP35 from the pMal-PfFKBP35-His_6 plasmid (previously produced by Paul Monaghan, [113]) with a *Eco*RI site and a *Pst*I site at the 5′ and 3′ ends, respectively, to facilitate subsequent cloning into the pLexA-N expression vector supplied by DualSystems. Primers (PfFKBP35fw and PfFKBDrev [Table 1]) were used to amplify the coding sequence for the FK506-binding domain (FKBD) of PfFKBP35 from pMal-PfFKBP35-His_6 with a *Eco*RI site and a *Pst*I site at the 5′ and 3′ ends, respectively, to facilitate subsequent cloning into the pLexA-N expression vector. PCR was performed using ~100 ng of pMal-PfFKBP35-His_6 template, 0.3 µM primers and 1X KAPA HiFi HotStart ReadyMix (KAPA Biosys-

tems) in a Techne TC-3000 thermocycler (95 °C for 5 min followed by 35 cycles of 98 °C for 20 s, 65 °C for 15 s, 72 °C for 30 s; followed by 72 °C for 5 min.).

2.3.2 *Generation of pLexA-N-FKBD and pLexA-N-PfFKBP35*

pLexA-N for use in the DualHybrid yeast-2-hybrid screen was transformed into *E. coli* XL1-Blue cells using the method described in section 2.3.6 using tetracycline (Tet) as the selective antibiotic. The plasmid was obtained by purification using a PureYield® Plasmid miniprep system (Medical Supply Company, Dublin) and screened for positive transformants using the restriction endonuclease *Eco*RI by the method detailed in section 2.3.7. Purified pLexA-N and the PCR-amplified PfFKBP35 and FKBD coding sequences purified from agarose gel slices (section 2.3.9) were digested with *Eco*RI and *Pst*I (Roche). Briefly, 3-µl reactions were set up in microcentrifuge tubes containing 0.02–1 µg DNA, 10 units of *Pst*I and *Eco*RI, 3 µl of 10X buffer 'H' (Roche), 0.3 µl of 100X (10 mg/ml) bovine serum albumin (BSA) and 20.7 µl of deionised water (dH_2O). Tubes were incubated at 37 °C for 3 h in a water bath. Ligation of pLexA-N-PfFKBP35 and pLexA-N-FKBD was performed using a total of ~100 ng DNA in 1:1 and 1:3 ratios of vector:insert with 1 unit of T4 DNA ligase (Roche) and the reaction incubated overnight at 4 °C. The ligation mixture was transformed by the heat-shock method (section 2.3.6) into competent cells (section 2.3.5) and plated onto L-agar supplemented with 100 µg/ml of Tet. Resulting colonies were screened for presence of the desired constructs as described in section 2.3.7 using *Eco*RI and *Pst*I endonucleases.

2.3.3 *Amplification of ΔNFKBD-His$_6$ by PCR*

Primers (PfΔNFKBDfw and PfΔNFKBDrev [Table 1]) were used to amplify the coding sequence for the FKBD of PfFKBP35, but without the 48 nucleotides at the N-terminus (coding for 16 amino acids) from the pMal-PfFKBP35-His$_6$ plasmid with a *Bam*HI site and a *Xba*I site at the 5′ and 3′ ends, respectively, to facilitate subsequent cloning into the pMal-c2x expression vector (New England Biolabs). PCR was performed using ~40 ng of pMal-PfFKBP35-His$_6$ template, 0.3 µM primers, 1X KAPA HiFi HotStart® ReadyMix (KAPA Biosystems) in a Techne TC-3000 thermocycler (95 °C for 2 min followed by 30 cycles of 98 °C for 20 s, 65 °C for 15 s, 72 °C for 15 c; followed by 72 °C for 2 min). The success of the PCR was assessed using electrophoresis through an agarose gel as described in section 2.3.8.

2.3.4 *Generation of pMal-ΔNFKBD-His$_6$*

pMal-c2x (NEB) was transformed into *E. coli* XL1-Blue cells using the method described in section 2.3.6 using ampicillin as the selective antibiotic. The plasmid was obtained by purification using a PureYield® plasmid miniprep system and screened for positive transformants using the restriction endonuclease *Bam*HI by the method detailed in section 2.3.7. Purified pMal-c2x and the PCR-amplified ΔNFKBD coding sequence (section 2.3.3) were digested with *Xba*I + *Bam*HI and *Xba*I + *Bam*HI + *Dpn*I (Roche) respectively. Briefly, 50-µl reactions were set up in microcentrifuge tubes containing ~3 µg DNA, 10 units of each restriction endonuclease, 5 µl of 10X 'buffer 4' (NEB), 0.3 µl of 100X bovine serum albumin (BSA) and made up to 50 µl with dH_2O. Tubes

were incubated at 37 °C overnight in a water bath. Both digestion mixes were subsequently purified using the method described in section 2.3.9. Ligation of pMal-ΔNFKBD-His_6 was performed using a total of ~100 ng DNA in 1:1 and 1:3 ratios of vector:insert with 1 unit of T4 DNA ligase (Roche) and incubated overnight at 4 °C. The ligation mixture was transformed by the heat-shock method (section 2.3.6) into competent *E. coli* TB1 cells (section 2.3.5) and plated onto L-agar supplemented with 100 µg/ml of Amp. Resulting colonies were screened for presence of the desired constructs as described in section 2.3.7.

2.3.5 *Preparation of competent E. coli cells*

Preparation of competent cells was performed essentially by the method of Chung [37]. A single colony of the desired strain of *E. coli* was used to inoculate 50 ml of L-broth (10% (w/v) tryptone, 5% (w/v) yeast extract, 5% (w/v) NaCl) and the culture grown overnight at 37 °C with agitation at 200 rpm. Four ml of this culture were used to inoculate 400 ml of fresh L-broth in a 2-l flask and incubated at 37 °C until the optical density at 595 nm (OD595) reached 0.375. The culture was split equally between four sterile polypropylene centrifuge tubes and left on ice for 5–10 min. Cells were centrifuged at 1,600 x *g* for 7 min in a GSA rotor using a Sorvall RC-50 Plus centrifuge at 4 °C and the centrifuge was decelerated without application of the brake. The supernatant was discarded and the cell pellets were resuspended in 20 ml of ice-cold $CaCl_2$ solution (60 mM CaCl2, 15% [v/v] glycerol, 10 mM piperazine-N,N´-bis(2-ethanesuphonic acid) (PIPES), pH 7.0). Cells were centrifuged at 1,100 x *g* for 5 min at 4 °C, the su-

pernatant was discarded and the cell pellets were resuspended in 20 ml of ice-cold $CaCl_2$ solution and incubated on ice for 30 min. Cells were centrifuged at 1,100 x g for 5 min at 4 °C, the supernatant was discarded and the cell pellets were resuspended in 3.5 ml of ice-cold $CaCl_2$ solution and divided into pre-chilled sterile microfuge tubes (~800 µl/tube), snap frozen in liquid N_2 and stored in a -80 °C freezer.

2.3.6 *Transformation of competent E. coli cells*

Competent *E. coli* cells of the desired strain were transformed using the heat-shock method as described by Maniatis *et al.* [106]. Two hundred-µl amounts of competent cells were thawed on ice for 30 min. One hundred ng of plasmid or ~100 ng of ligation mixture were mixed with the cells and incubated on ice for 30 min. Cells were heat shocked for 1 min 30 s at 43 °C and placed back on ice for 2 min. One ml of pre-warmed L-broth was added to the mixture and the tubes were incubated with shaking (~200 rpm) at 37 °C for 1 h. One hundred-µl volumes of each sample were plated in triplicate on L-agar supplemented with antibiotic selective for the plasmid being transformed and incubated at 37 °C overnight. Cells transformed with the parental vector served as positive controls, while cells transformed with the DNA sample digested with the relevant enzymes but left unligated served as negative controls.

2.3.7 *Screening of transformants*

Putative transformants obtained after overnight growth on L-agar (supplemented with appropriate antibiotic) were screened by a num-

ber of methods. All methods involved replica-plating colonies of putative transformants onto fresh L-agar (supplemented with appropriate antibiotic) using sterile pipette tips and using the remainder of the colony for the screening procedure. Once clones were identified, DNA sequence analysis (performed by Source Biosciences, Central Pathology Laboratory, St. James Hospital, Dublin) was used to confirm that the constructs included the correct sequence.

2.3.7.1 *Rapid colony screening*

Colonies were mixed with 30 µl of pre-warmed lysis buffer (10% [w/v] sucrose, 100 mM NaOH, 60 mM KCl, 5 mM EDTA, 0.25% [v/v] SDS, 0.05 [w/v] bromophenol blue) in microcentrifuge tubes and incubated in a water bath at 37 °C for 5 min. Samples were placed on ice for 5 min and centrifuged for 5 min at 18,000 x *g* for 5 min in a tabletop centrifuge to pellet cell debris. Fifteen µl of each supernatant were loaded directly onto an agarose gel as described in section 2.3.8. Following ethidium bromide staining, recombinant plasmids were identified by virtue of slower migration through the gel when compared with the parental vector.

2.3.7.2 *Screening by restriction endonuclease digestion*

The presence of the insert of interest was assessed by the ability of restriction endonucleases, for which specific recognition sites had been introduced to release the insert. Plasmids were obtained by purification using a PureYield® Plasmid miniprep system (Promega) and restriction endonuclease digestion was performed using the appropriate enzymes. Briefly, 30-µl reactions were set up in microcentrifuge tubes containing 0.02–1 µg DNA, 10 units of the desired restriction endonuclease, 3 µl of 10X of the appropriate buffer (Roche), 0.3 µl of

100X (10 mg/ml) bovine serum albumin (BSA) and 20.7 µl of dH_2O. The presence of the insert was assessed by migration relative to molecular mass standards following electrophoresis through an agarose gel.

2.3.8 *Visualisation of DNA by agarose gel electrophoresis*

DNA samples (PCR samples, purified plasmids, restriction enzyme-treated plasmids etc.) were analysed by mixing 5 µl of sample with 1 µl of 6X gel loading solution and running through a 1–2% (w/v) agarose gel prepared in Tris acetate EDTA (TAE) buffer (40 mM Tris-HCl, 1 mM EDTA, 20 mM acetic acid). Gels were typically run at 80-120 V until the desired degree of separation was achieved. Gels were stained by immersion in ethidium bromide (0.5 µg/ml) until the desired degree of staining was achieved (~15 min), washed in deionised H_2O (~20 min) and visualised on an AlphaImager 2200 gel imaging system using ultraviolet light (Alpha Innotech Corporation, San Leandro, California, USA).

2.3.9 *Purification of polymerase chain reaction (PCR) products*

PCR products were purified by one of two methods, both of which used the Wizard SV® Gel and PCR Clean-Up System (Promega). If only one product was visible on an ethidium bromide stained agarose gel then the PCR product was purified directly from the solution. If other products were visible as a result of non-specific primer binding, the product of interest was excised from an agarose gel and purified.

2.4 EXPRESSION AND PURIFICATION OF RECOMBINANT PROTEINS

2.4.1 *Harvesting and lysis of E. coli cells*

E. coli strains harbouring the desired plasmid were grown overnight and inoculated into L-broth, supplemented with 100 µg/ml Amp, and grown at 37 ºC with agitation at 200 rpm until an OD_{600} of 0.5–0.7 was reached. Protein expression was induced by the addition of 0.35 mM IPTG and the culture was incubated with agitation for a further 3 hours. Cells were harvested by centrifugation at 6000 x *g* for 15 min at 4 ºC in a Sorvall RC50 Plus centrifuge using a GSA rotor. Pellets were either used immediately or frozen at -20 ºC. Pellets were resuspended in MCAC-0 buffer (Section 2.4.2) supplemented with Complete Mini protease inhibitor tablets, EDTA-free (Roche). Cells were lysed by passage three times through a French Press at 1000 psi and the resulting lysate was clarified by centrifugation at 35,000 x *g* in a Sorvall RC50 Plus centrifuge using an SS-34 rotor for 1 h at 4 ºC.

2.4.2 *Nickel-chelate affinity chromatography*

A nickel-nitrilotriacetic acid-agarose column (HiTrap chelating column, Amersham Pharmacia, Buckinghamshire, UK) was equilibrated with 10 column volumes of metal-chelate affinity chromatography (MCAC) buffer (25 mM sodium phosphate, 500 mM NaCl, pH 7.4) prepared without imidazole (MCAC-0). Clarified lysate (prepared as in section 2.4.1) was applied to the column at a flow rate of 1 ml/min at 4 ºC using a peristaltic pump in a cold room. The column was washed with 10 column volumes of MCAC-75 (MCAC-0 supple-

mented with 75 mM imidazole), followed by elution with 10 volumes of MCAC-200 buffer (containing 200 mM imidazole). The eluate was either concentrated by ultrafiltration through an Amicon Ultra protein concentrator (Millipore) or dialysed against 5 l of IX-5% (prepared as described in section 2.4.3) in preparation for anion-exchange chromatography.

2.4.3 *Ion-exchange chromatography*

An anion-exchange column (Mono Q, Amersham Pharmacia) was equilibrated with 10 column volumes of IX-5% (19:1 mixture of IX-start buffer [20 mM Tris-HCl, pH 8.0, 25 mM NaCl] and IX-end buffer [20 mM Tris-HCl, pH 8.0, 1 M NaCl]). The dialysed MCAC-200 eluate was applied to the column at a flow rate of 1 ml/min and the resin was washed with 10 column volumes of IX-5% followed by elution with 5 column volumes of IX-20% (4:1 mixture of start buffer:end buffer). The eluted fraction was concentrated by ultrafiltration through an Amicon Ultra protein concentrator (Millipore) to approximately 500 µl.

2.5 PROTEIN ANALYSIS

Protein concentration was assayed using a Nanodrop 1000 spectrophotometer (Thermo Scientific). Protein samples were separated by SDS-polyacrylamide gel electrophoresis (SDS-PAGE) essentially according to the method of Laemmli [93]. Proteins separated by this technique were either visualised by staining with with Coomassie blue stain, sil-

ver stain or SyproRuby® stain (Sigma) (section 2.5.1), or transferred to a membrane for analysis by Western immunoblot (section 2.5.2).

2.5.1 *Staining of SDS-polyacrylamide gels*

2.5.1.1 *Coomassie Brilliant Blue staining.*

Gels were soaked in approx. 50 ml of Coomassie Blue reagent (0.15% [w/v] Coomassie Brilliant Blue R-250, 45% [v/v] methanol, 10% [v/v] acetic acid, filtered to remove particulate matter) with gentle shaking until the desired degree of staining was achieved. Destaining was performed by soaking the gel in several changes of a solution of 20% (v/v) methanol, 7.5% (v/v) acetic acid with shaking and imaging was performed using an AlphaImager 2200 gel imaging system.

2.5.1.2 *Silver staining.*

All steps were performed by placing the gels on a rocking table. Gels were stained by silver staining by first soaking in fixative solution (50% [v/v] methanol, 5% [v/v] acetic acid) in a clean glass container for 20 min and washed with 50% (v/v) methanol for 10 min. Gels were then washed in distilled water overnight. Gels were then soaked in 0.02% (w/v) sodium thiosulphate for 1 min, washed twice in distilled water for 1 min and removed to a fresh glass container. The gel was then stained with cold 0.1% (w/v) silver nitrate for 20 min and washed well with distilled water before development by soaking in pre-chilled developing solution (0.04% [v/v] formaldehyde, 2% [w/v] sodium carbonate) until the desired degree of staining was achieved (~10 min). Development was terminated by soaking the gel in 5% (v/v) acetic acid and gels were visualised on either an AlphaIm-

ager 2200 gel imaging system or a GE Imagequant LAS 4000 digital imaging system (GE Healthcare Life Sciences).

2.5.1.3 *SyproRuby® staining.*

Gels were stained by first soaking in fixative solution (50% [v/v] methanol, 7.5% [v/v] acetic acid) in a clean polypropylene dish, followed by staining overnight in SyproRuby® (provided as a liquid). Destaining was performed by soaking the gels in 10% [v/v] methanol, 7% [v/v] acetic acid for 30 min, with two changes. Imaging was performed by exposing the gels to ultraviolet light on either an AlphaImager 2200 gel imaging system or a GE Imagequant LAS 4000 digital imaging system.

2.5.2 *Western immunoblotting*

After electrophoresis, unstained polyacrylamide gels were sandwiched with polyvinylidiene difluoride (PVDF, Roche) and immersed in a blotting tank with transfer buffer (0.025 M Tris-HCl, 1.9 M glycine, 24% [v/v] methanol). Proteins were transferred at 120 V for 1 h. After transfer, the membrane was blocked by soaking in 5% (w/v) non-fat milk prepared in Towbin's solution (0.1 M Tris-HCl, pH 7.4, 0.9% [w/v] NaCl) for 1 h. The blocked membrane was soaked with a solution of primary antibody diluted to the desired concentration (typically between 1:500 and 1:10,000 depending on the antibody used) with 5% (w/v) non-fat milk in Towbin's solution for 1–4 h, after which time the membrane was washed in Towbin's/Tween solution (Towbin's solution supplemented with 0.05% [v/v] Tween-20) for 30 min with gentle rocking and two changes of Towbin's/Tween solu-

tion. These steps were repeated with a solution of the secondary antibody. Bands were detected using a chemiluminescence system (Pierce) according to the manufacturer's instructions using a GE Imagequant LAS 4000 digital imaging system.

2.6 GENERATION OF IMMUNOPHILIN ANTIBODIES

2.6.1 *Purification of PfFKBD and PfCYP19A*

E. coli strains previously generated by the Bell lab harbouring plasmids pMAL-PfFKBD-His_6 [113] and pET22b-PfCYP19A [107] were grown and the proteins encoded by these plasmids were overexpressed and purified as described in section 2.4. These proteins were used as antigens for generation of custom polyclonal antibodies as described in section 2.6.2 by CovalAb (St John's Innovation Centre, Cowley Road, Cambridge, UK).

2.6.2 *Immunisation*

Immunisation was performed on two female New Zealand white rabbits for each protein by the following method: Day 0, rabbits were bled (4–5 ml) to harvest pre-immune serum which was stored at -20 °C, 1 ml injection consisting of 0.5 ml antigen (between 0.5 and 1 mg/ml) and 0.5 ml incomplete Freund's adjuvant was administered. Injections were repeated on days 14, 28 and 42. Test bleeds were performed on day 39 (4–5 ml) and day 53 (10–15 ml) with storage of the sera at 4 °C, with final bleed performed on day 67. Antibodies were purified on a protein A column by standard methods [77].

2.7 DETECTION OF PROTEIN–PROTEIN INTERACTIONS

2.7.1 *Co-immunoprecipitation of PfCYP19B*

A preparation of 9.62 x 10^8 parasites harvested as described in section 2.2.3 were lysed as described in section 2.2.6. Parasites prepared in this manner formed the "bait and prey" fraction for use in co-immunoprecipitation (co-IP).

Co-IP was performed using the Pierce co-IP Kit (Product #26149) according to the manufacturer's instructions with the following modifications. To prepare the column, 100 µl of 50% (v/v) resin slurry were used with 100 µl of anti-PfCyp19B serum (previously generated in the lab [65]) . During co-IP all wash steps were increased to 400 µl, the 500 µl of "bait and prey" prepared as above was diluted in 400 µl IP lysis/wash buffer and mixed with the prepared column resin suspended in 200 µl IP lysis/wash buffer. This mixture was incubated with gentle shaking at 4 °C in a 1.5-ml microcentrifuge tube. The procedure was then completed as per the manufacturer's instructions. Immunoprecipitates were analysed on an SDS–15% polyacrylamide gel as described in section 2.5 and stained using silver stain as described in section 2.5.1. One sample of pre-concentrated immunoprecipitate was assessed by Western immunoblot as described in section 2.5.2 to confirm binding of PfCyp19B by the prepared column. The co-immunoprecipitation procedure was repeated a further 14 times using approximately the same number of parasites each time (approximately 1.443 x 10^{10} parasites in total) and the eluted "co-immunoprecipitates" were pooled and concentrated by approximately tenfold in a Pierce 9-kDa molecular weight cut-off (MWCO) protein concentrator in a Sorvall RT6000D benchtop centrifuge at

1,400 x *g* for 30 min at 4 °C for 35–40 min. The concentrated co-immunoprecipitates were analysed on a Pierce SDS 4–20% polyacrylamide gel stained with Sypro Ruby® as described in section 2.5.1. Bands corresponding to immunoprecipitating partners were cut out with a clean scalpel and analysed by mass spectrometry at the UCD Conway Institute mass spectrometry core facility (University Collge Dublin, Belfield, Dublin 4) on a Thermo Fisher Orbitrap LC/MS mass spectrometer. Two control columns were also prepared, one using 100 µl pre-immune serum from the same rabbit in which the anti-PfCyp19B serum was produced, the second using Pierce control agarose resin (crosslinked 4% (v/v) beaded agarose) and the co-IP procedure was repeated as above and analysed by SDS-15% PAGE in the same manner.

2.7.2 *Co-immunoprecipitation of PfCYP19A and PfFKBP35*

Due to optimisation of both the co-IP process and the protein concentration there are some minor differences in how the latter set of co-IP's were performed and analysed. The "bait and prey" fraction was prepared essentially as described above with an additional pre-clearing step on a control resin to remove non-specifically binding contaminating proteins. Columns were prepared using 200 µl of 50% (v/v) resin slurry and approximately 500 µg of the polyclonal antibody generated as described in section 2.6.2. Concentration of the eluted co-immunoprecipitates was performed using 0.5-ml Amicon Ultra 10-kDa centrifugal filter units (Millipore), in a benchtop centrifuge at 14,000 x *g* for 25 min at 4 °C. This was followed by a buffer exchange (by re-diluting the concentrated eluate in IX-5% buffer and

centrifuging at 14,000 x *g* for 25 min at 4 °C in the same centrifugal filter unit, repeated 4 times) to reduce background staining in subsequent SDS-PAGE analysis. The concentrated co-immunoprecipitates were analysed by SDS-10% PAGE (with component solutions filtered through a 0.2-µm filter to ensure removal of contaminating particles such as keratin) and bands corresponding to immunoprecipitating partners were cut out with a clean scalpel and analysed by mass spectrometry at the UCD Conway mass spectrometry facility on a Thermo Fisher Q-exactive LC/MS mass spectrometer. Control co-IP's were performed as above.

2.7.3 *Yeast-2-hybrid analysis with PfFKBP35*

2.7.3.1 *cDNA expression library construction.*

Library construction was performed commercially by Dualsystems Biotech AG, Zurich, Switzerland from harvested parasites provided as prepared in section 2.2.3. Briefly, first strand cDNA synthesis started from the 3'-end adapter comprising an oligo (dT) sequence to anneal to the poly(A)$^+$ stretch present at the 3' end of messenger RNA (mRNA). When the reverse transcriptase (RT) reached the 5' end of the mRNA, it added several non-template nucleotides, primarily deoxycytidines, to the 3' end of the newly synthesized first-strand cDNA (Schmidt & Mueller, 1999). This oligo (dC) stretch paired with a complementary oligo (dG) sequence present in the PlugOligo (Table 1). The RT then switched templates and continued first strand cDNA synthesis to the end of the oligonucleotide, thus incorporating the PlugOligo sequence into the 5' end of cDNA. The last 3'-dG residue of the PlugOligo is a terminator nucleotide comprising a 3'- phosphate

group. This blocking group prevented unwanted annealing and extension of the PlugOligo. The second adapter pair (3'-end adapter CDS-3M and 5'-end adapter PlugOligo-3M) comprised asymmetric sites with *Sfi*I restriction enzyme recognition sites, A & B. The incorporation of *Sfi*A and *Sfi*B sites into the 5' and 3' ends of the cDNA the sites allowed directional cloning of the cDNA library. Following first strand synthesis, the cDNA was amplified by PCR. The use of Easy-Clone polymerase and specially designed primers allowed synthesis of full-length enriched cDNA that is flanked by the PlugOligo and 3'-end adapter sequences. After digestion with *Sfi*I, size selection and purification, the resulting cDNA was ligated into a vector of choice using the *Sfi*I sites located in the 5' and 3' adapter sequences of the cDNA. *Sfi*I restriction sites are very rare in eukaryotic cDNAs and therefore allowed preferential cloning of full-length cDNAs. Following ligation, the cDNA library was amplified by transformation into *E. coli* for later use.

2.7.3.2 *Bait functional assay.*

This assay determines whether the bait enters the nucleus and binds to the LexA operators situated upstream of the reporter genes ("repression or blocking assay", [27]). A bait which enters the nucleus and binds to the LexA operator sites decreases transcription from the downstream *LACZ* gene (repression) and hence decreases β-galactosidase expression on galactose medium. Most LexA fusions that enter the nucleus and bind the operators but do not activate transcription repress β-galactosidase activity from 2 to 20 fold. >2 fold repression indicates >50% operator occupancy by the bait and signifies that the bait can be screened in the DUALhybrid assay.

2.7.3.3 *Yeast-2-hybrid screening.*

The yeast two-hybrid screen using the PfFKBD-His_6 bait was carried out by Dualsystems Biotech. The bait construct for yeast two-hybrid screening was constructed as described in section 2.3.2. The bait construct was transformed into the strain *S. cerevisiae* NMY32 (MATa his3Δ200 trp1-901 leu2-3,112 (*lexAop*)8-ADE2 LYS2::(*lexAop*)4-HIS3 URA3::(*lexAop*)8-*lacZ* GAL4) using standard procedures [67]. Correct expression of the bait was verified by Western blotting of cell extracts using a mouse monoclonal antibody directed against the LexA domain (Dualsystems Biotech, Switzerland). The absence of self-activation was verified by co-transformation of the bait together with a control prey and selection on minimal medium lacking the amino acids tryptophan, leucine and histidine (selective medium). For the yeast two-hybrid screen, the bait was co-transformed together with a *P. falciparum* cDNA library (generated by Dualsystems) into *S. cerevisiae* NMY32 (section 2.7.3.1). Transformants were screened, yielding transformants that grew on selective medium. Positive transformants were tested for β-galactosidase activity using a PXG β-galactosidase assay (Dualsystems Biotech). Initial positives which showed β-galactosidase activity were considered to be true positives. Library plasmids were isolated from positive clones. The identity of positive interactors was determined by sequencing.

2.7.4 *In vivo crosslinking*

2.7.4.1 *Photoactivatable amino acid crosslinking.*

Parasites were grown as in section 2.2.1 using complete leucine-free medium (RPMI-1640 without arginine, lysine and leucine made up

with 25 mM HEPES, 0.18% [w/v] sodium bicarbonate, 50 µg/ml hypoxanthine, 0.4% [w/v] Albumax®, 0.1 g/l L-arginine, 0.1 g/l L-lysine) completed with either 4 mM L-leucine or 4 mM photo-leucine (Pierce, Dublin, Ireland), grown for approximately 6 generations to high parasitaemia (~18–20%) and harvested as per section 2.2.3.

2.7.4.2 *Chemical crosslinking.*

Parasites harvested as per section 2.2.3 were incubated with 1 mM disuccinimidyl suberate (DSS) in PBS for 5 min at room temperature with samples taken every 1 min and quenched using 50 mM Tris-HCl, pH 7.5 for 20 min. Parasites were lysed by incubation with 0.05% (v/v) Triton X-100 solution in PBS on ice for 30 minutes. This was then centrifuged in a benchtop centrifuge at 13,200 x g at 4 °C for 10 min. The supernatant was removed and this was repeated twice more. The resulting parasite lysate was analysed by SDS 4–20% PAGE as described in section 2.5. Parasites incubated in PBS without DSS by the same method were used as a negative control.

2.7.5 *Histone purification*

Histones were harvested by the method of Longhurst and Holder, (1997) [102]. Briefly, cultures grown as per section 2.2 were centrifuged at 350 x *g* for 10 min at 4°C to pellet infected erythrocytes. The pellet was resuspended in PBS and centrifuged at 350 x *g* for a further 10 min to wash the erythrocytes. Two volumes of cold 1% (v/v) acetic acid were added and the pellet was resuspended and mixed by inverting, then left on ice for two min to allow for cell lysis. The erythrocyte lysate was washed in 5 volumes of PBS by centrifugation at

6,000 x *g* for 10 min at 4°C and the pellet was kept. This wash was repeated at least 4 times or until the supernatant was free of any visible haemoglobin. The pellet was further purified by the addition of 5 volumes of Nonidet P40 buffer (25 mM Tris-HCl, pH 7.8, 1 mM EDTA, 0.2% (v/v) Nonidet P40) and centrifugation at 12,000 x *g* for 30 s at 4 °C to remove contaminating haemoglobin and membranes. To extract the histones, the pellet was first washed three times in 0.8 M NaCl by centrifugation at 12,000 x *g* for 30 s at 4°C, then resuspended in 10 volumes of 0.25 M HCl and kept on ice for 1 h with frequent resuspension. The sample was then centrifuged at 12,000 x *g* for 2 min at 4°C to pellet any acid-insoluble components and the histone-containing supernatent was kept.

2.7.6 *Histone chaperone assay*

Circular plasmid DNA, pBluescript (0.1 pmol), was relaxed with 5 units of topoisomerase I in 20 µl relaxation buffer (40 mM Tris-HCl, pH 7.5, 100 mM KCl, 10 mM $MgCl_2$, 10 mM DTT, 0.5 mM EDTA, 30 µg/ml BSA) overnight at 37 °C. Relaxed pBluescript was combined with purified *P. falciparum* histones (1 pmol, purified as in section 2.7.5) and recombinant proteins (7 pmol, section 2.4) in assembly buffer (20 mM Tris-HCl, pH 8.0, 0.15 mM NaCl, 0.5 mM DTT) with a final volume of 50 µl. The reaction mixture was incubated at 30 °C for 1 h. The reaction was stopped by the addition of an equal volume of stop buffer 1 (60 mM Tris-HCl, pH 8.0, 30 mM EDTA, 0.5% (w/v) SDS, 25% (v/v) glycerol).

2.7.7 *Thermal melt and stability shift assay*

The protein being assessed (1 µM) was prepared in a final volume of 50 µl into 0.2 ml thin-walled PCR tubes (VWR, Dublin, Ireland) with one of eleven buffers. The buffers were as follows: Buffer 1 : 100 mM HEPES, 150 mM NaCl, pH 7.5. Buffer 2 : 100 mM potassium phosphate, pH 7.0. Buffer 3 : 100 mM sodium phosphate, pH 7.5. Buffer 4 : 100 mM sodium citrate, pH 5.5. Buffer 5 : PBS. Buffers 6-11 consisted of 100 mM NaCl and 50 mM HEPES at pH values 6.2, 6.6, 7.0, 7.4, 7.8, and 8.2 respectively.

The fluorescent dye used in this assay was SYPRO® Orange (Invitrogen™ Molecular Probes™) at a final concentration of 3.2 X. Triplicates of each sample were heated from 30 °C to 80 °C at a rate of 2 °C per minute. Fluorescence readings were taken for each sample at 0.2 °C increments at 470 nm excitation wavelength and 585 nm emission wavelength in a Rotor Gene-3000 thermal cycler (Corbett Research, Sydney, Australia). The melting temperature (T_m) was determined by obtaining the first derivative to the curve and identifying the curve's maximal point.

2.7.8 *Peptidyl-prolyl cis-trans isomerase assay*

The PPIase assay was performed by the method of Kofron *et al.* ([87]) using the tetrapeptide substrate succinyl-Ala-Leu-Pro-Phe-*p*-nitroanilide (Bachem, Bubendorf, Switzerland). All reagents were pre-equilibrated to 0 °C prior to use. In a 1-ml glass cuvette, recombinant protein (1 µM final concentration) was mixed with 100 µl α-chymotrypsin (60 mg/ml in 1 mM HCl), and the volume brought up to 980 µl with as-

say buffer (50 mM HEPES, 100 mM NaCl, pH 8.0 at 0 °C). The reaction was initiated by addition of 20 µl of substrate (5 mM tetrapeptide in 470 mM anhydrous LiCl prepared in trifluoroethanol). Changes in absorbance due to released *p*-nitroaniline were monitored at 390 nm at 0 °C over a 1 min period in a Shimadzu UV-1601PC UV-vis spectrophotometer with a thermostatted cuvette holder. The first order rate constant was calculated from the slope of the plot of $\ln(A_{max}\text{-}A_t)$ against t, where A_{max} is the maximum absorbance and A_t is absorbance at time t.

2.7.9 *Far-Western blotting*

Far Western blotting was performed essentially by the method of Wu et al. (2007) [177]. Briefly, after SDS-PAGE as described in section 2.5, and transfer to PVDF membrane as described in section 2.5.2, the membrane was incubated with 1 µg/µl of the protein probe in 5% (v/v) skimmed milk with gentle shaking overnight at 4 °C. Western blotting was then continued from primary antibody as described in section 2.5.2.

2.8 IMMUNOFLUORESCENCE MICROSCOPY

Eight-well multitest immunofluorescence microscopy slides (Thermo Scientific) were cleaned with 70% (w/v) methanol and pre-treated with 0.1% (w/v) poly-L-lysine overnight at room temperature in a humid chamber. They were then washed five times for 10 minutes with wash medium (RPMI 1640 supplemented with 25 mM HEPES, 0.18% w/v sodium bicarbonate, 50 µg/ml hypoxanthine, 0.16% w/v

glucose). Infected erythrocytes from cultures of *P. falciparum* at about 10% parasitaemia as described in section 2.2 or treated for 14–16 h overnight with relevant inhibitors were washed two times in wash medium at room temperature. Twenty µl of a solution of 4% (w/v) paraformaldehyde and 0.1% (v/v) Triton X-100 were pipetted into each window of the slide and 30 µl of cells resuspended in wash medium were added. This was incubated at room temperature for 3 h. Wells were washed five times for 10 min with PBS and incubated with 30 µl 5% (v/v) goat serum for 30 min at room temperature. Immunostaining was started by incubating the cells with 30 µl of the relevant antibody (0.2 mg/ml PfRAP$1_{1\text{-}14}$[kind gift from Prof. G Pluschke, Swiss Tropical and Public Health Institute, Basle], or a 1:40 dilution of PfCYP19B serum) for 1 h at room temperature. After five washes with 5% (v/v) goat serum, 30 µl of a 1:500 dilution of the relevant secondary antibody (donkey anti-mouse conjugated Alexafluor®-488, donkey anti-rabbit conjugated Alexafluor®-546 [Invitrogen], or goat anti-mouse conjugated fluorescein isothiocyanate [FITC, DakoCytomation]) were pipetted onto each window and incubated for 1 h at room temperature. Afterwards slides were washed five times for 10 min each with PBS, incubated for 2 min with 0.2 µg/ml 4',6-diamidino-2-phenylindole (DAPI), and washed again three times for 10 min with PBS. Slides were mounted with 2 µl per window Prolong Gold antifade reagent (Bio-Sciences, Dun Laoghaire) and covered with a coverslip. The coverslip was sealed to the slide using a clear nail varnish and left to set overnight. Antibody binding and DNA staining were assessed by confocal fluorescence microscopy (on an Olympus FV1200 Biological Laser Scanning Confocal Microscope).

2.9 3D STRUCTURE MODELLING

3D modelling of the PfFKBP35 protein was undertaken using the MODELLER software from Salilab (open source; UCSF, San Francisco, USA, www.salilab.org) and visualised using UCSF's Chimera software (open source; plato.cgl.ucsf.edu/chimera). All modelling was done on a Dell Precision M4400 laptop computer using the Ubuntu distribution 10 operating system. The Python scripts for the generation of all models are included in the appendices. Homology models were generated of the complete PfFKBP35 protein using the crystal structure of hFKBP12 (PDB code 2PPM) and the PfFKBP35 TPR domain (PDB 2FBN) as a template. A homology model of the FK506-binding domain (FKBD) was subsequently generated using hFKBP12 as the template for the Python script. The script was set to generate 50 iterative models and the model with the best lowest discrete optimised protein energy (DOPE) score was selected for use in further modelling. The FKBD homology model was then docked with calcineurin from the X-ray diffraction structure of hFKBP12–FK506–calcineurin 1TCO PDB structure file using the DOCK protocol in Chimera. Subsequent to generation of the homology models, a nuclear magnetic resonance (NMR) solution structure of the FKBD became available [86]. All of the above modelling was repeated to replace the homology model of the FK506 binding domain with this NMR solution structure. These models agreed almost perfectly.

3

INVESTIGATION OF THE IMMUNOPHILIN INTERACTOME

3.1 INTRODUCTION

P. falciparum possesses thirteen immunophilin or related genes, encoding eleven cyclophilin or cyclophilin-like proteins an FKBP and an FKBP like protein (see section 1.2) [107, 65, 113]. The immunosuppressive drugs CsA and FK506 show the ability to bind to the cyclophilins PfCYP19A and PfCYP19B, and the FKBP, PfFKBP35, respectively, and demonstrate antimalarial activity *in vitro* [20] and (in the case of CsA) *in vivo* [161]. Non-immunosuppressive derivatives of these compounds also possess antimalarial activity [114, 20], suggesting the immunosuppressive activity of the drugs as mediated by calcineurin in human T-lymphocytes is unrelated to the antimalarial activity and may be mediated through some other immunophilin–drug–protein interaction or direct action of the drug on the immunophilin itself. This chapter describes the work performed to identify the immunophilin–protein interaction network of the erythrocytic stages of *P. falciparum*, elucidation of which may lead to understanding of the antimalarial action of CsA and FK506.

Immunophilin–protein interactions appear to play a role in a wide variety of cellular functions in eukaryotes, including steroid receptor assembly in *Homo sapiens*, cytoskeletal organisation, and successful HIV virion formation. In protozoal parasites immunophilins have,

aside from the classic PPIase action, molecular chaperone activity [107, 113] and roles in host–parasite interactions such as the regulation of pro-inflammatory cytokines in the host by *Toxoplasma gondii* [5]. Since *P. falciparum* immunophilins demonstrate molecular chaperone activity they may play a role in protein folding and transport, export of parasite proteins to the host cell, and perhaps in parasite secretory organelles. Indeed a recent study by Singh *et al.* [147] demonstrated that treating merozoites with CsA and FK506 inhibits microneme secretion, though the concentrations of drugs used were exceptionally high in relation to their IC50. Parasite immunophilins may also have a role in protection from stress such as heat shock, and PfFKBP35 has been shown to interact with heat shock protein 90 *in vitro* [90]. This may be an important interaction *in vivo* since the parasite has to adapt to heat shock when it moves from the insect, (*Anopheles*) host to the human one, as well as to the heat shock encountered in the erythrocytic stages during febrile malaria.

No previous studies have looked specifically at the protein–protein interactions of these immunophilins, though whole interactome protein–protein studies have identified one cyclophilin–protein interaction. La Count *et al.* [92] using yeast 2-hybrid analysis, identified an interaction between PfCYP19A and the product of the gene PF3D7_0604500, a conserved *Plasmodium* protein of unknown function. Other studies have shown an interaction between PfFKBP35 and heat shock protein 90 (Hsp90) *in vitro* as mentioned above. Aside from these the only known immunophilin–protein interaction in the parasite is that between PfFKBP35 and calcineurin [90, 113]. Therefore almost nothing is known about the immunophilin interactome in *P. falciparum*. It should be possible to infer interactions from those seen in other organisms but the immunophilins are sufficiently different in sequence and

structure that these inferred interactions may not hold up under experimental scrutiny. It is also desirable to know if the immunophilins partake in interactions that are specific to *P. falciparum* as specific parasite protein–protein interactions make attractive drug targets and give insight into the biology of the organism.

3.2 METHODOLOGY

Materials and methods used in this chapter are described in detail in chapter 2. All experiments were performed with asynchronous cultures of the 3D7 clone of *P. falciparum*. Co-IPs were performed as described in section 2.7 and yeast-2-hybrid analysis was performed as described in section 2.7.3. Antibody generation was performed by CovalAb (Cambridge, UK). Mass spectrometry was performed at the Conway Institute core mass spectrometry facility (University College Dublin, Dublin, Ireland).

3.3 RESULTS

3.3.1 *Identification of putative interacting partners by co-IP*

3.3.1.1 *Generation of anti-immunophilin antibodies*

In order to investigate the interactome of the selected *P. falciparum* immunophilins it was first necessary to identify a method specifically to pull down these proteins from parasite cellular lysate. Gavigan *et. al* have demonstrated that CsA can specifically pull down PfCYP19A and PfCYP19B [65] but it was not possible to pull down meaningful amounts of PfFKBP35 with FK506 in a similar manner [Bell, A.,

personal communication]. It was decided that in order specifically to pull down large amounts of the immunophilins and their interacting partners, co-immunoprecipitation would be used. In order to do this an antibody specific to each immunophilin would be required. Antibodies for PfCYP19B were already available in the lab [65], but antibodies for PfCYP19A and PfFKBP35 would need to be generated. Both of these proteins were available in the laboratory, so PfFKBD was purified from the *E. coli* strain constructed by Monaghan *et al.* [113] as described in section 2.4 and pfCYP19A was available as a pure protein generated by Marin-Menendez *et al.* [107]. These proteins were used to produce the required antibodies commercially. The antibodies generated showed excellent specificity for each immunising protein (Figure 10). It is generally considered that a titre of >8000 constitutes good reactivity, and the antibodies produced both had titres >64000 and can be considered excellently immunoreactive.

PfFKBP35

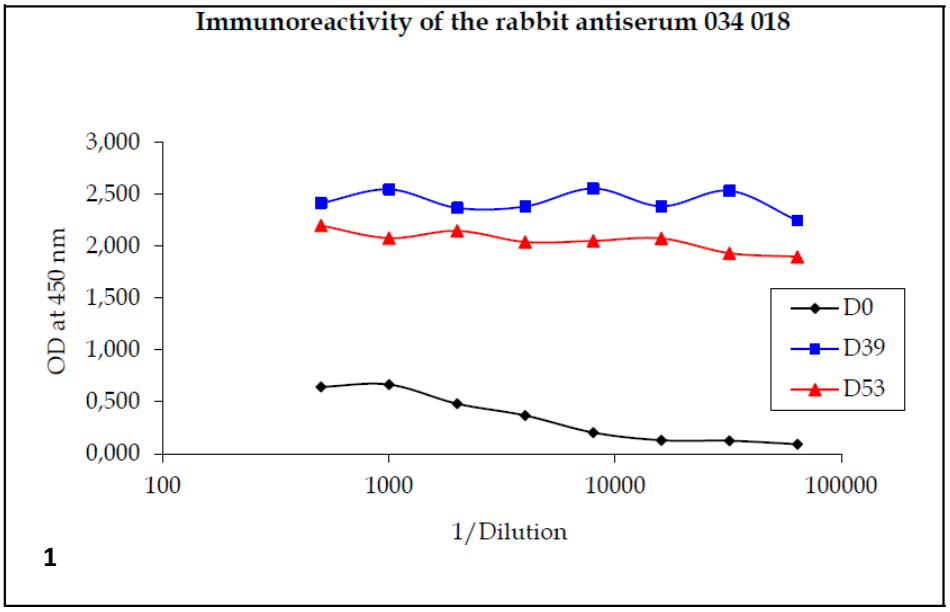

PfCYP19A

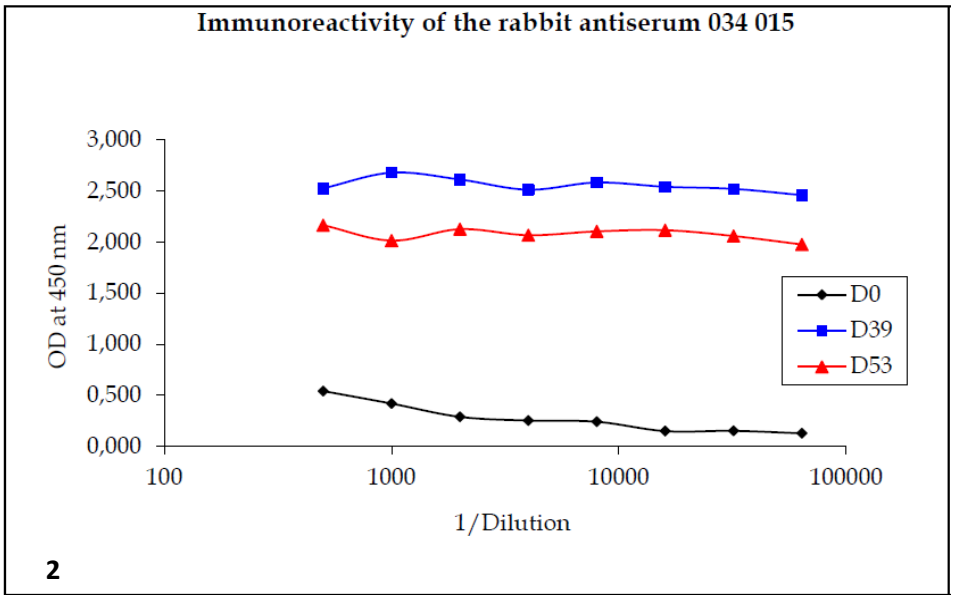

Figure 10: Immunoreactivity of rabbit antisera to immunising proteins. Rabbits were immunised with 1 ml consisting of 0.5 ml antigen (between 0.5 and 1 mg/ml) and 0.5 ml incomplete Freund's adjuvant on days 0, 14, 28 and 42. Serum samples were taken on day 0, 39 and 53. Immunoreactivity was assessed by ELISA against protein adsorbed to 96-well microtiter plates. Eight serum dilutions were assayed, between 1/500 and 1/64000. 1 ELISA of sera from PfFKBP35 immunised rabbits. 2. ELISA of sera from PfCYP19A immunised rabbits. In both cases graphs are representative of ELISAs from both rabbits immunised. Data provided by CovalAb.

3.3.1.2 *Co-immunoprecipitation of PfCYP19A, PfCYP19B and PfFKBP35*

Initial co-IP was performed against PfCYP19B since the antibodies were readily available at the start of the project. The co-immunoprecipitating eluates were analysed by silver stained SDS-PAGE and Western blot to assess both the total eluted protein content and the column's ability specifically to bind PfCYP19B (Figure 11). Early results indicated that there were at least three immunoprecipitating partners which were not present in the corresponding sample eluted from a pre-immune serum column. However, the protein content in the eluted fraction was at the threshold of what is detectable by silver staining (approx. 1 ng/band) and was therefore unsuitable for further analysis by mass spectrometry. Therefore immunoprecipitation was repeated 15 times and the resulting eluates were pooled and concentrated by ultracentrifugation approximately 15 fold, giving a sample volume the same size but which contained ~15 times more protein. The concentrated sample was again analysed by SDS-PAGE and in this second instance was stained using SyproRuby® (Figure 11). Successful staining of a band with SyproRuby® generally indicates that the protein is present in sufficient quantity for reliable identification by mass spectrometry. The concentrated immunoprecipitate revealed a further two interacting partners which were at too low a concentration to be visualised by silver staining previously. Co-IP partners A, B and C were excised from the gel and sent to University College Dublin's Conway Institute mass spectrometry facility for analysis. Due to the nature and cost of SyproRuby® it is not possible to show the actual gel used to excise the bands which were sent for mass-spectrometric analysis, though fig. 11 panel C is representative

of at least triplicate co-IPs and bands excised were reproduced across all gels.

After subsequent generation of antibodies to PfCYP19A and PfFKBP35, co-IP of these proteins was performed. The process of generating co-immunoprecipitating partners had been optimised successfully to require the use of fewer harvested parasites than in the initial study of PfCYP19B, and staining, imaging and mass spectrometry were all improved as a result. Co-IP partners for PfFKBP (Figure 12, Bands 1-6) and PfCYP19A (Figure 13, Bands 1-5) were excised from their respective gels and analysed by mass spectrometry. Again, the figures demonstrating co-IP results from these experiments are representative of multiple co-IPs and bands indicated as excised for mass-spectrometry are reproducible across all replicates.

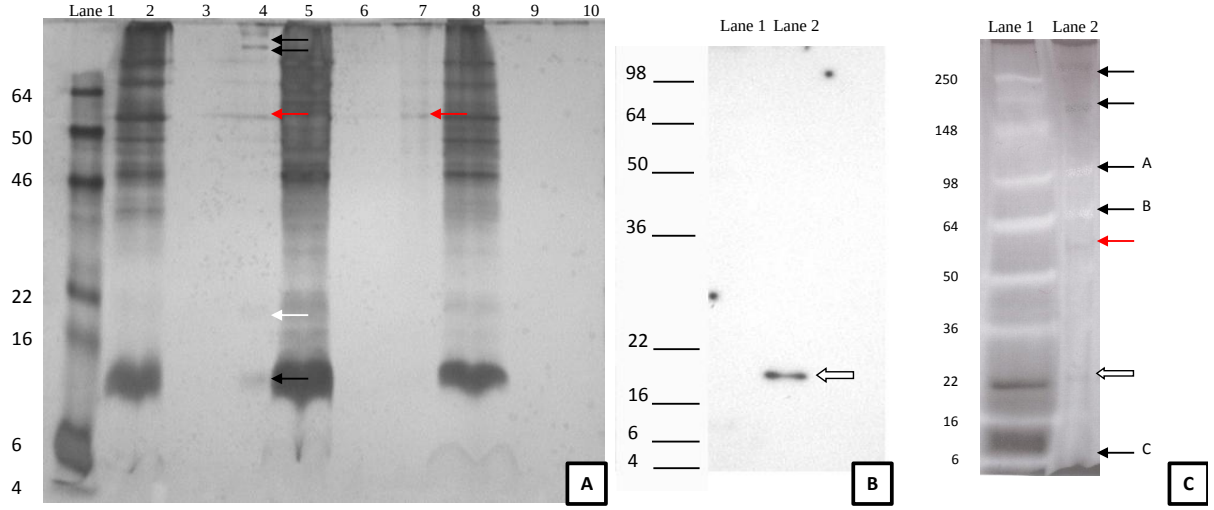

Figure 11: **A.** Silver stained SDS-15% polyacrylamide gel electrophoretogram showing PfCYP19B co-IPs. (Lane 1) molecular weight marker: numbers indicate mass in kDa. All co-IPs were performed using 500 µl saponin-released parasite suspension lysed by 0.5% (v/v) Triton X-100 on ice for 30 minutes. (Lanes 2–4) anti-PfCyp19B column, (Lanes 5–7) pre-immune serum column, (lanes 8–10) control resin (non-reactive) column. (Lanes 2, 5 and 8) 20 µl of initial flow through post-binding (total fraction volume 1 ml). (Lanes 3, 6 and 9) 20 µl post-binding wash fraction (total fraction volume 400 µl). (Lanes 4, 7 and 10) 20 µl final co-IP eluate fraction (total fraction volume 70 µl). White arrow = PfCyp19B. Black arrows = co-precipitating proteins at ~10 kDa, ~100 kDa and ~150 kDa (putative PfCyp19B interacting partners). Red arrow = ~60 kDa co-precipitating protein also present in pre-immune control. **B.** Western blot of SDS-12.5% polyacrylamide gel electrophoretogram. Co-immunoprecipitation used 228 µl saponin-harvested parasite suspension lysed by Triton X-100 on ice for 30 minutes and was performed using anti-PfCyp19B linked to Pierce AminoLink Plus Coupling Resin with parasite lysate as per the manufacturer's instructions. Blots were probed with 1:2000 anti-PfCyp19B serum. Lane 1: Flow-through post-incubation of whole parasite extract with resin. Lane 2: Immunoprecipitated eluate, White arrow = anti-PfCyp19B reactive band at ~19kDa. **C.** Sypro Ruby® stained SDS-4–20% polyacrylamide gel electrophoretogram showing concentrated co-immunoprecipitation eluate from an anti-PfCYP19B column. (Lane 1) molecular weight marker: numbers indicate mass in kDa. (Lane 2) 15 x co-immunoprecipitation eluates concentrated using a 9-kDa MWCO Pierce protein concentrator, 100% of the fraction was loaded, containing ~80 ng of protein. Concentration was performed at 5000 x g for 30 minutes. Red Arrow = co-precipitating protein also present in pre-immune control (Panel A, lane 7). White arrow = PfCyp19B. Black arrows = putative interacting partners.

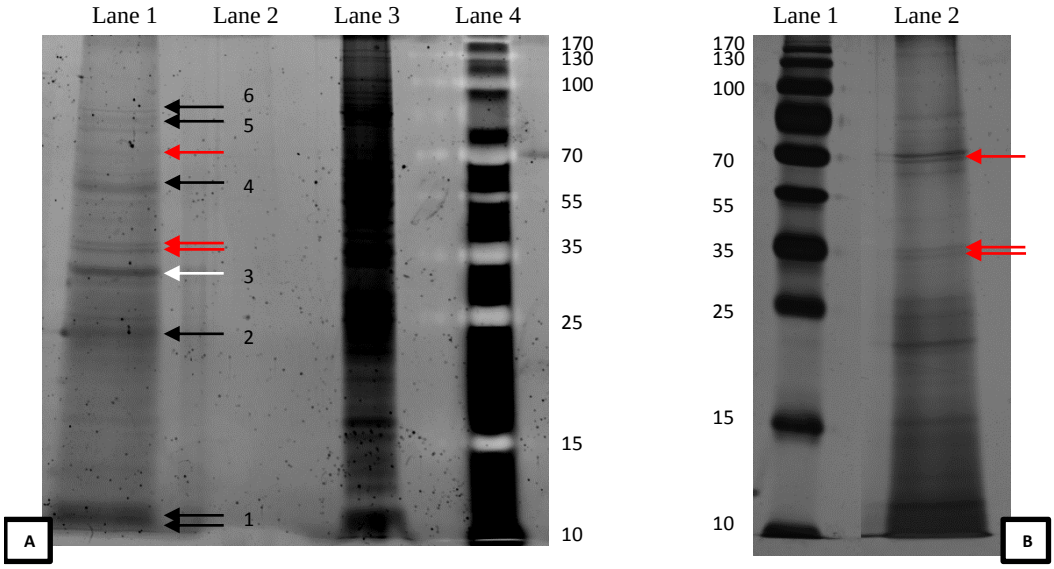

Figure 12: **A.** Silver stained SDS-12.5% polyacrylamide gel electrophoretogram showing concentrated anti-PfFKBP35 co-immunoprecipitation eluate. (Lane 1) Concentrated co-IP eluate (20 fold concentration). (Lane 2) Co-IP wash fraction (20 µl of 400 µl fraction). (Lane 3) Co-IP flow through (20 µl of 400 µl fraction). (Lane 4) Molecular weight marker (sizes are indicated in kDa). Arrows indicate major bands in concentrated co-IP eluate. **B.** co-IP using column generated with pre-immune serum. (Lane 1) Molecular weight marker (sizes are indicated in kDa). (Lane 2) Concentrated co-IP eluate (20 fold concentration). Black = putative interacting partners, Red = bands also present in pre-immune eluate, White = PfFKBP35. In both cases the eluate fraction corresponds to the total concentrated elution fraction from co-IP performed against 1.14 ml harvested parasite extract prepared as described in section 2.2.3.

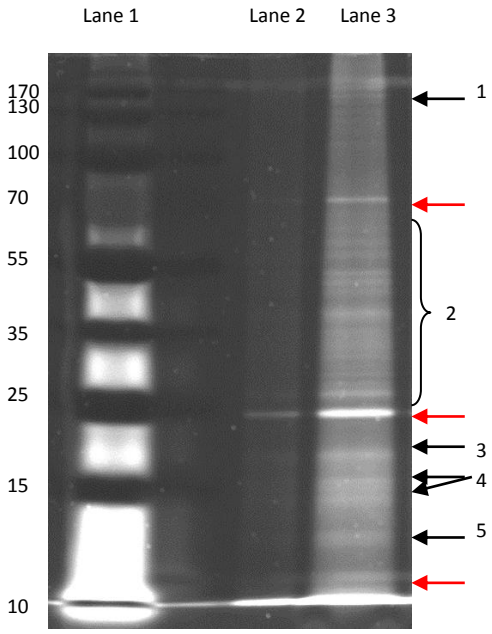

Figure 13: SyproRuby® stained SDS-12.5% polyacrylamide gel electrophoretogram showing concentrated anti-PfCYP19A co-immunoprecipitation. (Lane 1) Molecular weight marker (sizes are indicated in kDa). (Lane 2) Unconcentrated co-IP eluate (20 µl of 400 µl fraction). (Lane 3) Concentrated co-IP eluate (20 fold concentration, corresponding to the total concentrated elution fraction from co-IP performed against 1.14 ml harvested parasite extract prepared as described in section 2.2.3.). Arrows indicate major bands in concentrated co-IP eluate. Black = putative interacting partner,s Red = bands also present in pre-immune eluate (not shown).

3.3.1.3 *Mass Spectrometric Analysis of co-IP Proteins*

3.3.1.3.1 ANALYSIS AS A WHOLE DATASET Mass spectrometry results were analysed using the PEAKS software against a database generated from the complete list of Gene-Text-IDs of *P. falciparum* strain 3D7 on www.plasmodb.org. In the first instance the data from each band were grouped together for analysis; in this way we were able to increase the identification probability since we viewed the gel slices as a whole immunoprecipitate rather than discrete bands. This was done in order to include breakdown products in bands below a full length protein's position on the gel in the analysis. Of course this method doesn't distinguish between peptides identified where one wouldn't expect to see them, for example a peptide from a 15 kDa protein in a band at 90 kDa, and may lead to more false positives than if the results were analysed on a band-by-band basis. The disadvantages of false identifications are balanced, in the author's opinion, by the benefits of increasing the chances of identification of low-abundance proteins. This is illustrated by the difference between analysing the results of the PfCYP19B data as discrete bands vs. as a whole. In the analysis of this mass-spectrometric data PfCYP19B was not identified confidently by the band-by-band method, but when the data from all gel slices were analysed as a whole dataset the confidence of identification increased above a PEAKS score of 98%. Nonetheless, analysis on a band-by-band method, with subsequent elimination of proteins identified in positions above their predicted MW, was carried out (details below).

A sorting method was needed to sort high- from low-confidence identifications, so it was decided to base the sorting upon each protein identification's PEAKS score. The PEAKS score is a composite

score that takes into account results of the database search and *de novo* sequencing: as a rule of thumb, proteins with a PEAKS score higher than 95% can be considered confidently identified, but below this and down to approximately 70% there is a certain linear correspondence between PEAKS score and percent of probability that the identification is correct. Interactions with a score greater than 95% would be used in the first stage of further study, while those with lower scores would be returned to if it were deemed necessary. Those interactions that scored >95% will be referred to as group 1, those with a score <95% but >70% will be group 2, while those below 70% will be group 3. PEAKS analysis identified a total of 731 protein interactions for PfCYP19A, 105 interactions for PfCYP19B, and 480 protein interactions for PfFKBP35. One hundred and sixty one PfCYP19A interacting proteins, eleven PfCYP19B interacting proteins and 113 PfFKBP35 interacting proteins were sorted into group 1. The much lower number of proteins identified from the PfCYP19B co-IP was probably due to the sensitivity of the mass spectrometry: at the time the instrument available to us was a Thermo Orbitrap LC/MS machine, while for PfCYP19A and PfFKBP35 we had access to a Thermo Q-Exactive Quadropole Orbitrap which is a far more sensitive machine. Potentially important results are summarised in Table 2 while complete results can be found in appendix 1 (Table 5).

3.3.1.3.2 ANALYSIS BAND-BY-BAND In this instance, mass spectrometry results were again analysed using the PEAKS software against a database generated from the complete list of Gene-Text-IDs of *P. falciparum* strain 3D7 on www.plasmodb.org but analysed seperately on a band-by-band basis. Proteins identified from bands above their predicted or described MW were eliminated and the results were again

Table 2: **Potentially important protein interactions identified from co-IP screen**

Gene_ID	PEAKS Score (%)	Coverage (%)	No. of Peptides	Description
Triple Interactors				
PF3D7_0708400	99.2	18	13	heat shock protein 90 (Hsp90)
PF3D7_0818900	99.2	24	17	heat shock protein 70 (Hsp70)
PF3D7_0917900	99.2	42	33	heat shock protein 70 (Hsp70-2)
PF3D7_1134000	99.2	23	16	heat shock protein 70 (Hsp70-3)
PF3D7_0831700	99.2	9	7	heat shock protein 70, putative (Hsp70-x)
PF3D7_1410400	99	9	8	rhoptry-associated protein 1 (RAP1)
PF3D7_1357000	99.2	43	22	elongation factor 1-alpha
PfFKBP35 Interactors				
PF3D7_1246200	97.7	6	2	actin I (ACT1)
PF3D7_0903700	98.9	11	4	alpha tubulin 1
PF3D7_1008700	99.1	10	4	tubulin beta chain
PF3D7_0617800	98.9	32	5	histone H2A (H2A)
PF3D7_1105100	99.2	57	8	histone H2B (H2B)
PF3D7_0610400	96.2	5	1	histone H3 (H3)
PF3D7_1105000	98.9	39	4	histone H4 (H4)
PF3D7_0919000	99	14	4	nucleosome assembly protein (NAPS)
PF3D7_0501600	98.3	7	3	rhoptry-associated protein 2 (RAP2)
PF3D7_0322000	99	22	4	peptidyl-prolyl cis-trans isomerase (CYP19A)
PF3D7_1115600	98.3	14	3	peptidyl-prolyl cis-trans isomerase (CYP19B)
PF3D7_0708800	95.1	2	2	heat shock protein 70 (Hsp70-z)
PF3D7_1118200	97	1	1	heat shock protein 90, putative
PF3D7_1434300	97.6	5	3	Hsp70/Hsp90 organizing protein (HOP)
PF3D7_1473200	98.2	3	2	DnaJ protein, putative
PfCYP19A				
PF3D7_1015600	99.2	41	21	heat shock protein 60 (Hsp60)
PF3D7_0708800	99.2	14	11	heat shock protein 70 (Hsp70-z)
PF3D7_1434300	99	15	9	Hsp70/Hsp90 organizing protein (HOP)
PF3D7_0929400	99.2	13	20	high molecular weight rhoptry protein 2
PF3D7_0905400	99.2	9	8	high molecular weight rhoptry protein 3
PF3D7_1252100	97.9	2	4	rhoptry neck protein 3 (RON3)
PF3D7_1116000	97.7	1	1	rhoptry neck protein 4 (RON4)
PF3D7_0501600	98.5	6	3	rhoptry-associated protein 2 (RAP2)
PfCYP19B				
PF3D7_1246200	99.1	18	5	actin I (ACT1)

sorted into groups 1, 2 and 3. It is important to note that while the number of overall interaction identifications was reduced in each case, the interactions that we have highlighted as important in table 2 are still confidently identified. In general, confident protein identification came from bands below the predicted MW of the protein: this was not unexpected since co-IP for these immunophilins appears to pull down components of the proteolytic machinery of the parasite. For example, Hsp90 and 3 Hsp70 isoforms were identified with a PEAKS score of >99%, by multiple peptides covering >10% of the protein in the band labelled #4 in the PfCYP19A co-IP SDS-PAGE, which is at approximately 14–22 kDa. Since the highlighted interactions are unaffected by analysis by this method the complete results are not included in this document, but the data are available on request from the author.

3.3.2 *Identification of putative interacting partners for PfFKBP35 using yeast 2-hybrid analysis*

3.3.2.1 *Generation of pLex-A-PfFKBP35-His$_6$ and pLex-A-PfFKBD-His$_6$*

Due to the difficulty encountered while identifying interacting partners through parasite based methods (>8 months needed to get enough parasites for co-IP) it was decided to identify interacting partners for PfFKBP35 using a commercial yeast-2-hybrid screening service. To this end, plasmids containing both the full length FKBP and the FK506 binding domain (FKBD) were constructed using the vector supplied by DualSystems, pLexA-N (Figure 14).

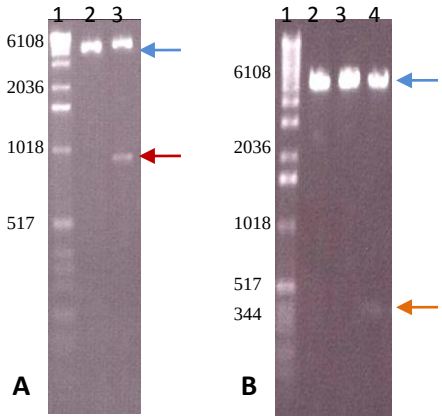

Figure 14: Analysis of pLexA-N bait plasmid constructs. Plasmid isolated from transformant colonies was subjected to *Eco*RI and *PstI* digestion, run through a 1% agarose gel and stained with ethidium bromide. (A) Lane 1, Molecular weight marker (MW in bp). Lane 2, ~0.2 µg unligated pLexA-N plasmid. Lane 3, ~0.2 µg pLexA-N ligated with PfFKBP35 PCR product. Blue arrow: band at ~5600 bp corresponding to pLexA-N. Red arrow: band at ~900 bp corresponding to PfFKBP35 PCR product. (B) Lane 1, Molecular weight marker (molecular weight in bp). Lanes 2+3, ~0.2 µg unligated pLexA-N plasmid. Lane 4, ~0.2 µg pLexA-N ligated with FKBP-domain PCR product. Blue arrow: band at ~5600 bp corresponding to pLexA-N. Orange arrow: band at ~380 bp corresponding to FKBP-domain PCR product.

3.3.2.2 *Functional Bait Assay*

These constructs were then assessed by a functional bait test assay. This assay determines whether the bait protein enters the nucleus and binds to the *LEXA* operators situated upstream of the reporter genes (10). A bait which enters the nucleus and binds to the *LEXA* operator sites decreases transcription from the downstream *LACZ* gene (repression) and hence decreases β-galactosidase expression on galactose medium. Most *LEXA* fusions that enter the nucleus and bind the operators, but do not activate transcription, repress β-galactosidase activity from 2 to 20 fold. More than 2 fold repression indicates >50% operator occupancy by the bait and signifies that the bait can be screened in the DUALhybrid® assay. The assay determined that the FKBD construct was better able to enter the nucleus of the yeast than the full-length PfFKBP35 and repressed β-galactosidase activity better than at least one of the positive controls. It was therefore the more suitable of the two constructs for use in the screen against the *P. falciparum* library (Figure 15).

3.3.2.3 *Yeast-2-hybrid analysis*

This screen ultimately yielded eleven putative interacting partners (Table 3): three "Class B" interactors which have been identified two times and represent highly likely interactors with the bait, and eight "Class C" interactors which were found only once in the screen. "Class A" interactors are those which have been rescued three or more times. They represent highly likely interactors of the bait protein, but unfortunately no interactors of this class were identified. Although some of the results from this analysis may indeed represent true interactors of the protein of interest, others may represent common false positives.

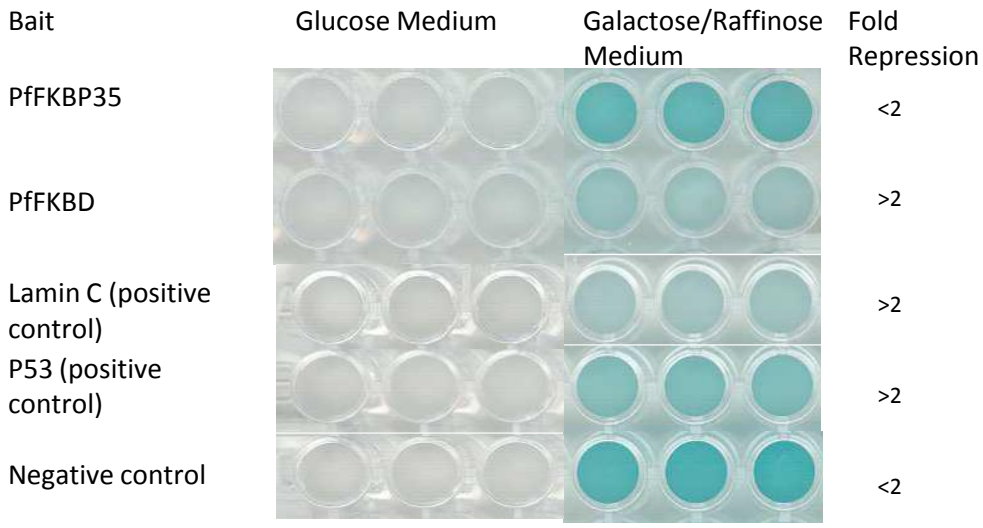

Figure 15: Functional bait assay of pLexA-N-PfFKBP35 and pLexA-N-FKBD constructs. Expression strains containing FKBP construct, positive controls or empty construct vector were grown on either glucose medium (negative for β-galactosidase activity) or galactose/raffinose medium (positive for β-galactosidase activity). A blue colour indicates β-galactosidase activity: the weaker the blue colour, the more the *LACZ* operator is repressed and the more bait is entering the nucleus. This assay was performed by DualSystems.

Table 3: **Putative PfFKBD-protein interactions identified through yeast-2-hybrid screening.**

Class*	Gene ID	Product Description
B	PF3D7_1473200	DnaJ protein, putative
B	PF3D7_0519800	conserved protein, unknown function
B	PF3D7_0731300	*Plasmodium* exported protein (PHISTb), unknown function (PfG174)
C	PF3D7_0408400	conserved *Plasmodium* protein, unknown function
C	PF3D7_0206500	conserved *Plasmodium* protein, unknown function
C	PF3D7_1035200	S-antigen
C	PF3D7_0730300	transcription factor with AP2 domain(s) (ApiAP2)
C	PF3D7_1333700	histone H3 variant, putative (CenH3)
C	PF3D7_1105100	histone H2B (H2B)
C	PF3D7_1025100	glucosamine-fructose-6-phosphate aminotransferase, putative
C	PF3D7_1013800	conserved *Plasmodium* protein, unknown function

*See Text for explanation

3.3.3 *An immunophilin-protein interaction map*

The data generated in this study generated a large number of putative protein–protein interactions for the three *P. falciparum* immunophilins studied. Due to the large nature of the dataset it is desirable to represent the results in a meaningful visual manner from which a reader can draw observations and conclusions easily and quickly, albeit with the caveat that the interactions (save those between PfFKBP35 and histone H2B & DnaJ [PF3D7_1105100 & PF3D7_1473200] which were detected by both methods, and that between PfFKBP35 and Hsp90 which was reported previously [90]) are unconfirmed (but see chapter 4). It was decided to construct an "interaction map" of the putative results generated by both the co-IP and Y2H studies. The network visualisation software Cytoscape (www.cytoscape.org) was used to generate network node maps of each protein which were then merged, colour coded by GO process annotation and separated into singly, doubly and triply interacting groups (Figure 16). Gene_IDs of each in each node of the double and triple interactors can be found in the appendix (Table 4).

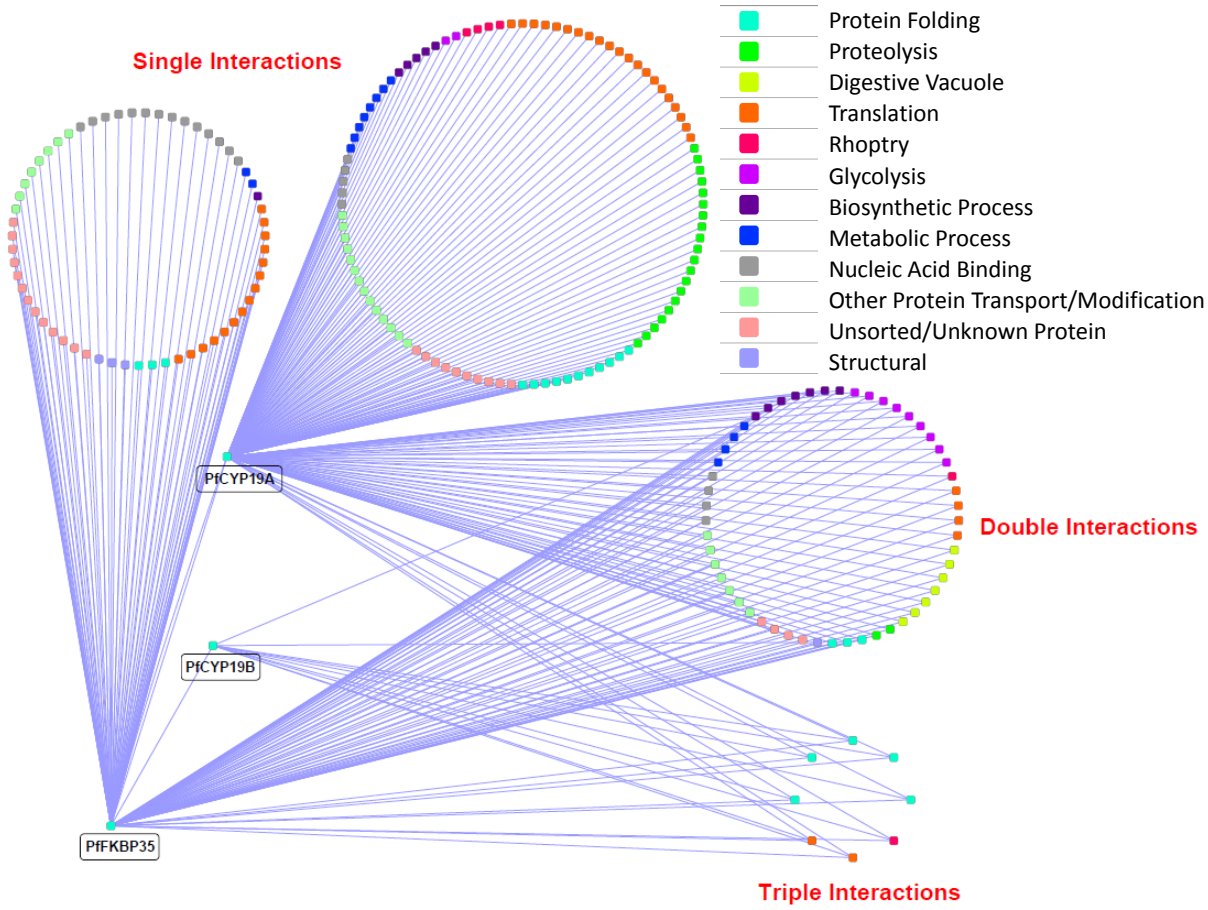

Figure 16: Network map showing putative singly, doubly and triply interacting proteins for PfCYP19A, PfCYP19B and PfFKBP35. Interactors are colour coded by GO-annotation. Identification of the interactors in each node can be found in the appendix (Table 4).

3.4 DISCUSSION

The primary aim of the research described in this chapter was to identify putative interacting partners for the two most abundant blood stage cyclosporin A binding cyclophilins PfCYP19A and PfCYP19B and the FK506 binding protein PfFKBP35. Co-immunoprecipitation is a powerful tool to study novel protein–protein interactions and has previously been used to demonstrate protein–protein interactions in *P. falciparum* [69]. Similarly yeast-2-hybrid screening is a well established methodology for studying protein–protein interactions and large scale studies have used it to analyse the proteome of *Plasmodium* [92]. Use of both of these methods to identify putative immunophilin protein interactions is described herein.

Prior knowledge of immunophilin–protein interactions in *P. falciparum* was limited to *in vitro* evidence of the interaction between PfFKBP35 and the protein phosphatase calcineurin [90, 113] as well as its interaction with Hsp90 [90]. This study represents the first attempt to characterise the interactome of the major drug binding immunophilins in *P. falciparum*. We have demonstrated that co-IP specifically and reproducibly pulls down a number of protein bands when separated by SDS-PAGE and subsequent analysis by mass spectrometry identified 284 putative protein identifications by whole dataset analysis. Though this list may include a large number of false positives due to the nature of the analysis, we feel that it represents an excellent starting point for further research, especially when coupled with data on other immunophilin interactions in the literature. Analysis on a band-by-band basis was performed but these results didn't affect the confidence of the interactions which we have highlighted as interesting sufficiently to warrant a separate discussion of analysis

by this method. Discussion of each of these proteins individually is clearly not practical so we will begin by discussing those for which there is supporting evidence for the interaction from other organisms and will follow up by discussion of interesting novel (putative) interactions.

As mentioned in the first paragraph, Kumar *et al.* (2005) demonstrated that PfFKBP35 interacted with PfHsp90 by its TPR domain and inhibition of both PfFKBP35 and PfHsp90 has a synergistic antimalarial effect. The data presented by this study also indicate an interaction between PfFKBP35 and PfHsp90 by the FKBP's ability to pull down PfHsp90 from a crude parasite lysate. While not a novel interaction this datum serves as an indication of the validity of the co-IP/mass-spectrometry methodology used herein.

A large body of evidence exists which suggests a role for immunophilins as part of high-affinity ligand-binding forms of unactivated steroid receptors in humans. This receptor consists of a multicomponent complex which includes Hsp90, CYP40, FKBP52 (or FKBP51), and an additional p23 protein component, assembly of which is mediated by Hsp70 in association with accessory chaperones Hsp40, Hip and Hop [133, 32, 123]. Other organisms also show evidence of similar interactions, for example Hsp90, Hsp70, Hop and FKBP73 have been shown to interact in protein chaperone complexes in *Arabidopsis* [56]. All three *P. falciparum* immunophilins demonstrate an the ability to pull down Hsp90 and at least four Hsp70 isoforms, though it is difficult to determine whether the interaction between the immunophilins and the Hsp70 proteins is distinct for each Hsp70 or if the multiple identifications come from their high degree of sequence similarity. PfCYP19A and PfFKBP35 pulled down Hsp70/Hsp90 organising protein (Hop), PfCYP19A pulled down PfFKBP35, and the inverse was

also true. Also of note is the fact that PfFKBP35 demonstrated an interaction with PfDnaJ (a putative *Plasmodium* homologue of Hsp40) in both the co-IP and the Y2H screens. These data all point to the tentative conclusion that a cyclophilin–FKBP–Hsp70–Hsp90–Hop protein chaperone complex also exists in *P. falciparum*. Work attempting to follow up on these data will be discussed in chapter 4.

FK506-binding proteins have been demonstrated to have a number of histone-related functions. Specifically nuclear FKBPs in *Schizosaccharomyces pombe* and *Saccharomyces cerevisiae* were shown to possess histone chaperone activity [91] and the nuclear FKBP Fpr4p in *S. cerevisiae* is responsible for regulating methylation of amino acid lysine-36 on histone H3. This regulation is governed by *cis-trans* isomerisation of the bonds preceding the prolines P30 and P38 on histone H3 by Fpr4p. [119]. PfFKBP35 has been demonstrated to be located in the nucleus of the erythrocytic stage of *P. falciparum* [90]. Our data have indicated that the *P. falciparum* FKBP may possess the ability to interact with histones. Specifically, co-IP with PfFKBP35 pulled down the 4 histones involved in nucleosome formation (H2A, H2B, H3 and H4) as well as the nucleosome assembly protein (NAPS). The case for an FKBP–histone interaction is further strengthened by our Y2H data which indicate that the FK506-binding domain of PfFBKP35 may interact with the histones H2A and H3. Again, follow up work will be discussed in the next chapter.

Immunophilins also demonstrate a role in cytoskeletal organisation in humans; FKBPs have been experimentally associated with microtubules [126, 46], particularly on neurite length in early neuronal differentiation [131] and cyclophilin B has a functional interaction with neuronal actin [116]. Our data implicated PfFKBP35 as undertaking a similar cytoskeletal interaction in *P. falciparum*, being able to pull

down actin I and both of the subunits of microtubules, α- and β-tubulin. Similarly PfCYP19B was able to pull down actin I in our co-IP experiments.

Moving on to discuss interactions of interest which are not predicted by data from other sources we will first consider the indication from our data of an interaction of all three immunophilins with the rhoptry associated protein 1 (RAP1). PfFKBP35 also pulled down RAP2, as did PfCYP19A, which also pulled down a number of other rhoptry proteins, two rhoptry neck proteins (RON3 and RON4) and two high-molecular weight rhoptry proteins (RhopH2 and RhopH3). This interaction caught our interest for a number of reasons: first it is the only protein which interacts with all three immunophilins tested that is not predicted from other organisms or involved in protein processing (as the immunophilins are). Secondly, data from past research has indicated that binding and inhibition of RAP1 by an antibody raised against a heterologous peptide sequence inhibits *P. falciparum* growth in culture [115]. We hypothesise that *P. falciparum* immunophilins are potentially important molecular chaperones in transport of rhoptry proteins to their ultimate location. Currently little is known about rhoptry trafficking between protein synthesis and arrival at the rhoptry. The next chapter will detail the work undertaken to investigate this interaction.

Among the other co-IP proteins for PfYP19A and PfFKBP35, there is a significant representation of proteins in the digestive vacuole (DV). Both proteins pulled down plasmepsins I–IV as well as falcipains 2, 2a and 3. Components of the DV have been predicted to be potential druggable targets in antimalarial therapy [99]. PfCYP19A also pulled down a large number of proteins involved in proteolysis, in particular 18 proteasome subunits, components or regulatory sub-

units, while both PfCYP19A and PfFKBP35 pulled down a large number of proteins involved in translation such as ribosomal subunits, elongation factors and translation initiation factors. This is expected because of immunophilins' close relationship with protein synthesis via their PPIase activity. Finally, there was a large number of proteins involved in glycolysis, biosynthetic or other metabolic processes pulled down by both PfCYP19A and PfFKBP35. All of the identifications of the interacting proteins are listed in the appendix (Table 5).

Overall the work detailed in this chapter suggests that the major drug binding immunophilins of *P. falciparum* partake in a number of interactions analagous to immunophilin–protein interactions in other organisms, but also in several potentially novel interactions which may represent suspects in the antimalarial therapeutic action of CsA and FK506. Of course these interactions are only indicated through this one method and are unconfirmed, and further research will be required to identify true immunophilin–protein interactions from the potentially large number of false identifications due to the mass-spectrometric analysis methodology utilised. We feel that the drawbacks of the analysis method used are outweighed by having as large a dataset as possible as a starting point for further study since false positives can be eliminated by further experimentation but true interactions which are disregarded early due to too stringent analysis would be missed entirely. The first steps in studying the potential immunophilin-interactions identified will be discussed in the next chapter.

4

EXPERIMENTAL ANALYSIS OF PUTATIVE PROTEIN–IMMUNOPHILIN INTERACTIONS

4.1 INTRODUCTION

We selected three putative interactions (Chapter 3) for further study in this chapter: the PfCYP19B–Hsp70 interaction, the interaction between PfFKBP35 and histones/nucleosomes and the interaction between the immunophilins and RAP1.

PfCYP19B is a major cytosolic cyclophilin of *P. falciparum* [65] and it makes sense that at least one of the parasite's immunophilins is involved in a high molecular weight chaperone complex analagous to that seen in humans and other species, as discussed in the previous chapter. *P. falciparum* encodes five Hsp70 genes: PfHsp70-I, PfHsp70-II, PfBip-II PfHsp70-III and PfHsp70-IV [1]. PfHsp70-I is the major cytosolic Hsp70 in the intra-erythrocyte life cycle, and it is predicted to be involved in a chaperone complex with Hsp90 [49, 16]. This potential interaction between PfCYP19B and PfHsp70 is interesting for a number of reasons. Chaperones have drawn attention as potential malarial vaccine candidates, and PfHsp70 was shown to be immunogenic in both infected humans [108] and experimentally infected monkeys [73]. Hsp70s have been reported to be associated with the surfaces of both the liver–stage parasites [135] and merozoites [9], and sera from malaria infected patients show increased reactivity to Hsp70s [51]. Chaperones are also of particular interest in malaria be-

cause of the exposure to heat shock that the parasite undergoes. The temperature difference between the mosquito vector and the human host is over 10 °C [1], and during infection and intra-erythrocytic growth in the human host the parasite experiences heat shock caused by cyclical febrile episodes suffered by the patient. The parasite seems to require a robust response to heat shock and has dedicated approximately 2% of its genome to chaperones expressed at various stages of the life cycle [1]. Disrupting the parasite's ability to cope with heat stress makes an attractive drug target.

Histones too make attractive drug targets, and there has been a lot of recent focus on disrupting histone modifications such as acetylation and methylation as an approach to antimalarial therapy [8, 155, 105]. It has been shown that small molecule histone methyltransferase inhibitors have activity against malaria parasites both in culture and in an *in vivo* mouse model [105]. Histone deacetylase (HDAC) inhibitors have also shown promise as antimalarial therapies, and several promising leads have emerged from the current trend of repurposing existing drugs, particularly anti-cancer drugs, as antimalarials [155]. Any role of parasite immunophilins in epigenetic modification of histones could prove to be of major importance.

Plasmodium rhoptries are complex secretory organelles, and to date we know of more than 30 proteins which are classified as rhoptry proteins in *P. falciparum* [40], with a further 27 potential rhoptry proteins of unknown function identified through proteome analysis [142]. Rhoptry associated protein 1 (RAP1) is one of these proteins, believed to be located in the rhoptry bulb, that is highly conserved in both laboratory-adapted strains and clinical isolates [82]. Antibodies to RAP1 appear to inhibit the invasive ability of merozoites [78, 115], and peptides derived from RAP1 demonstrate erythrocyte binding

capacity [45]. RAP1 appears to be essential for the invasive ability of merozoites, since a RAP1 gene disruption was only possible in a culture-adapted *P. falciparum* strain which uses alternative parasite ligands for invasion [13]. That study also demonstrated that RAP1 was required for correct RAP2 localisation. RAP1's apparent critical role in the parasite life cycle and the unique molecular pathway to which it belongs make it an attractive drug target.

Confirming that protein–protein interactions occur *in vitro* is often a difficult process, let alone confirming that the interaction is biologically relevant *in vivo*. Even more difficult is assessing that the new interaction is a possible drug target. Having said this, there are a wide variety of experimental techniques that are popularly used to demonstrate protein–protein interactions both *in vitro* and *in vivo*. The techniques we have utilised in this chapter include confocal microscopy, far Western blotting, chaperone assays, thermal stability shift assays and co-immunoprecipitation.

Most often confocal microscopy is used to determine whether two or more proteins are co-located in the cell. Co-location in a specific organelle or structure usually indicates that interactions between the proteins being studied are possible. Co-immunoprecipitation was discussed in the introduction to the previous chapter with regards to identifying novel protein–protein interactions, and it can also be used as a method to confirm that these interactions take place. If antibodies to both proteins are available it should be possible to detect the presence of an interacting partner of "protein 1" by Western blotting for "protein 2" from a co-immunoprecipitate of the first. Far Western blotting uses a non-antibody protein probe to bind to proteins on a Western blot, usually followed by detection of the probe protein by

standard Western blotting methods if the probe is not tagged in some way e.g. flourescently.

4.2 METHODOLOGY

Materials and methods used in this chapter are described in detail in chapter 2. All experiments were performed with asynchronous cultures of the 3D7 clone of *P. falciparum*. Co-IPs were performed as described in section 2.7, far Western blotting as described in section 2.7.9, and confocal microscopy was performed as described in section 2.8. Anti $RAP1_{1\text{-}14}$ was a kind gift from Prof. G Pluschke, Swiss Tropical and Public Health Institute, Basle. The histone chaperone assays were performed by Michael Prunty under the author's supervision.

4.3 RESULTS

4.3.1 *Co-IP with anti-Hsp70*

In order to confirm that PfCYP19B interacts with PfHsp70 we attempted to pull down the cyclophilin using co-IP of the heat shock protein. Antibodies to heat shock protein 70 from other organisms are readily available. We sourced an polyclonal antibody which had been generated against a recombinant full length Hsp70 from *H. sapiens* to increase the possibility of cross-reactivity, due to the high level of sequence similarity between Hsp70s, and confirmed that it was able to detect a 70-kDa band when used in a Western blot of a crude parasite lysate (Figure 17).

After confirming cross-reactivity of the HsHsp70 antibody we used it to generate a co-IP column as described in section 2.7.1. The co-IP eluate from this column contained PfCYP19B when analysed by Western blot with an anti-PfCYP19B antibody (Figure 18, lanes 1 & 2). We can conclude that this ability to pull down PfCYP19B is specific to the anti Hsp70 column since co-IPs performed using a column made with an irrelevant antibody (Fig. 18, lane 3 & 4) and a non-reactive column which is unable to bind antibody (Fig. 18, lane 5) were unable to pull down PfCYP19B. Similarly the co-IP eluate from the anti-Hsp70 column is negative for an irrelevant protein (Figure 18, lane 6 & 7). Taken together, these results lead to the conclusion that PfCYP19B specifically interacts with PfHsp70 *in vitro*.

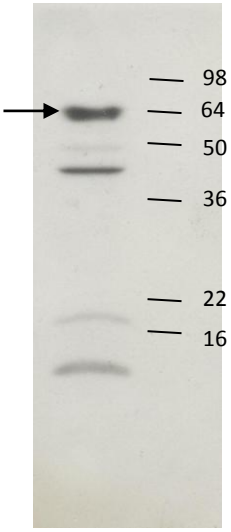

Figure 17: Western blot of ~100 µg crude parasite lysate separated by SDS–12.5% PAGE, transferred to PVDF membrane and probed with anti-Hsp70. The black arrow indicates a band at ~70 kDa; numbers indicate molecular weight marker size in kDa. Lower bands may be the result of protein breakdown in the sample.

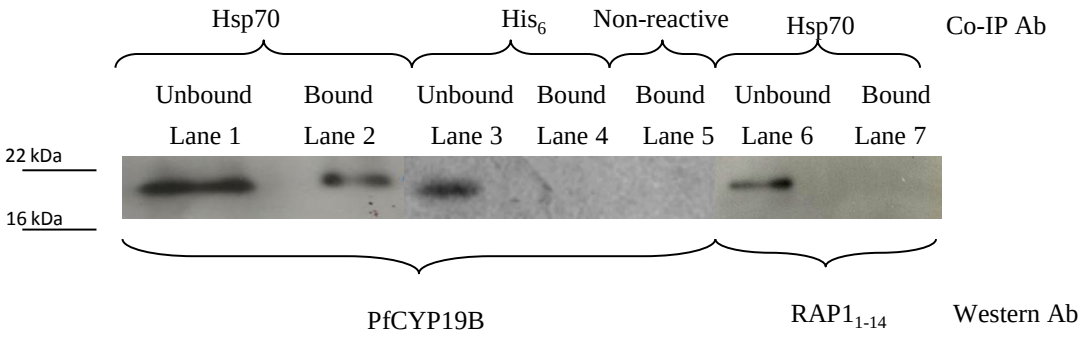

Figure 18: Co-IP and Western blot investigation of PfCYP19B–Hsp70 interaction. Co-IP was performed using anti-Hsp70 to pull down PfCYP19B by its affinity for Hsp70 (Lane 1 & 2). Controls comprising an irrelevant antibody column (anti-His_6: Lane 3 & 4), a non-reactive column (Lane 5) and a Hsp70 co-IP Western blot probed with an antibody for an irrelevant protein (Lane 6 & 7) are also shown. In the cases of the unbound fraction approximately 20 µl of a 400 µl fraction were loaded, and in the cases of the bound fractions the eluate was concentrated and a volume equalling the total fraction was loaded onto the SDS-PAGE. Bars on the left of the image indicate the positions of molecular size markers in kDa.

4.3.2 *Investigation of the PfFKBP35–histone interaction*

The discovery, by both Y2H and co-IP, that PfFKBP35 potentially interacts with *P. falciparum* histones is a promising avenue of further investigation since FKBPs in other organisms have demonstrated histone interactions. As discussed in section 3.4, nuclear FKBPs in *S. pombe* and *S. cerevisiae* were shown to possess histone chaperone activity [91] and the nuclear FKBP Fpr4p in *S. cerevisiae* is responsible for regulating methylation of amino acid lysine-36 on histone H3. This regulation is governed by *cis-trans* isomerisation of the prolines P30 and P38 on histone H3 by Fpr4p. [119].

4.3.2.1 *Histone purification*

To investigate this interaction we required histones from *P. falciparum* upon which to experiment. We employed the method of Longhurst et al. (1997) [102] as described in section 2.7.5 to purify histones from *P. falciparum* cultures. By this method we were able to purify proteins of the correct molecular weight when analysed by separation on SDS-15% PAGE, matching the results observed by Longhurst and Holder [102], as shown in figure 19.

4.3.2.2 *Far-Western blot analysis of PfFKBP35–histone interaction*

The first step in studying this interaction was to investigate whether purified recombinant *P. falciparum* FKBD was able to interact in any way with purified histones. The FKBD was chosen since the Y2H study identified a potential interaction using only the FKBD. The method chosen to study this initially was far-Western blotting, since we had an antibody available for PfFKBD. By this method we employ standard Western blotting techniques to assess whether a non-

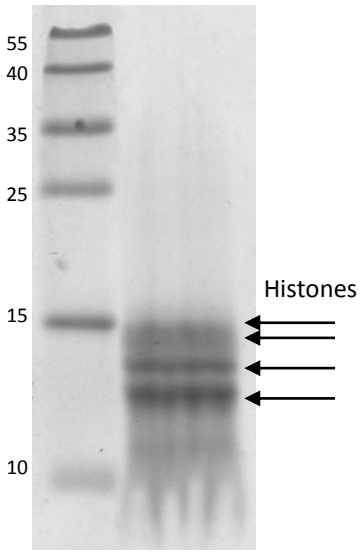

Figure 19: Purification of *P. falciparum* histones. Approximately 30 μg of *P. falciparum* histones (right lane) purified by the method of Longhurst et al. (1997) [102] separated by SDS 15%-PAGE. Masses of molecular weight markers (left lane) are indicated in kDa on the left. Arrows indicate bands corresponding to the 4 low MW proteins isolated in the original study.

antibody protein probe (in this case PfFKBD) has bound to a protein (in this case histones) first separated by SDS-PAGE and subsequently transferred to a membrane such as nitrocellulose or PVDF. Figure 20 demonstrates that FKBD purified as described in section 2.6.1 is specifically able to bind to *P. falciparum* histones purified as described in section 2.7.5 and separated by SDS-PAGE and subsequent transfer to PVDF membrane. There was no interaction observed between PfFKBD and an irrelevant protein (BSA), nor an interaction between an irrelevant protein (PfCYP19B) and *P. falciparum* core histones by this method.

4.3.2.3 *Histone chaperone assay of PfFKBP35*

We next investigated the ability of PfFKBP35 to act as a histone chaperone, by the same method employed by Kuzuhara *et al.* (2004) [91]. In

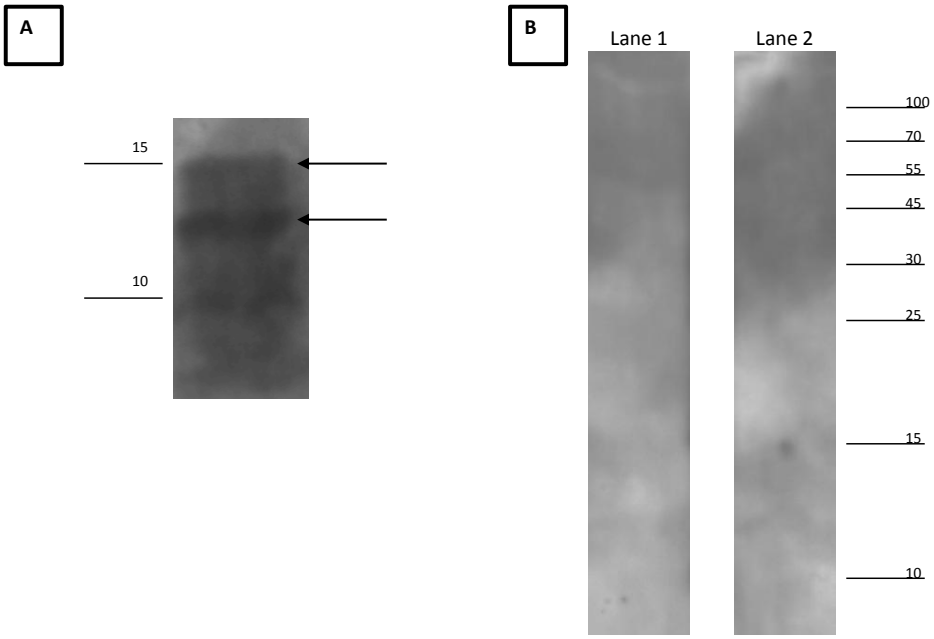

Figure 20: Far-Western blotting analysis of *P. falciparum* histone interactions. 30 µg *P. falciparum* histones (**A** and **B,** lane 1) or 10 µg bovine serum albumin (**B,** lane 2) were separated by SDS-15% PAGE and transferred to PVDF membrane, which was probed with 1 µg/µl recombinant PfFKBD-His_6 (**A** and **B**, lane 2) or 1 µg/µl recombinant PfCYP19B (**B**, lane 1), extensively washed and the interaction was detected by standard Western blot using an antibody for PfFKBD-His_6 (**A** and **B**, lane 2) or PfCYP19B (**B**, lane 1). Arrows indicate bands corresponding to the apparent MW of histones as seen in figure 19. Numbers and lines to the left and right indicate the position and size of molecular weight marker in kDa.

brief, this assay demonstrates the ability of a histone chaperone to assist in DNA supercoiling in the presence of histones. When supercoiling is relaxed by the action of an enzyme such as topoisomerase I the DNA appears to increase in molecular size as measured by agarose gel electrophoresis, with increasing levels of DNA relaxation leading to higher apparent MW. The addition of histones and a histone chaperone protein (but not histones alone) facilitates the formation of nucleosomes and the apparent high-MW relaxed DNA becomes supercoiled and returns to an apparently low-MW state on agarose gels. As can be observed in figure 21, there is no apparent increase in the ability of histones to form nucleosomes regardless of the presence of the full length PfFKBP35 or the FK506 binding domain of the protein. Unfortunately we were unable to perform a positive control for this experiment due to lack of a protein which is known to act as a histone chaperone. This experiment was performed by Mr. Michael Prunty as part of a final year research project under the author's supervision.

4.3.2.4 *Effect of FK506 on H3K36 methylation*

Finally we investigated whether the action of FK506 has an effect on the amount of H3K36 methylation. Previously, researchers have shown that H3K36 methylation is controlled by the PPIase action of the yeast FKBP Fpr4p. This regulation is governed by *cis-trans* isomerisation of the prolines P30 and P38 on histone H3 by Fpr4p [119]. In this experiment we incubated parasites in culture with FK506 or chloroquine for 14 h. As shown in figure 22, there is an increase in H3K36 methylation with increasing concentrations of FK506, which is known to inhibit the PPIase activity of PfFKBP35, but this was not seen with the standard antimalarial drug chloroquine, whose primary action is to disrupt haemozoin formation.

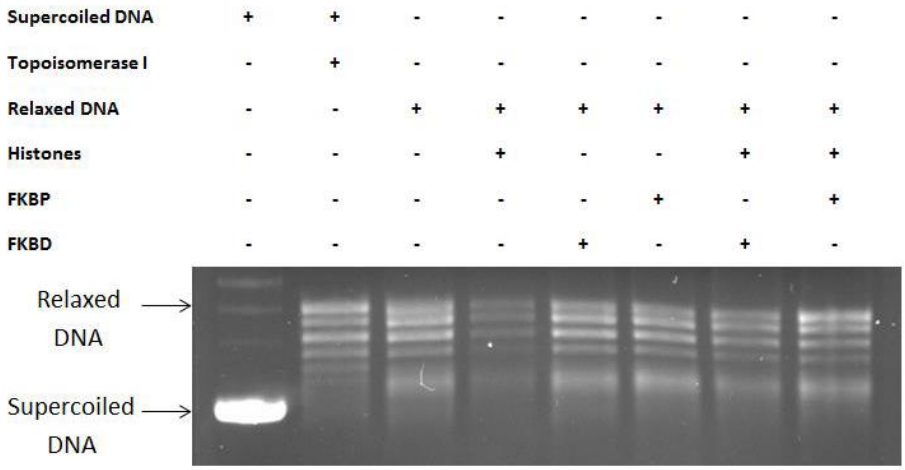

Figure 21: Histone chaperone assay of PfFKBP35 and its FKBD. Circular pBluescript plasmid DNA (Lane 1) was relaxed with 5 units of Topoisomerase I overnight at 37 °C. Relaxed pBluescript (Lanes 2-8) was combined with purified *P. falciparum* histones (Lane 4, 7 & 8) and recombinant proteins (Lanes 5, 6, 7 & 8) in assembly buffer with a final volume of 50 µl. The reaction mixture was incubated at 30 °C for 1 h. The reaction was stopped by the addition of an equal volume of stop buffer and the level of DNA supercoiling was analysed on a 1% agarose gel. In all cases the reactions were performed with 0.1 pmol of plasmid and 7 pmol of protein and 10 µl of the 50 µl total reaction volume were loaded onto the agarose gels. This experiment was performed by Mr. Michael Prunty as part of a final year research project under the author's supervision.

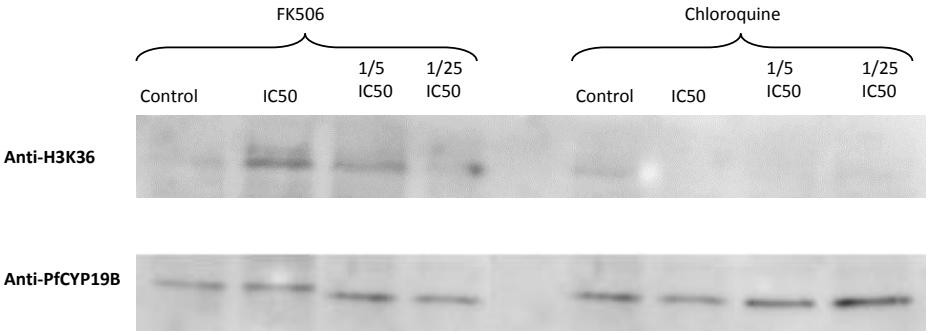

Figure 22: Western blot of extracts from parasites incubated with decreasing concentrations of either FK506 or chloroquine for ~14 h. Parasites were lysed by incubation on ice with Triton X-100 for 30 min and the clarified lysate was separated by SDS-12.5% PAGE. The blot was probed with either anti-H3K36 (Abcam®, ab9050) (a kind gift from Dr. Alastair Fleming) or anti-PfCYP19B as a loading control.

Overall it appears that PfFKBP35 does not act as a histone chaperone under the conditions employed but does appear to play a role in the methylation of H3K36 by it's PPIase activity.

4.3.3 *Investigation of RAP1–immunophilin interaction*

4.3.3.1 *Confocal immunofluorescence microscopic analysis of locations of RAP1 and PfCYP19B*

As mentioned, confocal immunofluorescence microscopy is usually used to confirm a protein–protein interaction is possible by showing that the proteins being studied are present in the same subcellular compartment. Previous data from Gavigan *et al* have shown that PfCYP19B is mostly located in the cytoplasm [65], while Moreno *et al* demonstrated that PfRAP1 exhibits the characteristic bipunctate staining of a rhoptry protein in mature merozoites [115]. We concluded that attempting to show co-location would be unreasonable based on the information about each protein's location in the cell, but we hy-

pothesised that PfCYP19B might be involved in chaperoning PfRAP1 during transport to its ultimate location and so instead undertook work to study the effect of cyclosporin A, non-calcineurin targeting immunophilin-ligands and two non-immunophilin ligands (as negative controls) on PfRAP1 location.

Immuno-staining schizonts for RAP1 under normal conditions resulted in the bi-punctate staining characteristic of rhoptry proteins, while PfCYP19B was seen located in the cytoplasm as expected (Figure 23, Control). After 14–16 h of incubation with CsA at 5x IC50 we demonstrate that the characteristic bipunctate staining of PfRAP1 was disrupted and RAP1 and PfCYP19B were seen to co-locate (Figure 23, 5xIC50 CsA). The disruption was still evident at the IC50 and somewhat evident at 0.2x IC50 and 0.04x IC50 while the characteristic bipunctate staining for RAP1 was restored after reduction below this concentration. At all concentrations tested there is no evidence of an effect on the location of PfCYP19B.

In order to exclude the possibility that this effect was due to calcineurin inhibition by the drug/cyclophilin complex we tested the effects of the non-calcineurin binding immunophilin-ligands [MeVal]^4-cyclosporin and BC-556 on RAP1. These ligands were both able to disrupt RAP1 location in schizonts at similar relative concentrations to CsA, i.e 5x IC50 (Figure 24) and IC50 (not shown). Also tested were the classic antimalarial drugs chloroquine and artemisinin, but these ligands had no effect on RAP1 location after 14–16 h at 5x IC50 (Figure 24). Taken together these results suggested that the disruption of proper RAP1 location was not associated in a non-specific way with parasite damage or growth inhibition but was likely mediated by interference with the action of one or more cyclophilins.

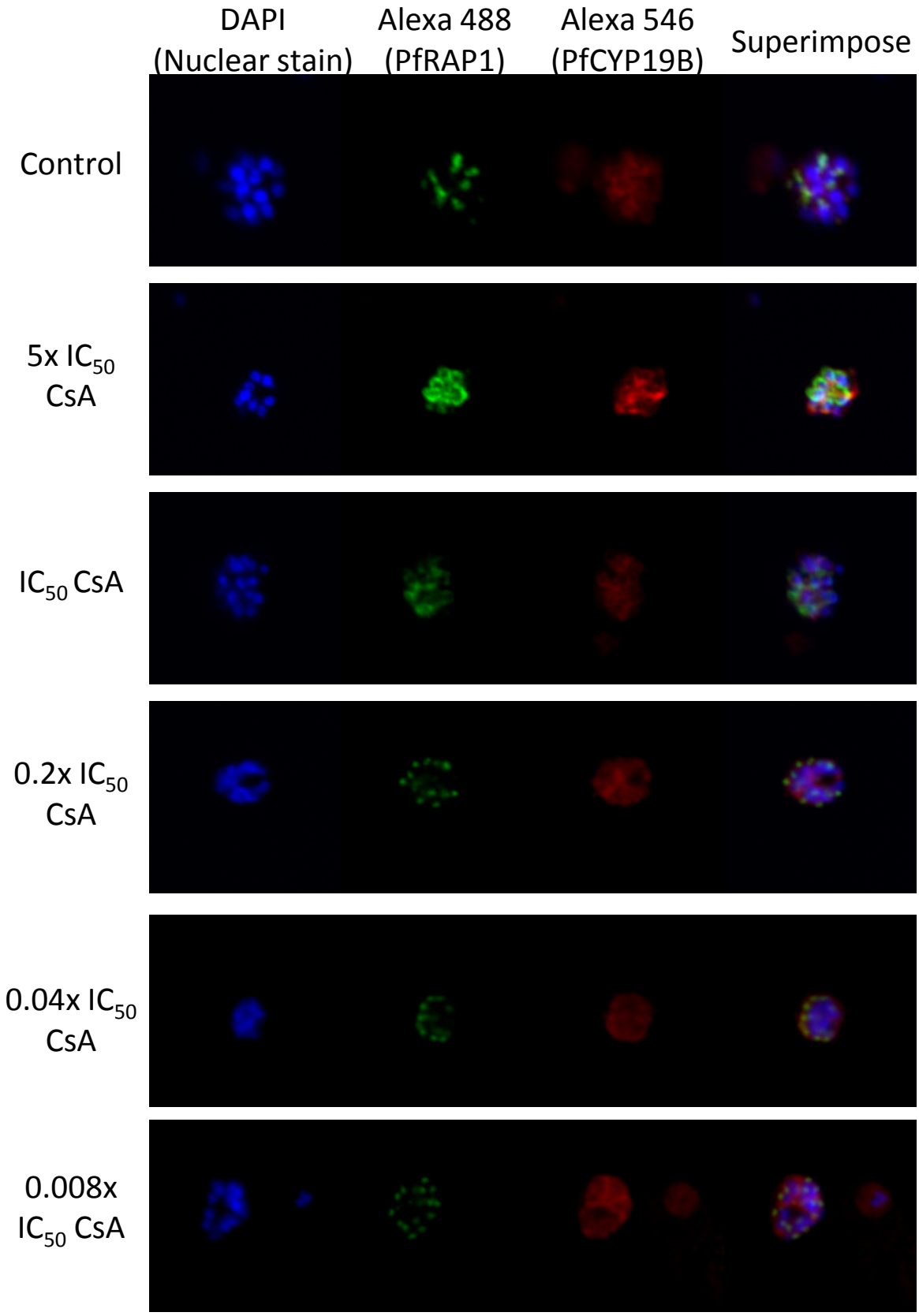

Figure 23: Confocal immunofluorescence microscopy of *P. falciparum* schizonts treated with decreasing concentrations of cyclosporin A. Shizonts were stained with DAPI (nuclear), Alexafluor-488 (PfRAP1) and Alexafluor-546 (PfCYP19B).

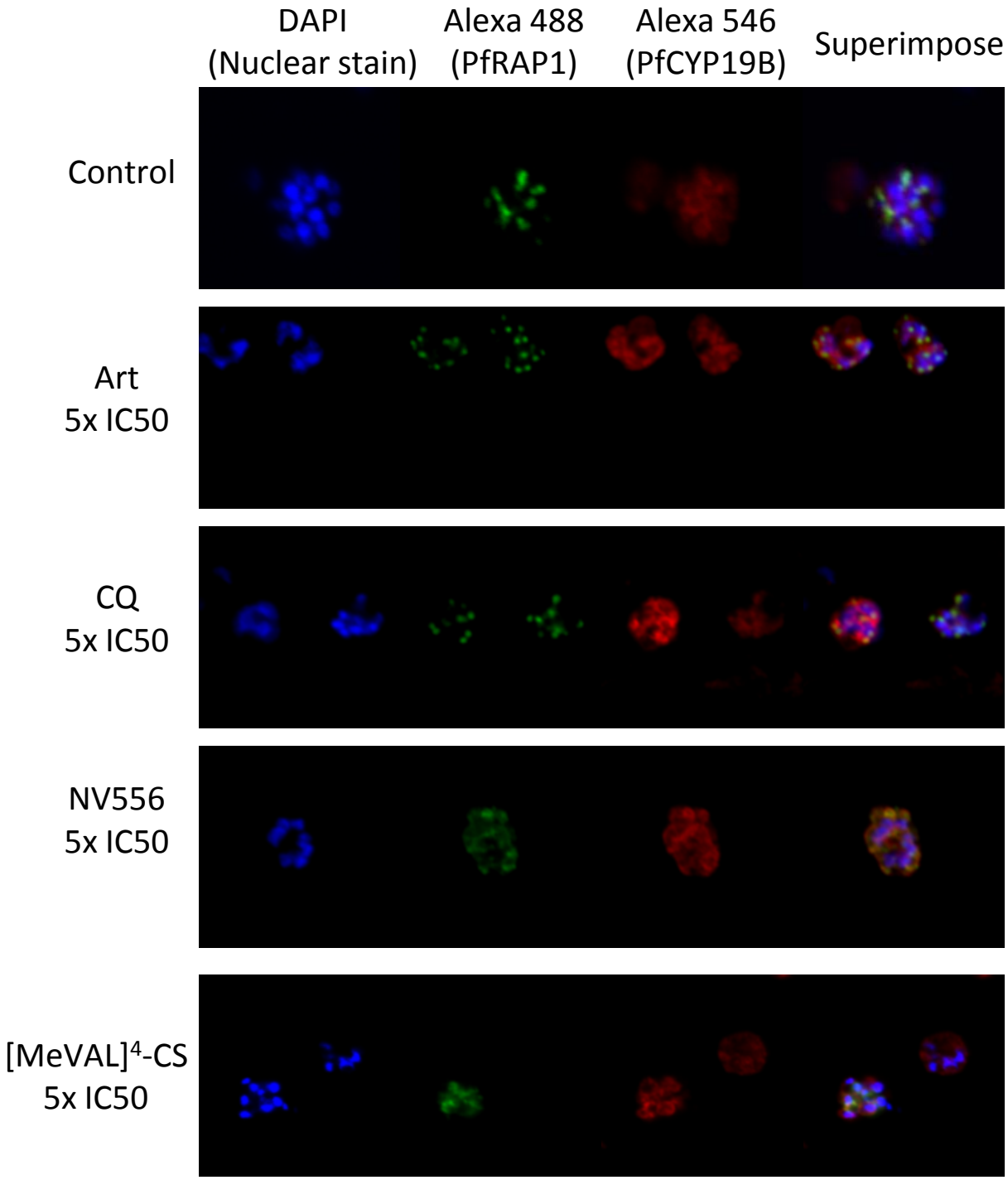

Figure 24: Confocal immunofluorescence microscopy of *P. falciparum* schizonts treated with artemisinin, chloroquine, [MeVal]^4-Cs and BC-556. Shizonts were stained with DAPI (nuclear), Alexafluor-488 (PfRAP1) and Alexafluor-546 (PfCYP19B).

It is well characterised that NV556 binds to other cyclophilins, however the ability of this ligand to bind to Plasmodium cyclophilins was unproven. In order to assess ligand binding to PfCYP19B we utilised the thermal stability shift assay described in section 2.7.7. This technique is discussed in more detail in section 5.3, briefly an increase in the peak of the first derivative of the melting curve indicates binding of a ligand to a protein. Utilising this technique we demonstrated clearly that NV556 is able to bind to recombinant PfCYP19B (Figure 25).

4.3.3.2 *Effect of immunophilin ligands on invasion of erythrocytes by merozoites*

To test whether the effect on RAP1 transport was mediated (i) directly by the action of cyclophilin ligands on some interaction in the rhoptry between cyclophilins and RAP1, perhaps causing it to become prematurely exported from the rhoptry once in place, or (ii) on earlier events in the erythrocytic cycle such as transport of RAP1 to the rhoptry, we also assessed the effect of the ligands used in the immunofluorescence assay on the ability of the parasite to invade erythrocytes. It is well known that RAP1 is critical for the invasive ability of merozoites and this assay (Section 2.2.5) was a relatively crude way to assess this process. It cannot differentiate between effects on merozoite release from schizonts, merozoite viability and invasion itself but it served well enough our purposes to show an effect by an inhibitor on the relative number of newly infected erythrocytes resulteing from treated parasites versus from an untreated control. The assay relies on the ability to generate high-purity schizont cultures at high parasitaemia by magnetic selection. Higher schizont numbers relative to trophozoites (which are also pulled out by magnetic selection,

but with lower affinity) were assured by over-loading the magnetic column with high-parasitaemia cultures to out-compete the binding of trophozoites with more schizonts. Schizonts were then incubated with whatever ligand was being tested at the desired concentration for ~2 h, washed to remove the ligand and introduced to fresh erythrocytes. The number of rings in the resulting culture was counted 14-16 h later and any reduction in this parasitaemia compared to a control was judged an effect on "invasion".

As shown in figure 25 the effect of these cyclophilin ligands on invasion was minimal. This supported our hypothesis that they are acting on cyclophilins at some point in the erythrocytic cycle before RAP1 is already in place in the rhoptry. As a whole these data indicate that inhibition of cyclophilins in early to mid stages of the erythrocytic cycle has an effect on the parasite's ability to transport RAP1 to its ultimate location in the rhoptry, and potentially indicate a role for cyclophilins in one or more of the transport pathways of rhoptry proteins.

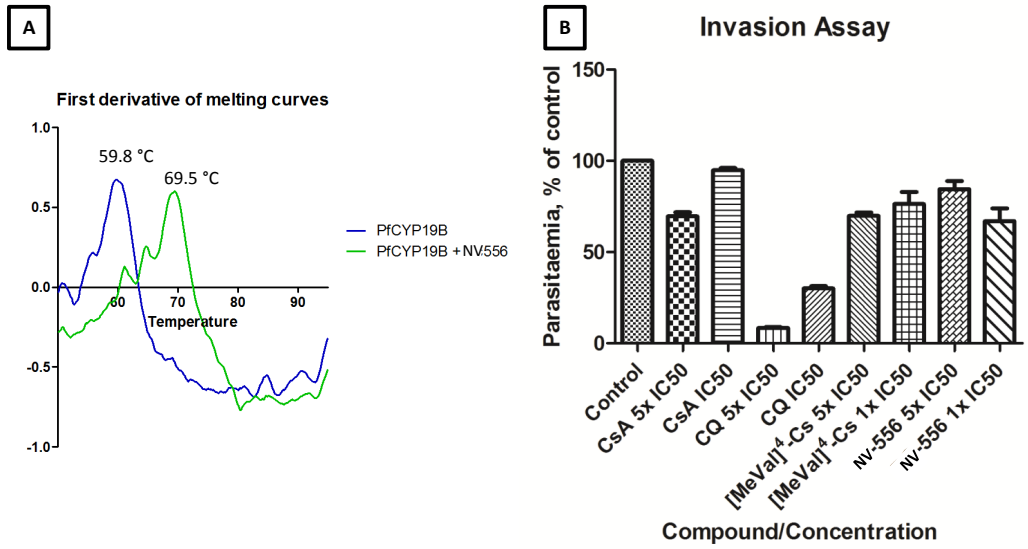

Figure 25: Binding of NV556 to PfCYP19B & Effect of various ligands on merozoite invasion of erythrocytes. (A) Binding of NV556 to PfCYP19B was assessed by thermal stability shift assay. Binding is indicated by an increase in the peak of the first derivative of the melting curves of a protein in the presence of a ligand. (B) The cyclophilin ligands CsA, [MeVal]^4-Cs and BC-556 and the antimalarial drug chloroquine (CQ) were incubated for 2 h with schizonts purified by magnetic selection followed by washing and mixing with fresh erythrocytes. The parasitaemia 14–16 h later was assessed by counting rings in giemsa-stained blood smears microscopically and expressed as a percentage of a control culture incubated with a vehicle only control.

4.4 DISCUSSION

The experimental work detailed in this chapter consist of the investigation of three potential immunophilin–protein interactions raised by the co-IP and yeast-2-hybrid analyses performed in the previous chapter.

We demonstrated by co-immunoprecipitation from whole parasite lysates that PfCYP19B was specifically able to interact with PfHsp70 *in vitro*. This has important implications in our understanding of the chaperone machinery in *P. falciparum*. PfHsp70 and PfHsp90 are known to interact in the parasite, and are apparently involved in a

high molecular weight chaperone machinery complex under normal erythrocytic growth conditions [16]. In other organisms this machinery consists of Hsp90, CYP40, FKBP52 (or FKBP51), and an additional p23 protein component, assembly of which is mediated by Hsp70 in association with accessory chaperones and co-chaperones Hsp40, Hip and Hop [133, 32, 123]. This complex is intimately involved in correct folding of certain nascent polypeptides, the most studied of which is the glucocorticoid receptor. The Hsp90 chaperone cycle is thought to progress as follows: an immature, incompletely folded protein is first bound by Hsp70 and its cochaperone Hsp40. These assembly chaperones then form an intermediate complex consisting of Hsp70, Hsp40, Hop, the incompletely folded protein and the Hsp90 dimer. The final complex is stabilised by PPIases and p23 binding to specific recognition sites on the Hsp90 dimer, followed by catalysis of protein folding, release of the folded protein and disassociation of Hsp90 from the rest of the complex components [97].

We hypothesise that in *Plasmodium* the major components of an analagous complex would be Hsp90, PfCYP19B, perhaps PfFKBP35 and PfP23 and their assembly is mediated by PfHsp70-I, DnaJ (putative Hsp40), PfHip and PfHop. Recent work by our lab has shown that inhibition of PfHsp70 has an antimalarial effect (W. Shaw, unpublished data, [38]). While there is a tendency in science to infer protein function, interactions and processes from data available in other organisms, it is important to confirm them experimentally. Simply inferring that an interaction occurs may lead one to miss out major differences in host-parasite biology, for example if one were to infer that FKBP–calcineurin interaction requires the presence of FK506 in all organisms, one would miss the fact that this interaction appears to take place without the drug in the parasite (discussed in more detail

in the next chapter). In all, the work detailed in this and the previous chapter supports but does not prove the involvement of *P. falciparum* immunophilins in the Hsp90 chaperone cycle and machinery.

We next demonstrated that PfFKBP35 specifically interacts with *P. falciparum* histones by far Western blotting. This is a relatively crude method for determining that two proteins interact, but the position of the bands on the blot indicated that the recombinant PfFKBD-His_6 used as the probe in the experiment interacts predominantly with PfH2B and PfH3 (~13.1 and ~15.5 kDa respectively). This agrees excellently with the data generated by Y2H analysis in chapter 3 which showed an interaction between the same proteins. The interaction with PfH3 is supported in the literature by evidence that the yeast FKBP Fpr4p acts as a PPIase on residues P30 and P38 on histone H3 in *S. cerevisiae*, but a review of the available literature reveals no evidence for a direct interaction between FKBPs and H2B in any organism.

The work to investigate whether PfFKBP35 was able to act as a histone chaperone analagous to FKBPs in *S. pombe* and *S. cerevisiae* led us to the conclusion that PfFKBP35 doesn't possess this ability under the conditions employed. This is not inconsistent with the literature, since the original researchers observed that histone chaperone action is independent of the PPIase domain and instead relies on an acidic/acidic/basic domain [91] which PfFKBP35 does not possess. There is evidence that nuclear FKBPs without this domain are able to act on histones, but this is an indirect action mediated through a secondary protein (Nelson CJ, poster, Functions of Nuclear FKBP proteins, conference on Cyclophilins and other Foldases, Halle, Sept 2013).

Positive results came from our investigation of the levels of H3K36 methylation in asynchronous parasites in culture. We know that yeast FKBPs act on histones by regulating methylation of H3K36, a methylation which is also present in *P. falciparum*, and that inhibition of the PPIase activity by rapamycin induces an increase in the levels of H3K36 methylation [119]. Parasites incubated with FK506, to inhibit the PPIase activity of PfFKBP35, demonstrated a dose dependent increase in the level of H3K36 methylation. A recent study demonstrated that methylation of H3K36 by the protein PfSETvs is important in silencing *var* genes and may have an important role in virulence [83]. Follow up work on the type of methylation regulated by PfFKBP35 and the effect of the methylation state regulated by the protein will be of great interest.

Finally we undertook an investigation into the putative interaction between the rhoptry protein RAP1 and the cyclophiln PfCYP19B. Currently there is only limited understanding of how rhoptries form and how proteins are transported to these structures. We hypothesised that since PfCYP19B is an abundant chaperone, it may potentially be involved in chaperoning RAP1 during transport to its ultimate location. The authors of a recent review into *Plasmodium* rhoptry proteins hypothesised a model for protein sorting in which proteins destined for the rhoptries are co-translationally inserted through Sec61 at the endoplasmic reticulum (ER) via their signal sequence and trafficked to the Golgi in COPII-coated vesicles. At the Golgi rhoptry-associated membrane antigen (RAMA) aggregates with other rhoptry bulb cargo, such as RAP1, and is transported to the rhoptry by budding off into clathrin-coated vesicles [40]. *Plasmodium* cyclophilins may be involved at any number of points along this modelled pathway. PfCYP19B has a cleavable signal peptide which appears to be

cleaved during the erythrocytic stage [65] but for which a function remains unclear perhaps it is involved during one or more of these rhoptry trafficking pathways.

We analysed sub-cellular location of RAP1 and PfCYP19B under normal culture conditions and in the presence of cyclophilin-ligand antimalarials as well as non-cyclophilin antimalarials. We reproduced clearly the bi-punctate staining characteristic of rhoptry proteins observed by Moreno *et al.* (2001) [115] as exhibited by RAP1 under normal culture conditions. We also demonstrated for the first time that in late schizont stages of *P. falciparum* in culture, PfCYP19B is clearly located in the cytosol of the developing merozoite, following on from work by Gavigan *et al.* (2003) [65] which demonstrated that PfCYP19B was cytosolic in the trophozoite stage of the parasite. In the presence of the cyclophilin-binding ligand CsA we demonstrated that the characteristic bi-punctate staining of RAP1 was disrupted in a concentration dependent manner, that RAP1 appeared to co-locate with PfCYP19B to some extent in the treated cells. With decreasing concentrations of CsA, the disruption of RAP1 location was lessened and that at very low concentrations of CsA (<0.04 x IC_{50}) there was no evidence of disruption. In order to decide whether this effect was mediated through the action of calcineurin or was as a direct effect of the inhibition of the cyclophilin we also assessed the ability of the non-calcineurin binding, cyclophilin ligands [MeVal]^4-Cs and BC-556 to disrupt the location of RAP1. Both of these compounds showed a similar effect on RAP1 location at similar concentrations to CsA (relative to their IC_{50}). Finally in order to determine whether this was just a general antimalarial effect we tested the classic antimalarial compounds artemisinin and chloroquine, neither of which disrupted RAP1 location. Our hypothesis therefore is that RAP1 location is de-

pendent on the action of one or more of the parasite's cyclophilins, most likely PfCYP19A or PfCYP19B since they are the major CsA binding cyclophilins.

To test whether this effect was directly on some interaction in the rhoptry between cyclophilins and RAP1 we also assessed the effect of the inhibitors used in the immunofluorescence assay on the ability of the parasite to invade erythrocytes. We saw very little effect on the invasive ability of merozoites, especially when compared to chloroquine, which is not thought to act particularly on merozoites. From this we concluded that the effect of these inhibitors, and most likely the cyclophilin–RAP1 interaction occur before the events which culminate in location of RAP1 in the rhoptry.

The data presented in this chapter (i) served to confirm *in vitro* the interaction between PfCYP19B and Hsp70, lending credence to the inferral of a Hsp90 based chaperone machinery/cycle in the parasite from other organisms; (ii) showed a possible new role for PfFKBP35 in the regulation of histone methylation, and (iii) demonstrated a potential role of *P. falciparum* cyclphilins in chaperoning RAP1, and possibly other proteins to the rhoptry.

5

INVESTIGATION OF A NOVEL PFFKBP35–CALCINEURIN INTERACTION

5.1 INTRODUCTION

FKBP's are named for their ability to bind FK506. Binding the drug leads to formation of a complex which binds to calcineurin in human T-cells, preventing the dephosphorylation of the cytosolic subunit of nuclear factor of activated T-cells (NF-AT). Phospho-NF-AT is then unable to translocate to the nucleus and initiate T-cell activation. This is classic description the immunosuppressive action of FK506. However, recently it was determined that the FK506-binding protein of *P. falciparum* is able to interact with and inhibit calcineurin (both mammalian [113] and parasite [90]) in an FK506-independent manner. Indeed, addition of FK506 to an assay measuring calcineurin phosphatase activity inhibition by PfFKBP35 had no measurable effect in the two independent studies of Monaghan & Bell (2005) [113], and Kumar et al. (2005) [90] though another group of investigators did observe FK506 dependence under their experimental conditions [178]. The *Plasmodium* FKBP is a multi-domain protein, consisting of a FKBD, three tetratricopeptide domains and a putative calmodulin binding site (figure 7). Previous work in our lab indicated that the FKBD was responsible for the protein's ability to bind calcineurin [113]. Obviously from a drug discovery point of view this is interest-

ing as any difference between host and parasite molecular biology might be an attractive drug target.

This chapter describes the work undertaken by *in vitro* and *in silico* methods to elucidate the nature of the difference between the *P. falciparum* FKBP and other FKBPs, such as the major human one hFKBP12, that causes this unusual interaction. In parallel to this was the attempt to confirm that the FK506-independent PfFKBP35–calcineurin interaction occurs *in vivo* (i.e. in intact parasites) by a number of protein-crosslinking techniques. The purpose of the latter study was to indicate that this is not just an *in vitro* artefact but is physiologically relevant to the parasite.

5.2 METHODOLOGY

Materials and methods used in this chapter are described in detail in chapter 2. Briefly, 3D modelling of the PfFKBP35 protein was undertaken using the MODELLER software from Salilab (UCSF, San Francisco, USA, www.salilab.org) and visualised using UCSF's Chimera software (plato.cgl.ucsf.edu/chimera). Cloning and protein purification were performed by standard methods. Functional and ligand-binding assessment by PPIase, thermal stability shift and phosphatase assays were performed as per previously published methods or manufacturer's instructions with minor modifications where appropriate. Construction of pMal-ΔNFKBD-His_6 was performed by Anais Roche under the author's supervision.

5.3 RESULTS

5.3.1 *3D Modelling of PfFKBP35–calcineurin complex*

Three dimensional modelling was undertaken to investigate *in silico* possible structural differences between the FK506-independent PfFKBP35–calcineurin interaction and the FK506-dependent interaction between hFKBP12 and calcineurin and to generate a model of the complete PfFKBP35 protein. Using the existing crystal structure of the hFKBP12 [72] as a template and subsequently the NMR solution structure of *P. falciparum* FK506-binding domain (FKBD) [86], homology models were generated of FKBD both from amino-acid sequence and from overlap of the Kang *et al.* (2008) [86] NMR solution structure (2VN1) using the MODELLER and CHIMERA programmes. More than 50 iterative models were generated for each and the best model was selected using its Discrete Optimised Protein Energy (DOPE) score. These models were then docked with the human calcineurin structure (1TCO) from the Griffith *et al.* (1995) [72] using CHIMERA's docking protocol. The model resulting from docking of the FKBD homology model to calcineurin is shown in figure 26 A, and the model generated by docking the NMR solution structure of the FKBD–FK506 complex to human calcineurin is shown in figure 26 B. Using the existing solution NMR structure of the FKBD and the X-ray diffraction structure crystal structure of the TPR domain [4], a composite model of PfFKBP35 was also developed using 50 iterative generations and the best model was selected by DOPE score (model not shown).

This 3D model highlights two interesting structural differences. The first is a possible role for the 15-AA N-terminal extension in the *Plas-*

modium FKBP's interaction with calcineurin (blue region in Fig. 26). The second difference is the loss of an α-helix on the composite surface that directly contacts calcineurin. In other models generated by this method, we observed that the "loop" structure (green in Fig. 26) turns over to occupy part of the FK506 binding pocket in the FKBD. It is possible that the loss of structure is as a result of the modelling conditions since the helix is present in the 2VN1 NMR solution structure of the FKBD complexed with FK506, but it is also possible that binding of FK506 induces a conformational change in the protein and causes the alpha helix to form. In terms of sequence similarity, this N-terminal extension is the most obvious difference between the *P. falciparum* FKBP35 and the human FKBP12 (Figure 27). As a result of these investigations we decided to attempt to make a truncation to the PfFKBD which removes the 15 amino acid N-terminal extension and to assess whether this was the causative agent of the FK506-independent interaction with calcineurin.

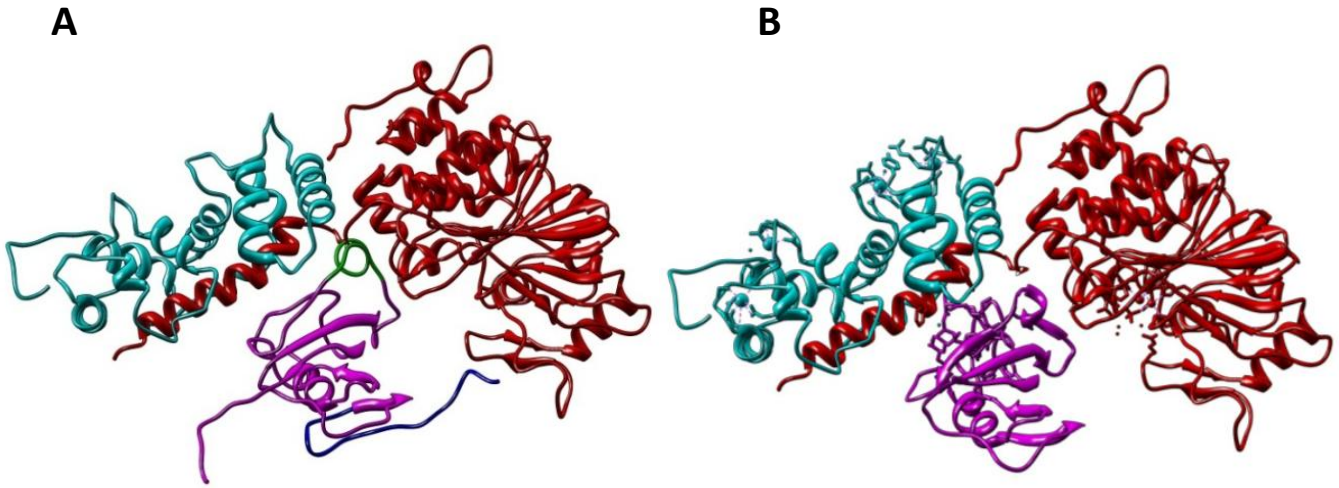

Figure 26: 3D modelling of PfFKBD. **A.** 3D model generated using MODELLER and CHIMERA showing PfFKBP's FKBD region docked with human calcineurin. **B.** hFKBP12-FK506-calcineurin crystal structure [86]. Side chains forming hydrogen bonds are shown in model **B** and hydrogen bonds are shown by dotted lines. Red – Calcineurin subunit A. Cyan – Calcineurin subunit B. Purple – part of PfFKBD (**A**) / FKBP12 (ribbons) and FK506 (sticks) (**B**). Blue – FKBD N-terminal extension. Green – loop structure of PfFKBP35 that differs in conformation from the homologous region in hFKBP12.

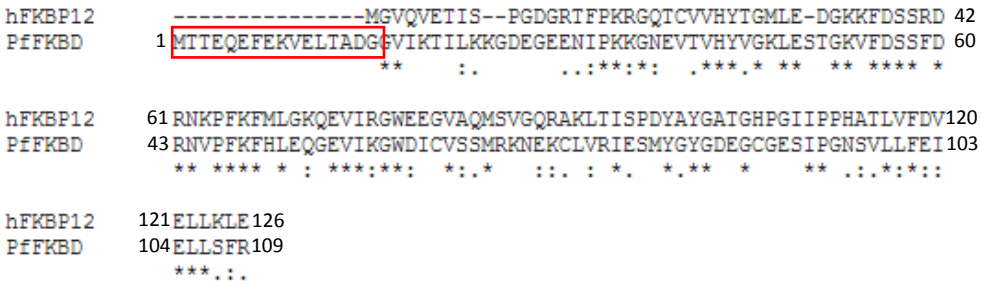

Figure 27: Sequence alignment of human FKBP12 with PfFKBD. The red box indicates 15 AA N-terminal extension. Identical residues are indicated with an asterisk, a colon indicates conservation between groups of strongly similar properties and a full stop indicates conservation between groups of weakly similar properties.

5.3.2 *Construction and purification of ΔNFKBD*

We successfully constructed a recombinant gene for the FK506-binding domain lacking the N-terminal 15 amino acids in the pMal-c2x vector plasmid and carrying a C-terminal hexa-histidine tag (Figure 28). This work was performed by Anais Roche under the author's supervision. This plasmid contained an N-terminal MBP-fusion protein which could be cleaved following nickel-chelate affinity chromatography. In our experience FKBD expressed in *E. coli* without this MBP tag is insoluble. The MBP tag perhaps assists in correct folding and the FKBD is soluble and functional following enzymatic cleavage. We successfully expressed the modified FKBD in *E. coli* and purified the protein by successive nickel chelate affinity chromatography, cleavage, and a final nickel-chelate chromatography (Figure 29). Though purification of the protein was successful the purity of the protein was very difficult to get to a level sufficient for protein based assays. As shown in figure 30 FKBD-His_6 purified by standard methods and concentrated ~35x was significantly more pure than ΔNFKBD-His_6 purified in the same manner, and optimisation attempts improved

the quality very little. We hypothesise that removal of those 15 amino acids from the N-terminus moves the two proteins (MBP and FKBD) much closer together and restricts access of the enzyme to the cleavage site. This in turn leads to more uncleaved protein purified in the eluate. In view of this problem it was determined that the uncleaved MBP-ΔNFKBD-His_6 would be used in further protein-based assays. This should present little problem since Monaghan et al. (2005) [113] demonstrated the FK506 independent interaction between calcineurin and PfFKBP35 using MBP-FKBD-His_6 in their experiments. Obviously we would have preferred to use the cleaved protein as it is perhaps slightly more convincing in terms of its physiological relevance but in this case it was not possible.

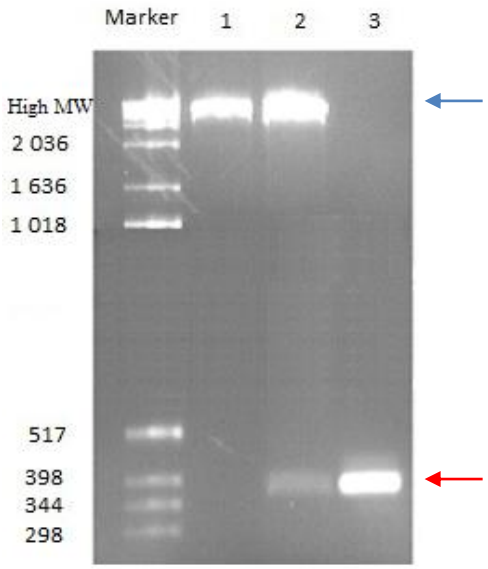

Figure 28: Analysis of pMal-ΔNFKBD-His_6 plasmid construct. Plasmid isolated from transformant colonies was subjected to digestion with *Bam*HI and *Xba*I, run through a 1% agarose gel and stained with ethidium bromide. Molecular weight marker sizes are in bp. Lane 1. ~0.2 µg unligated pMal-c2x plasmid. Lane 2. ~0.2 µg pMal-c2x ligated with ΔNFKBD-His_6 PCR product. Lane 3. ~2 µg ΔNFKBD-His_6 PCR product. Blue arrow: band at > 6800 bp corresponding to pMal-c2x. Red arrow: band at ~360 bp corresponding to ΔNFKBD-His_6 PCR product.

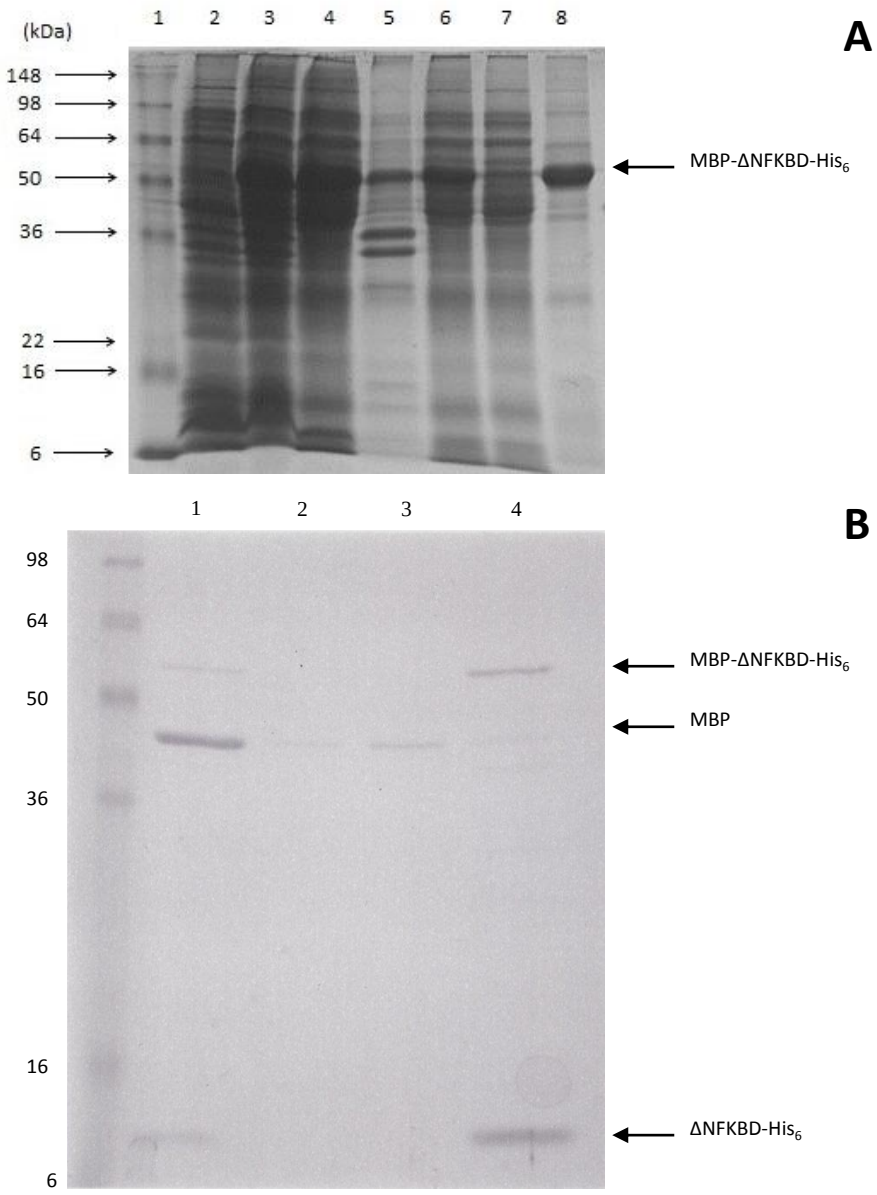

Figure 29: **A.** SDS-12.5% PAGE analysis of expression of pMal-ΔNFKBD-His_6 in *E. coli* and cleavage of the MBP-tag. Lane 1. Molecular weight marker; masses are in kDa. Equal volumes of lysates of *E. coli* transformed with pMal-ΔNFKBD-His_6 were loaded (Lane 2, pre-induction; Lane 3, post-induction with 0.35 mM IPTG). Cells lysed by passage through a French Press were centrifuged and equal volumes of clarified lysate (Lane 4) and insoluble pellet (Lane 5) were loaded. Clarified lysate was diluted ~1:5 and applied to a nickel chelate column (Lane 6, sample applied). The flow-through was checked to ensure binding of MBP-ΔNFKBD-His_6 (Lane 7). MBP-ΔNFKBD-His_6 was eluted with 200 mM imidazole (Lane 8). **B.** The eluate was dialysed overnight at 4 °C against 5 l MCAC-0 and 6.25 mg of recombinant protein were cleaved by incubation at 22 °C with factor Xa for 27 h. This was diluted ~1:7 in MCAC-0 and re-applied to a nickel chelate column (Lane 1, sample applied). The flow through was checked to ensure binding of ΔNFKBD-His_6 (Lane 2), washes were performed with 75 mM imidazole to remove loosely bound MBP (lane 3) and ΔNFKBD-His6 was eluted with 500 mM imidazole (Lane 4).

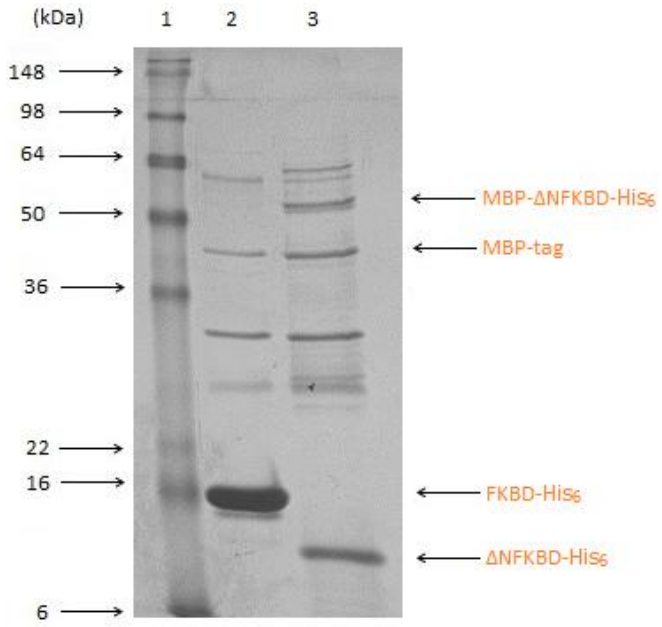

Figure 30: Purity comparison of FKBD-His_6 and ΔNFKBD-His_6 by electrophoretic separation on SDS 12.5%-PAGE. (Lane 1) Molecular weight marker; sizes in kDa. (Lane 2) ~ 5 µg total protein from nickel chelate FKBD-His_6 purification. (Lane 3) ~ 5 µg total protein from nickel chelate ΔNFKBD-His_6 purification. The arrows on the right hand side indicate the position of bands of interest.

5.3.3 *Functional assessment of ΔNFKBD*

5.3.3.1 *Thermal stability shift assay of FKBD and ΔNFKBD*

This assay (Section 2.7.7) is based on the ability of a fluorescent dye to bind to exposed hydrophobic regions in an unfolded protein. Denaturation by increasing temperature leads to the protein unfolding and the hydrophobic regions becoming exposed resulting in the dye binding and an increase in fluorescence. By this method it is possible to assess the quality of a protein preparation and to give some indication of whether a protein is folded [44].

Eleven buffers were tested to find the conditions in which the FKBDs would give the best melting curves: these buffers are detailed in section 2.7.7. Figure 31 shows the results of the buffer selection. Panel A and B are reproduced from Crowther *et al.* (2010) [44] to indicate melt curves representative of enzyme preparation quality for the reader's benefit. As can be seen in panels C and D both MBP-FKBD-His_6 and MBP-ΔNFKBD-His_6 had curves indicative of higher quality preparations in most of the buffers tested. From these buffers we selected buffer 4 (100 mM sodium citrate, pH 5.5) for use in further thermal melt experiments. It is important to note that in these graphs it is not the height of the curve (which is measured in arbitrary fluourescence units), but rather the *shape* of the curve which is indicative of the enzyme preparation's quality: low fluorescence at lower temperatures leading to a well defined peak which returns to low fluorescence as temperature increases.

Thermal melt can also be used to assess whether a protein binds to a ligand by a method known as thermal stability shift. In essence, if a protein or enzyme binds to a ligand that protein may become more stable and therefore more resistant to denaturation by heating resulting in a shift in the melting temperature of the protein. The melting temperature can be determined by finding the point of inflection (by first derivative) of the curve, which is the point at which the protein becomes completely unfolded and fluorescence starts to decrease due to protein aggregation. Once again it is important to note that it is not the height of the curve, but the point at which the curve peaks that is the important datum in this experiment. As seen in figure 32 the melting temperature of both MBP-FKBD-His_6 and MBP-ΔNFKBD-His_6 were the same, 57.9 °C, indicating that removal of the N-terminal 15-amino acid extension had no effect on

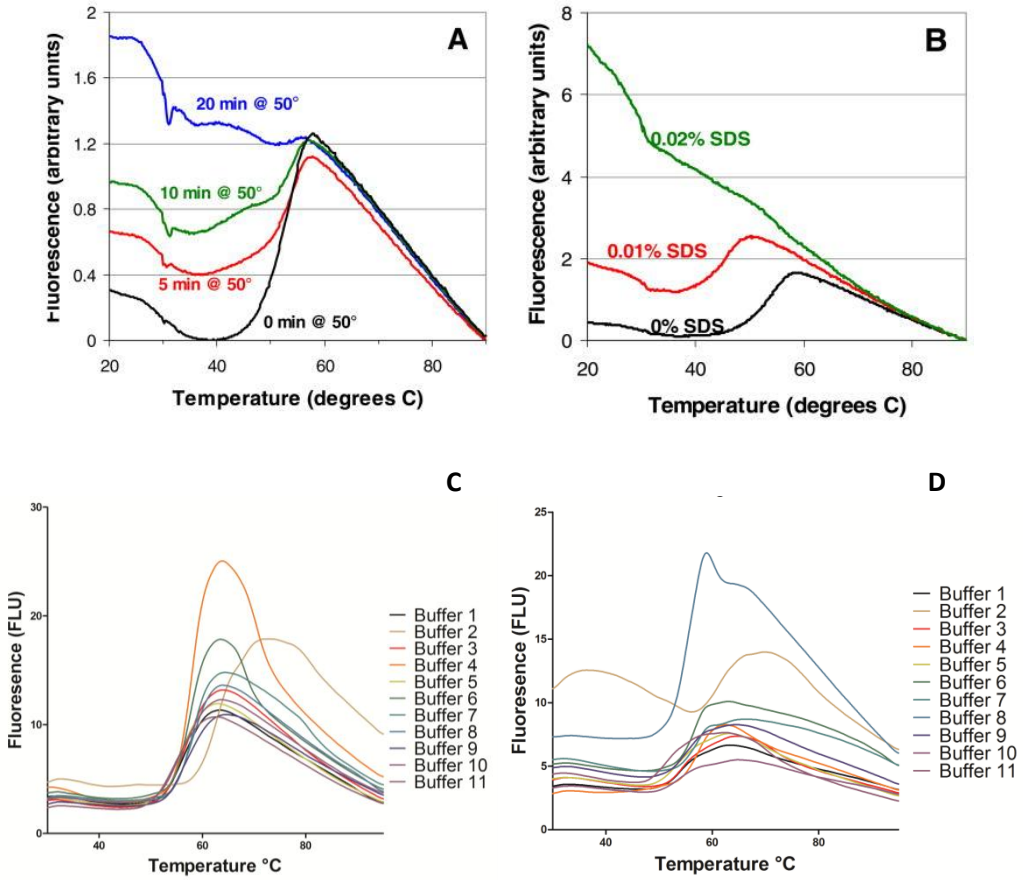

Figure 31: Thermal melt assay of MBP-FKBD-His_6 and MBP-ΔNFKBD-His_6. **A&B** are reproduced from Crowther *et al.* (2010) [44] for the reader's benefit to indicate melt curves representative of glyceraldehyde-3-phosphate dehydrogenase preparation quality. Also indicated on these graphs are the effects of denaturing the enzymes by heat or SDS on the resulting thermal melt curve. The lower two panels show the thermal melt curves of **C.** 1 µM MBP-FKBD-His_6 and **D.** 1 µM MBP-ΔNFKBD-His_6 in 11 buffers (Section 2.7.7) to identify the optimum buffer for further experimentation.

the thermal profile of the protein. This is in keeping with data from 3D homology modelling in which the N-terminal extension appeared to be quite disordered and didn't possess secondary structure. We also confirmed that MBP-FKBD-His_6 possessed FK506-binding ability, demonstrated by the shift in melting temperature from 57.9 °C to 59.7 °C (figure 32, panel B). Interestingly MBP-ΔNFKBD-His_6 appeared to be unable to bind FK506 at the same concentration (figure 32, panel C) according to this method. This could mean one of two things: either the 15 amino acid extension is somehow involved in the ability of the protein to bind FK506, or (in spite of the indication from these thermal melt experiments that MBP-ΔNFKBD-His_6 appeared to possess a folded profile similar to that of the untruncated protein) it did not possess the correct secondary structure. If, in the second case, ΔNFKBD-His_6 was unfolded, perhaps the signal from unfolding maltose binding protein masks that of the unstructured ΔNFKBD-His_6. We believe the second possibility not to be the case since an unfolded protein should give a high fluorescence reading starting at low temperatures as its hydrophobic residues are exposed and bound to the flourescent substrate, and we saw no evidence of this. In order to investigate this further we performed the thermal stability shift assay using rapamycin (RAP), another FKBP ligand. Once again MBP-ΔNFKBD-His_6 appeared unable to bind the ligand tested (figure 32, panel D). Also tested was the effect of increasing concentration of both FK506 and RAP at 5, 25, 125 and 625 µM on MBP-ΔNFKBD-His_6 (data not shown). Once again no shift in melting point was observed, suggesting that there was not just a reduced affinity for FK506 and RAP but a complete loss of ligand binding ability.

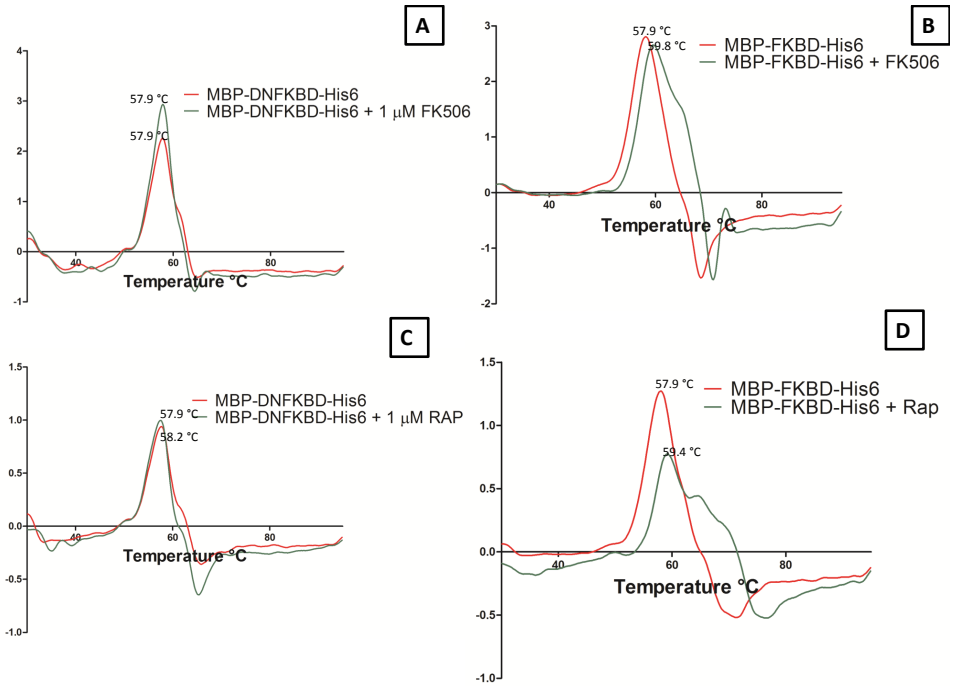

Figure 32: Thermal stability shift assay, showing **A.** 1 µM MBP-ΔNFKBD-His_6(red) and 1 µM MBP-ΔNFKBD-$His_6$with 1 µM FK506 (green). **B.** 1 µM MBP-FKBD-His_6(red) and 1 µM MBP-FKBD-$His_6$with 1 µM FK506 (green). **C.** 1 µM MBP-ΔNFKBD-His_6(red) and 1 µM MBP-ΔNFKBD-$His_6$with 1 µM rapamycin (green). **D.** 1 µM MBP-FKBD-His_6(red) and 1 µM MBP-FKBD-$His_6$with 1 µM rapamycin (green).

5.3.3.2 *PPIase activity of FKBD and ΔNFKBD*

Next, the recombinant protein was assayed in order to determine whether it retained the characteristic peptidyl-prolyl *cis-trans* isomerase (PPIase) activity. This assay is based on measuring the isomerisation of a peptidyl-prolyl bond in an artificial tetrapeptide substrate. The substrate, N-succinyl-Ala-Leu-Pro-Phe-*p*-nitroaniline, is linked at the C-terminus to the chromagen *para*-nitroaniline (*p*-NA), which is cleavable from the peptide by the action of α-chymotrypsin if the Leu-Pro bond is in the *trans* conformation. The amount of free p-NA in solution can then be measured spectrophotometrically by absorbance at 390 nm. The PPIase activity of an enzyme added to this assay can be determined by measuring the change in the rate of the release *p*-NA compared to an enzyme free control.

The PPIase activity is determined by the shape of the curve. The steeper the curve is the closer to t = 0, the more activity the protein has. Background conversion is assessed and subtracted from rate constants in the presence of enzyme. We purified FKBD-His_6 (Monaghan & Bell, 2005) [113] and assessed PPIase activity at 250 nM. It is clear from the resulting curve FKBD-His_6 has PPIase activity (Figure 33, A), and that it is strongly inhibited in the presence of the ligands FK506 and Rap. Conversely ΔNFKBD-His_6 at 250 nM had no discernible difference in slope compared to the background (data not shown). The concentration was subsequently increased to 5 µM and did appear to have a slight difference in slope compared to background (Figure 33, B) but the effect of FK506 and Rap is not apparent from just the shape of the curve.

After analysis of the curves, the data were transformed mathematically in order to generate the rate constants for PPIase activity of each

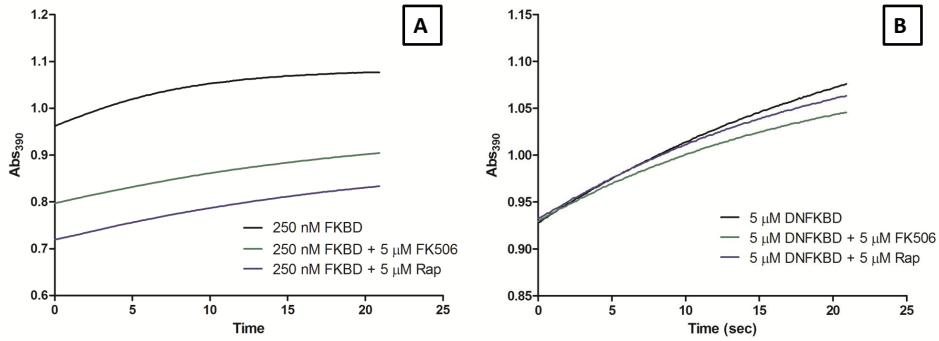

Figure 33: PPIase activity of FKBD-His_6 (FKBD) and ΔNFKBD-His_6 (DNFKBD). FKBD and DNFKBD were used in the assay at 250 nM and 5 μM respectively, either on their own or in the presence of 5 μM FK506 or Rap. Representative curves show increase in absorbance over time.

enzyme, as shown in figure 34. According to these data, FKBD-His_6 at 250 nM has a rate constant of 0.08432 ± 0.00982 s^{-1}. ΔNFKBD-His_6 by contrast has no discernible rate constant above background (data not shown). Indeed, we needed to raise the concentration of ΔNFKBD-His_6 to 5 μM before a rate concentration was apparent: this value was 0.0121 ± 0.00085 s^{-1}. In terms of the effect of FK506 and Rap on ΔNFKBD-His_6, we observed that Rap had no statistically significant effect but FK506 did. Though the rate constants in each case were very close (0.0035 ± 0.00035 s^{-1} for FK506 in the presence of and 0.00815 ± 0.003055 s^{-1} in its absence) and it is not easy to draw convincing conclusions from these data. What is clear though is that the N-termial truncation has a very significant effect on the PPIase activity of the FKBD, reducing it by ~200 fold.

5.3.3.3 *Phosphatase inhibition assay of binding to calcineurin by FKBD and ΔNFKBD*

The ProFluor® Ser/Thr PPase Assay measures purified serine/threonine protein phosphatase activity. The assay begins with a stan-

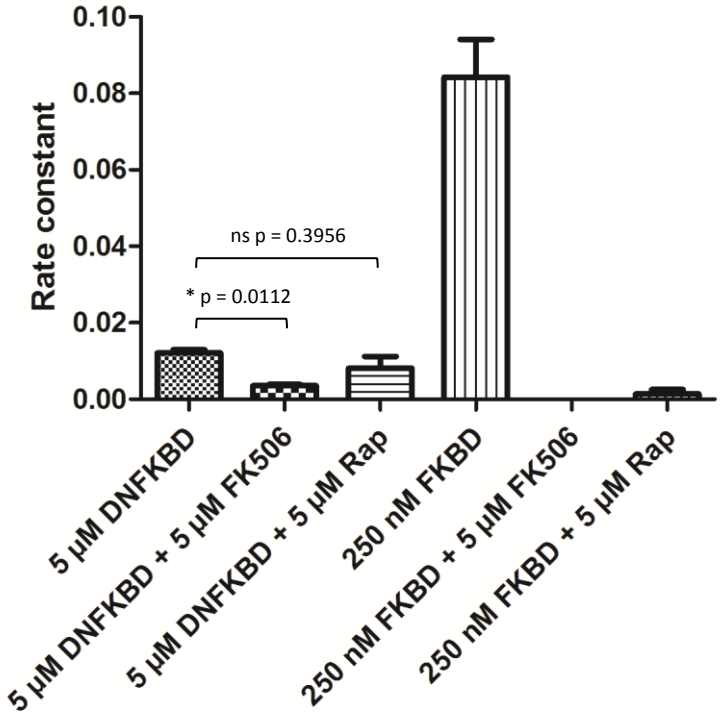

Figure 34: Rate constants of the PPIase activity of FKBD-His_6 and ΔNFKBD-His_6. The rate constants for FKBD and ΔNFKBD, in the presence or absence of ligands, were determined by calculating the natural logarithm of the remaining substrate (by the formula $(A_{max}-A_{390})/0.0133$ = *cis* remaining [in µM]) vs. time and taking the slope of the resulting curve.

dard phosphatase reaction performed in the reaction buffer with the provided phosphorylated bisamide rhodamine 110 peptide substrate (S/T PPase R110 Substrate) and Control AMC Substrate that serves as a control for compounds that may inhibit the protease. In this configuration, both the S/T PPase R110 Substrate and Control AMC Substrate are nonfluorescent. Following the phosphatase reaction, adding a protease solution simultaneously stops the phosphatase reaction and completely digests the dephosphorylated S/T PPase R110 Substrate and the Control AMC Substrate, producing highly fluorescent rhodamine 110 and AMC. Phosphorylated S/T PPase R110 Substrate, however, is resistant to protease digestion and remains nonfluorescent. Thus, the R110 fluorescence intensity measured in the assay is correlated with phosphatase activity in the presence of active protease, and the AMC fluorescence intensity is an indication of protease activity. A compound that only inhibits the phosphatase will decrease the R110 fluorescent signal as will a compound that only inhibits the protease. In this way the assay distinguishes between phosphatase inhibition and protease-inhibition.

As shown in figure 35, recombinant ΔNFKBD had a much reduced ability to inhibit the phosphatase activity of calcineurin at the concentrations tested regardless of the presence of FK506. There is no statistically significant difference between calcineurin on its own or in the presence of 1 µM MBP-ΔNFKBD-His_6 or 1 µM MBP-ΔNFKBD-His_6+ 1 µM FK506. We were also able to replicate the results of Monaghan et al (2005) showing ~50% inhibition of calcineurin by MBP-FKBD-His_6. This inhibition of calcineurin by MBP-FKBD-His_6 was statistically significant.

Overall the results of the experiments in this section indicate that the truncated form of FKBD appears to be folded, is unable to bind

FK506 and Rap, possesses very little PPIase activity, and is unable to inhibit the phosphatase activity of calcineurin.

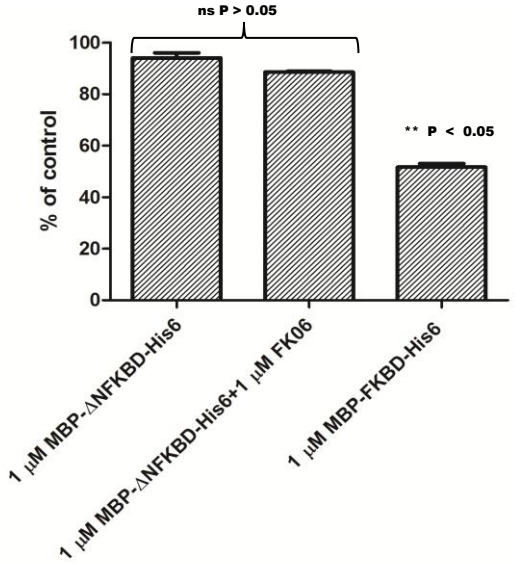

Figure 35: Inhibition of calcineurin phosphatase activity by FKBD and ΔNFKBD. Activity of calcineurin was measured by the fluorescence of a rhodamine-conjugated peptide substrate that, upon dephosphorylation by calcineurin, is digested by a protease, releasing highly fluorescent rhodamine. The fluorescence attributable to 40 nM calcineurin was set as 100%. The effects of various proteins and/or drugs on the activity of calcineurin were assessed. Bars show the SEM of three or more replicate experiments. To ensure that reduced fluorescence was not due to inhibition of the protease, a control peptide whose fluorescence is independent of phosphorylated state was incorporated into each reaction. No inhibition of protease occurred (data not shown).

5.3.4 *Studies of PfFKBP35–calcineurin interaction in intact parasites*

In vivo crosslinking is a powerful tool for investigating protein–protein interactions. We attempted two methodologies to crosslink PfFKBP35 to calcineurin. The first, photo-crosslinking, used a photoactivatable amino acid derivative, photo-leucine, which contains a diazirine ring for ultraviolet (UV) photo-crosslinking of proteins. Photoactivation

of the diazirine ring creates a reactive carbine intermediate that irreversibly crosslinks proteins that closely interact with each other. Parasites grown in leucine-free medium supplemented with photo-leucine should incorporate it into newly synthesised proteins and this should allow *in vivo* crosslinking. The second, chemical-crosslinking, used the chemical-crosslinking reagent disuccinimidyl suberate (DSS). DSS is a noncleavable and membrane permeable crosslinker that contains an amine-reactive N-hydroxysuccinimide (NHS) ester at each end of an 8-carbon spacer arm. NHS esters react with primary amines at pH 7–9 to form stable amide bonds, along with release of the N-hydroxysuccinimide leaving group. Proteins generally have several primary amines in the side chain of lysine (K) residues and the N-terminus of each polypeptide that are available as targets for NHS-ester crosslinking reagents.

5.3.4.1 *Photo-crosslinking analysis of PfFKBP35–calcineurin interaction*

In order to confirm that PfFKBP35 interacts with calcineurin in an FK506 independent manner in intact *Plasmodium* cells, parasites were grown in leucine free culture medium which had been supplemented with either 4 mM L-leucine (Fig. 36, A) or 4 mM photo-leucine (Fig. 36, B) for approximately 6 generations (3–5 days depending on initial parasitaemia). As shown in Fig. 36, those parasites grown in photo-leucine showed complete loss of viability when compared to those grown in culture medium supplemented with L-leucine. This is in contrast to mammalian cells; a wide variety of cell lines (including HeLa, HepG2, 239T and others) have been successfully grown in 4 mM photo-leucine [152]. Total loss of growth was evident after a very short period of time. This leads to the conclusion that photo-leucine is unsuitable for use with *P. falciparum* in erythrocyte culture.

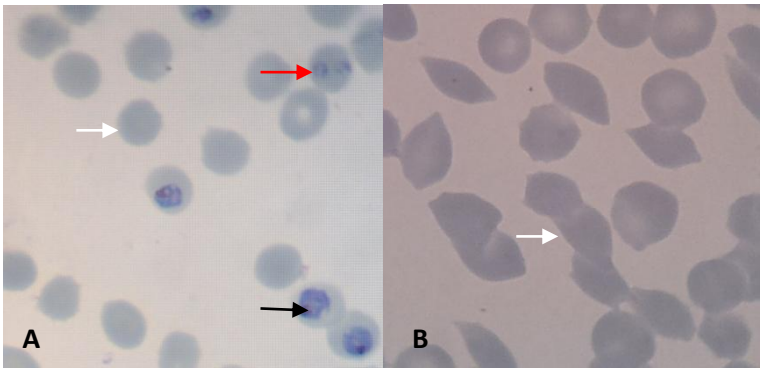

Figure 36: Giemsa stained smear of erythrocytic *P. falciparum* culture treated with L-leucine or photo-leucine. White arrows indicate erythrocytes. **A.** Parasites grown for 6 generations in leucine free culture medium, supplemented with 4 mM L-leucine. Arrows indicate stained parasites (black = trophozoite, red = ring stage) **B.** Parasites grown for 6 generations in leucine free culture medium, supplemented with 4 mM photo-leucine.

5.3.4.2 *Chemical crosslinking*

We attempted chemical-crosslinking by a number of methods. First, crosslinking in culture, then crosslinking after lysis of erythrocytes but before parasite harvesting, then on intact parasites after harvesting. In all cases, where it was possible to analyse samples by SDS-PAGE and Western blotting (in the second case large scale crosslinking of haemoglobin from erythrocytes rendered samples unuseable), there was no evidence of protein crosslinking. At the time these experiments were performed the anti-PfFKBP35 antibody had not yet been produced so Western blots were performed using anti-PfCYP19B as a proof-of-concept, the intention being to optimise crosslinking using the antibody available and subsequently repeat the experiment when anti-PfFKBP35 was produced. We quickly came to the conclusion that DSS does not appear to crosslink proteins in *P. falciparum* under the conditions tested. Whether this is because of differences in the parasite membrane that render it impermeable or that the conditions tested weren't suitable for crosslinking (though they were the condi-

tions described in the literature and in protocols for protein crosslinking in other cell types) is unclear. Figure 37 is representative of the Western blots from *in vivo* chemical crosslinking experiments. We also tested DSS crosslinking in parasite lysates, in which case it did appear that DSS was able to crosslink proteins. Unfortunately the crosslinking appeared to be total in a very short amount of time, rendering much of the protein unable to enter the SDS polyacrylamide gel (Figure 38). From these results we concluded that while DSS does appear to effectively crosslink parasite proteins when they are in solution, it seems to be unable to perform the same function on parasite proteins in the cell, perhaps because the parasite membrane is impermeable to the compound.

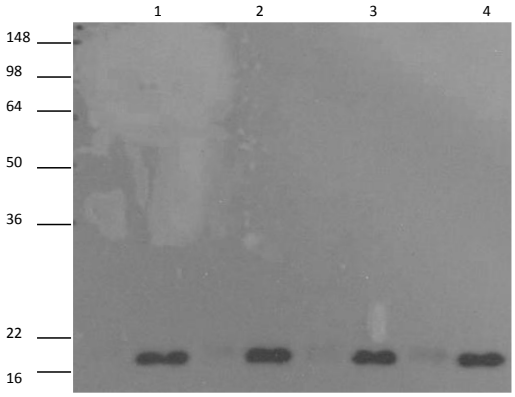

Figure 37: Treatment of saponin harvested parasites with disuccinimidyl suberate. Saponin harvested parasites were incubated with the chemical crosslinker DSS for 1 min, quenched with 250 mM Tris-HCl pH 8.0 for 20 min before being lysed by incubation with 0.5% (v/v) Triton X-100 on ice for 30 min and analysed by SDS-12.5% PAGE and Western blot with anti-PfCYP19B. Lane 1. 5 mM DSS. Lane 2. 1 mM DSS. Lane 3. 0.2 mM DSS. Lane 4. 0.05 mM DSS. Molecular weight is indicated on the left in kDa.

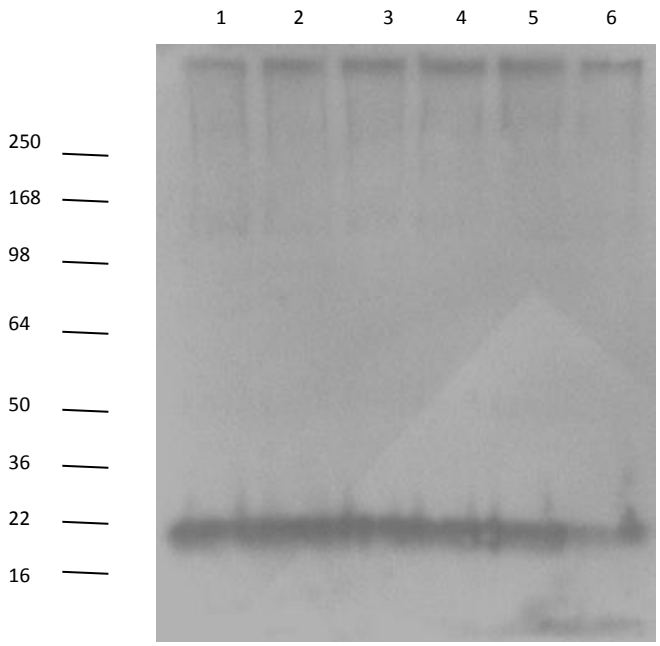

Figure 38: Treatment of saponin harvested parasites, lysed and subsequently incubated with the chemical crosslinker DSS. Saponin harvested parasites were lysed by incubation with 0.5% (v/v) Triton X-100 on ice for 30 min, incubated with the 0.5 mM DSS for 1 min, quenched with 250 mM Tris-HCl pH 8.0 for 20 min before being analysed by SDS 12.5% PAGE and Western blot with anti-PfCYP19B. Lane 1. 2 min incubation. Lane 2. 4 min incubation. Lane 3. 6 min incubation. Lane 4. 8 min incubation. Lane 5. 10 min incubation. Lane 6. 12 min incubation. Molecular weight is indicated on the left in kDa.

5.4 DISCUSSION

The primary aim of the research described in this chapter was to investigate the nature of the FK506-independent interaction between PfFKBP35 and calcineurin reported in the literature. There is some disagreement on whether this interaction with calcineurin occurs at all [113, 90, 86]. As mentioned in the introduction (section 5.1) two groups have demonstrated that PfFKBP35 and calcineurin interact in an FK506 independent manner [113, 90], while another group demon-

strated that they require FK506 to interact [86]. This disagreement may be due to differences in the methodology. For example the Kumar *et al.* (2005) study used recombinant *P. falciparum* calcineurin, the Monaghan & Bell (2005) study used calcineurin purified from bovine brain and Kang *et al.* (2008) used recombinant human calcineurin. Monaghan & Bell (2005) recombinantly expressed PfFKBP35 tagged at the N-terminus with MBP and at the C-terminus with His_6, Kumar *et al.* (2005) used recombinant N-terminally His_6 tagged PfFKBP35 and Kang *et al.* (2008) recombinantly expressed only the FKBP with no tag. All three studies also used different concentrations from one-another of FKBP, calcineurin and FK506 as well as different ratios between them in their assays.

Initially we studied the interaction between the two proteins *in silico* by constructing a homology model based on available crystal structures of FKBPs from other organisms in complex with calcineurin. By this method we were able to point out two major differences between *P. falciparum* FKBD and hFKBP12. The first is the presence of an N-terminal 15 amino acid extension, which appears to be in a position to interact with the B-subunit of calcineurin according to our 3D model. The second is the loss of secondary structure of an alpha-helix near the active site of the protein. We hypothesised that since the N-terminal extension was such a major difference between the FKBPs it may play a role in this novel interaction (also data from our 3D homology modelling indicated that this region was particularly disordered, in that it fell into no particular conformation). We were successfully able to construct a recombinant protein which lacked this extension.

Cleavage of the purified protein from its maltose-binding protein tag proved to be difficult. It appeared that due to the truncation the enzymatic cleavage was far less efficient than in the full–length

protein. This led to two problems. The first was contamination of the final product by uncleaved protein and the second was that due to increased incubation time there was a very significant increase in protein breakdown. Since the FK506-independent interaction was however shown with MBP-FKBD-His_6 [113] we decided that studying MBP-ΔNFKBD-His_6 would still provide relevant results. Interestingly MBP-ΔNFKBD-His_6 no longer possessed the ability to bind the well known FKBP ligands FK506 and rapamycin according to the thermal stability shift experiments. We then investigated whether the truncated protein retained PPIase activity, and demonstrated that MBP-ΔNFKBD-His_6 did have *cis-trans* isomerase activity but approximately 200 fold lower than the activity of the untruncated protein. Two possible conclusions could be drawn from these data, either that the truncation rendered the recombinant protein unable to fold correctly or that the N-terminal domain was somehow involved in enzymatic activity and ligand binding. Neither of these conclusions seems likely, since the truncated protein retains PPIase activity (albeit significantly reduced) and FKBP's from other species lacking the N-terminal extension still have activity, as well as the experiments that demonstrated that the truncated protein retains a 'normal' thermal melt profile. We then proceeded to investigate whether this truncated recombinant protein was able to interact with calcineurin in the manner described for the untruncated FKBD by Monaghan & Bell (2005) [113]. The basis for this investigation is that the presence of an interacting protein in solution interferes with calcineurin's ability to dephosphorylate a substrate. We saw the same result demonstrated previously, that MBP-FKBD-His_6 inhibited dephosphorylation of the R110 substrate by approximately 50%, in the author's opinion this datum contributes to the confidence that the FK506 independent in-

teraction is indeed a valid observation, by eliminating one of the differences (purified bovine vs. recombinant human calcineurin) as the source in the different results observed by the three research groups. MBP-ΔNFKBD-His_6 appeared to be unable to inhibit dephosphorylation in the same manner, but if this effect were ~200 fold reduced, as was the PPIase activity, we would be unable to detect it.

These data are difficult to interpret. It seems unlikely that this relatively disordered 15-amino acid extension could have such an effect on the FKBD but it is clear that this is the case. The protein is likely folded, since the thermal melt profile is characteristic of a folded protein, so the question that then arises is: is it folded correctly? The answer to this question is unclear. The apparent lack of the ability of the protein to bind FK506 and Rap in the thermal stability shift would tend to indicate that ΔNFKBD-His_6 does not possess the correct secondary structure (though 200 fold reduced FK506 and Rap binding would be undetectable), but then again it does possess at least some PPIase activity for which correct secondary structure is absolutely required. Perhaps what has occurred is that removing the N-terminal extension has a significant effect on the protein's ability to spontaneously adopt the correct secondary structure but a small subset (say 1 in 200) of ΔNFKBD-His_6 units do manage to fold correctly. This would lead to the observed decrease in PPIase ability, and also to the apparent lack of ligand binding (since the fluourescent signal from incorrectly folded ΔNFKBD-His_6 would mask the shift in fluorescent signal of the folded protein due to the relative abundance of each). In light of this it is difficult to draw conclusions based on the phosphatase inhibition assay. If we could conclusively say that the protein was correctly folded but lacked PPIase and ligand binding activity then it would be easy to conclude that the N-terminal extension plays

a major role in these effects and in the ability to bind calcineurin independently of the presence of FK506. But since we cannot say that the truncated protein is definitely folded correctly we cannot say whether or not the FKBP–calcineurin interaction is affected at all from the data presented herein. In the author's opinion incorrect protein folding is an unlikely explanation for the results presented herein, due to the observation that the truncated and wild type FKBD possess the same thermal melt profile. One would expect an altered secondary structure to have an effect on both the profile and the melting temperature of the protein and there is no sign of this occuring, nor can protein aggregation explain the results observed adequately since an aggregated FKBD would similarly affect the melt profile and melting temperature.

One further possibility which should be considered is that the *P. falciparum* possesses two significant amino acid substitutions. Substitution of the hydrophobic doublet (Gly89/Ile90) from hFKBP12 to a hydrophilic doublet (Glu108/Ser109) in PfFKBP35. This region is exceptionally conserved in the FKBP family, occurring within a region where two loops that interconnect β-strands cross each other – a highly unusual topological feature that, prior to the determination of the structure of FKBP domains, was thought to be prohibited in anti-parallel β-sheets due to difficulties in packing side chains efficiently [136]. In the wild type protein these substitutions may change the active site of PfFKBP35 sufficiently to prohibit FK506 and Rap binding and greatly reduce PPIase activity and calcineurin inhibitory activity, but the N-terminal extension performs some allosteric function which changes the conformation of the active site sufficiently to restore these properties. If this case is true then the N-terminal extension could be considered of major importance for the activity

of PfFKBP35 despite seeming relatively disordered. This hypothesis seems like it would be relatively expensive in terms of fitness, as synthesising a 2-kDa extension must surely be more costly to the parasite than simply mutating two protein coding sequences from Glu/Ser to Gly/Ile. Perhaps the N-terminal extension encodes some novel signal sequence that is required for its correct transport to perform some important function in the life cycle and this prohibits these mutations. Further work may elucidate whether the N-terminal extension has an effect on the protein's ability to fold correctly, or it is involved in altering the active site in some way. Particularly it would be interesting to revert Glu108/Ser109 to Gly108/Ile109 in concert with the N-terminal truncation to see what effect that has on PPIase activity and calcineurin inhibition.

In parallel with the discussed *in vitro* work was the attempt to demonstrate the interaction *in vivo* by several protein-crosslinking techniques. Unfortunately it appears that *P. falciparum* is particularly intractible to study by these methods. There is some evidence that the parasite keeps PfFKBP35 and calcineurin in separate parts of the cell during its life cycle [90], (PfFKBP35 in the nucleus and calcineurin in the cytoplasm). This may be because of the ability of PfFKBP35 to inhibit calcineurin, and perhaps the parasite needs to appropriate host FKBPs for cytoplasmic use. Still, because of the definite difference between the parasite FKBP and most other FKBPs, PfFKBP35 remains an attractive drug target.

6

GENERAL DISCUSSION

This study has investigated the protein–protein interactome of the major immunophilins PfCYP19A, PfCYP19B and PfFKBP35 of *P. falciparum* with a view to understanding better the mechanism of antimalarial action of the immunosuppressive ligands CsA and FK506 and the cellular functions of these immunophilins. In addition this study investigated the basis of the FK506-independent PfFKBP35–calcineurin interaction previously reported [113]. The work has encompassed studies with intact parasites, parasite extracts and recombinant parasite proteins and has added to the understanding of the biological roles of these proteins during the parasite erythrocyte life cycle.

6.1 THE INTERACTION NETWORK OF PARASITE IMMUNOPHILINS

The molecular characteristics of PfCYP19A, PfCYP19B and PfFKBP35 were well established before this study began [113, 65]. All three immunophilins were known to possess PPIase activity, which was inhibited by CsA and FK506 in the cases of CYPs and FKBPs respectively, and they were also known to possess molecular chaperone activity in assays with model substrates. PfFKBP35 was known to interact with PfHsp90 via its TPR domain *in vitro*. No other data were available to indicate which parasite proteins these immunophilins interact with

or what the molecular target or targets of CsA, FK506 and their non–immunosuppressive derivatives were.

The work performed in this study illustrated for the first time a number of putative immunophilin–protein interactions. These interactions were identified by two methodologies, co-IP and Y2H. We have demonstrated that co-IP specifically and reproducibly pulls down a number of protein bands and identified a large cohort of putative immunophilin–protein interactions, 161 PfCYP19A interacting, eleven PfCYP19B interacting, and 113 PfFKBP35 interacting proteins. Many of these interactions overlapped between immunophilin targets and we were able to generate an interaction map consisting of 211 unique protein identifications not counting the immunophilins themselves. In addition to these data we identified 11 putative PfFKBP35 interacting proteins by Y2H analysis, which were also included in the interaction map.

These interactions can be broadly grouped in two ways, firstly into singly, doubly and triply interacting proteins and secondly into 10 categories based on each protein's GO annotation. By grouping the putative interacting partners in this way we were able to generate an interaction map (Figure 16) which provided an excellent way to visualise these interaction data.

We have highlighted a number of interactions which we believe to be important to the biology of the parasite, for which there are strong supporting data from other organisms, or for which we have an indication of interaction from two sources. Specifically we believe all three immunophilins interact with large portions of *P. falciparum's* heat shock machinery; all co-IPs pulled down Hsp90 and four Hsp70 isoforms (Hsp70, Hsp70-2, Hsp70-3 and Hsp70-x). PfFKBP35 pulled down a putative Hsp90 and a putative DnaJ (Hsp40) protein, though

with low peptide coverage; DnaJ was also indicated as a putative interaction by our Y2H study. PfCYP19A pulled down Hsp60 with 21 peptides identified by mass spectrometry covering 41% of the protein. Additionally both PfCYP19A and PfFKBP35 pulled down another Hsp70 isoform (Hsp70-z) and Hsp70/Hsp90 organising protein. We believe these to be important putative interactions because of analagous interactions in other organisms such as the steroid receptor complex in humans [134], as well as the general importance of heat shock proteins for parasite biology [1].

We also highlighted the putative interaction of PfFKBP35 with the nucleosome complex of *P. falciparum*. Our Y2H study indicated a putative interaction between PfFKBP35 and the histones H2B and H3. Co-IP with PfFKBP35 also pulled down H2B and H3, along with the other histones H2A and H4 and the nucleosome assembly protein (NAPS). We believe that the direct interactions may be between H2B and H3 and since these proteins exist as heterodimers of H2A–H2B and H3–H4 they pull down H2A and H4 by that association. These interactions are supported in the literature by evidence that nuclear FKBPs in *S. pombe* and *S. cerevisiae* were shown to possess histone chaperone activity [91] and the nuclear FKBP Fpr4p in *S. cerevisiae* is responsible for regulating methylation of amino acid lysine-36 on histone H3 [119].

The co-IP study also indicated a putative interaction between all three immunophilins and RAP1, as well as between PfFKBP35 & PfCYP19A and a number of other rhoptry proteins. RAP1 is known to be critical for invasion of erythrocytes by *P. falciparum* merozoites [41] and we have highlighted this putative interaction because we believe it is worthy of further investigation due to this critical role.

Aside from these highlighted interactions, among the large number of other putative interacting partners which were identified from the Y2H and co-IP studies, there was a significant representation of proteins involved in protein translation, chaperoning and digestion. From these data it appears that these major *P. falciparum* cytosolic immunophilins may be involved in a wide variety of cellular functions in the parasite. Some of these interactions may be analogous to immunophilin–protein interactions in other organisms, like the known role of immunophilins in cytoskeletal architecture, molecular chaperone machinery, and nucleosome assembly and modification while some may represent novel immunophilin–protein interactions specific to *P. falciparum* or critical for its life cycle.

6.2 SPECIFIC IMMUNOPHILIN–PROTEIN INTERACTIONS

Following on from the studies on whole parasite extracts by co-IP and whole genome analysis by Y2H we undertook specific investigation of some of the putative interactions indicated in these screens. We investigated three in particular; Hsp70–PfCYP19B, PfCYP19B–RAP1 and PfFKBP35–histones. The results from these investigations have contributed to our knowledge of the roles of immunophilins in the parasite.

We demonstrated that PfCYP19B is specifically pulled down by Hsp70 in co-IP experiments against whole parasite lysate *in vitro*. These data lend confidence to the inferral that *P. falciparum* possesses a chaperone complex similar to the high molecular weight chaperone machinery known to exist in other organisms. This machinery, consisting of immunophilins, Hsp90 and p23 along with accessory

proteins Hsp70, Hsp40, Hip and Hop, appears to be present in most eukaryotes. It is not surprising that *P. falciparum* also possesses a similar machinery, whose role is closely involved in chaperoning correct protein folding. In other organisms different immunophilins are associated with this complex depending on the substrate which is chaperoned, for example FKBP51/52 are associated with the complex during steroid receptor assembly, while cyclophilin D is associated during oestrogen receptor chaperoning [63]. This may explain in part why the parasite requires a large repertoire of immunophilins.

Experiments on live parasites indicated a potential role for parasite cyclophilins, specifically those that bind CsA and its derivatives which don't possess immunsuppressive activity, in the process of RAP1 chaperoning at some point between protein synthesis and its final location in the rhoptry body. When analysed by immunofluorescent microscopy with antibodies directed against it, RAP1 exhibits a characteristic bi-punctate staining in parasite schizonts, indicative of location in the rhoptry body [115]. We demonstrated by immunofluorescent confocal microscopy that when parasites were grown in the presence of the cyclophilin ligands CsA, BC-556 and [MeVal]^4-Cs RAP1 did not exhibit the characteristic bi-punctate appearance but instead appeared to locate in the cytosol of immature merozoites within the schizont. There was no effect of ligand treatment on PfCYP19B location. Experimentation consisting of short treatment of parasite schizonts with same ligands indicated that they have little effect on merozoite invasion, consistent with the hypothesis that the action of these ligands occurs at some point before arrival of RAP1 at the rhoptry.

Work investigating the interaction between histones and PfFKBP35 confirmed in vitro an interaction between recombinant FKBP and pu-

rified *P. falciparum* histones. We demonstrated that recombinant PfFKBD bound to purified histones immobilised on PVDF membrane by far-Western blot and appeared to bind with higher affinity to bands corresponding to the molecular weight of PfH2B and PfH3. This experiment appeared to agree excellently with the data generated by Y2H. Further research shed light into the roles that these interactions play in the parasite's growth and survival. Our initial hypothesis was that PfFKBP35 acts as a histone chaperone since it is known to have protein chaperone action and yeast nuclear FKBPs are known to be histone chaperones. This hypothesis remains unconfirmed, and is perhaps unlikely since PfFKBP lacks the acid/acid/base domains which appear to be required for histone chaperone action. Our investigation into the effect of FK506 treatment on the methylation state of H3K36 demonstrated that parasites treated with FK506 have increased H3K36 methylation. In *S. cerevisiae* H3K36 methylation is regulated by the PPIase activity of the FKBP Fpr4p, and inhibition of this protein leads to increased H3K36 methylation. It appeared that PfFKBP35 is also involved in regulation of H3K36 methylation by its PPIase activity.

6.3 THE PFFKBP35–CALCINEURIN INTERACTION

We also investigated the apparent interaction between PfFKBP35 and calcineurin that takes place regardless of the presence of FK506. Undertaking a complete investigation, beginning with 3D modelling, progressing to gene truncation and protein expression to *in vitro* protein assays we assessed the role of a major structural difference in this interaction.

We determined that PfFKBP35 possessed a 15-amino acid N-terminal extension and 3D modelling suggested that this extension may play a role in the protein's interaction with calcineurin. We proceeded to truncate this gene and subclone the truncated gene into an expression vector, from which we were able to express and purify an MBP tagged form of the truncated protein. Unfortunately this form of the protein didn't possess characteristic activities of the wild-type protein. The protein was unable to bind to the classic FKBP ligands FK506 and Rap, and appeared to possess greatly reduced PPIase activity. In spite of the fact that the protein appeared to be folded by thermal melt assay, we were unable to determine whether it was correctly folded and so were unable to deduce whether these losses were due to loss of correct fold or loss of the N-terminal extension. The truncated protein was unable to inhibit the phosphatase activity of calcineurin, but once again we were unable to determine whether this was due to loss of correct fold or loss of the N-terminal extension *per se*.

It is possible that the N-terminal extension is asserting some allosteric effect on the PPIase active site of the protein and that removing the extension disrupts both PPIase activity and ligand binding and that this effect is independent from the protein's ability to bind calcineurin. It is also possible that removing the extension eliminates the protein's ability to bind to calcineurin independently of the presence of FK506. It is difficult to discriminate between these possibilities with confidence since we are unable to determine whether the protein is correctly folded. One way to detemine this would be to be to assess the chaperone activity of the truncated protein, as chaperone activity of FKBPs is independent of PPIase activity and if the protein maintains the same level of chaperone activity as full length protein we could say with more confidence that the protein was folded correctly.

Finally we attempted to detect by various *in vivo* crosslinking methods whether this interaction occurs in intact parasites. Unfortunately *P. falciparum* appeared to be particularly intractable to study by these methods.

6.4 FINAL PERSPECTIVES AND FUTURE DIRECTIONS

There is much that remains unknown about the roles of immunophilins in *P. falciparum*. Before the outset of this study, without the ability to easily knock out or knock down the proteins individually and as a group and observing the resulting phenotype we were left having to infer function from organisms in which this is possible in order to determine the possible roles immunophilins play in the parasite. With the results from our co-IP experiments and our Y2H screen we have been able to generate an interaction map which provides an excellent body of evidence not only to support these inferrals but also as a starting point for further research.

Our own follow up work confirmed a number of these inferrals, namely immunophilin interactions with Hsp70 and histones. We were also able to demonstrate a potential novel role for immunophilins in parasite biology, that of chaperoning RAP1. As a body of work we have provided new insights into the function of immunophilins in the parasite. It has become increasingly clear that the antimalarial activity of CsA, FK506 and their non-immunosuppressive derivatives may not be just on one specific immunophilin–protein interaction but rather be a more general disruption of a variety of chaperone and protein folding functions. This would tend to agree with the fact that these drugs seem to be most active against the most metabolically

active erythrocytic stages of the parasite, namely trophozoites [114]. What is apparent is that immunophilins play an important role in the parasite and that despite evidence from yeast that they are not essential for growth under laboratory conditions, that may not hold to be true in *P. falciparum*.

The field of malaria research is progressing rapidly, in particular in the area of identifying new targets, and discovering lead coupounds that could be used for antimalarial therapy. There is no doubt that these and potentially other immunophilins have potential as chemotherapeutic targets. The studies of this thesis have added to the understanding of the biological function of *P. falciparum* immunophilins and have identified at least one novel potential function. The next steps after this work are research into immunophilin interactions *in vivo*, but unfortunately the parasite is difficult to manipulate genetically and doesn't possess siRNA machinery to allow knockdown interference. Hopefully these obstacles can be overcome and we can begin to further clarify the functions of these proteins in *P. falciparum*.

7

APPENDIX

Table 4: **Gene_IDs of double and triple interacting partners.**

Double Interactions			
PfCYP19B-PfFKBP35		**PfCYP19B-PfCYP19A**	
PF3D7_1246200		PF3D7_0511800	
PfCYP19A-PfFKBP35			
PF3D7_0818200	PF3D7_1347500	PF3D7_0812400	PF3D7_1408100
PF3D7_1105400	PF3D7_1010700	PF3D7_1324900	PF3D7_1407800
PF3D7_0627500	PF3D7_1451100	PF3D7_1446200	PF3D7_1361900
PF3D7_1130200	PF3D7_1222300	PF3D7_1311800	PF3D7_0827900
PF3D7_1029600	PF3D7_1015900	PF3D7_0930300	PF3D7_0621200
PF3D7_1008900	PF3D7_1468700	PF3D7_1416500	PF3D7_0626800
PF3D7_1223100	PF3D7_1444800	PF3D7_0608800	PF3D7_1011800
PF3D7_1226300	PF3D7_1462800	PF3D7_1129100	PF3D7_0826700
PF3D7_0721100	PF3D7_0708800	PF3D7_1343000	PF3D7_0501600
PF3D7_1104400	PF3D7_0624000	PF3D7_0922500	PF3D7_0922200
PF3D7_1115700	PF3D7_1105100	PF3D7_1120100	PF3D7_1129000
PF3D7_1115300	PF3D7_1434300	PF3D7_1407900	PF3D7_1439900
PF3D7_1115400	PF3D7_1012400	PF3D7_1408000	
Triple Interactions			
PF3D7_0708400	PF3D7_0917900	PF3D7_1357100	
PF3D7_0818900	PF3D7_1134000	PF3D7_1410400	
PF3D7_0831700	PF3D7_1357000		

Table 5: **Full list of co-IP partners and their mass spectrometric results.**

Gene_ID	PEAKS Score (%)	Coverage (%)	No. of Peptides	Description
PfCYP19A				
Unsorted				
PF3D7_0934500	97.3	12	3	vacuolar ATP synthase subunit e, putative
PF3D7_1311900	99.1	12	7	vacuolar ATP synthase subunit a (vapA)
PF3D7_0930300	99.2	30	64	merozoite surface protein 1 (MSP1)
PF3D7_1428300	98.3	7	3	proliferation-associated protein 2g4, putative
PF3D7_0419600	99	16	6	ran binding protein 1, putative
PF3D7_1335100	99.1	17	7	merozoite surface protein 7 (MSP7)
PF3D7_0703500	98.6	1	3	erythrocyte membrane-associated antigen
Unknown Function				
PF3D7_1457300	98.3	5	4	conserved *Plasmodium* protein, unknown function
PF3D7_1244100	98	1	1	conserved *Plasmodium* protein, unknown function
PF3D7_0811400	97.1	3	3	conserved *Plasmodium* protein, unknown function
PF3D7_0721100	96.9	8	2	conserved *Plasmodium* protein, unknown function
PF3D7_1104400	98.1	6	3	conserved protein, unknown function

PF3D7_1427900	97.5	9	2	conserved protein, unknown function
Protein Folding				
PF3D7_1015600	99.2	41	21	heat shock protein 60 (Hsp60)
PF3D7_0818900	99.2	42	30	heat shock protein 70 (Hsp70)
PF3D7_0917900	99.2	34	23	heat shock protein 70 (Hsp70-2)
PF3D7_1134000	99.2	15	10	heat shock protein 70 (Hsp70-3)
PF3D7_0708800	99.2	14	11	heat shock protein 70 (Hsp70-z)
PF3D7_0831700	99.2	16	12	heat shock protein 70, putative (Hsp70-x)
PF3D7_0708400	99.2	22	17	heat shock protein 90 (Hsp90)
PF3D7_1434300	99	15	9	Hsp70/Hsp90 organizing protein (HOP)
PF3D7_0827900	99.2	26	17	protein disulfide isomerase (PDI8)
PF3D7_1132200	99.2	34	20	TCP-1/cpn60 chaperonin family, putative
PF3D7_1247400	99.2	31	12	FK506-binding protein (FKBP)-type peptidyl-prolyl isomerase (FKBP35)
PF3D7_1333000	97.6	7	2	20 kDa chaperonin (CPN20)
PF3D7_0608700	99.2	17	9	chaperone, putative
PF3D7_1128100	97	8	2	cochaperone prefoldin complex subunit, putative
PF3D7_0320300	99.2	23	15	T-complex protein 1 epsilon subunit, putative

PF3D7_1229500	99.2	30	20	T-complex protein 1, gamma subunit, putative
PF3D7_0214000	99.2	22	14	T-complex protein 1, putative
PF3D7_0306800	99.2	20	11	T-complex protein beta subunit, putative
PF3D7_1357800	99.2	35	16	TCP-1/cpn60 chaperonin family, putative
PF3D7_0308200	99.1	12	7	TCP-1/cpn60 chaperonin family, putative
PF3D7_1222300	99	4	3	endoplasmin homolog precursor, putative

ners and their mass spectrometric results.

Proteolysis				
PF3D7_0803800	99.2	35	12	20S proteasome beta subunit
PF3D7_0312300	98.8	16	4	26S proteasome regulatory subunit S14, putative
PF3D7_1129200	99	13	6	26S proteasome regulatory subunit, putative
PF3D7_0912900	98.9	12	4	26S proteasome regulatory subunit, putative
PF3D7_1030500	98.1	7	4	26S proteasome regulatory subunit, putative
PF3D7_1466300	97.7	2	3	26S proteasome regulatory subunit, putative
PF3D7_0205900	96.7	3	3	proteasome 26S regulatory subunit, putative
PF3D7_0317000	99	20	6	proteasome component C8, putative
PF3D7_1338100	99.1	11	6	proteasome regulatory subunit, putative
PF3D7_0608500	99	20	6	proteasome subunit alpha type 2, putative
PF3D7_0727400	99.1	25	7	proteasome subunit alpha type 5, putative
PF3D7_0807500	99.1	35	9	proteasome subunit alpha, putative

PF3D7_0518300	99.1	23	7	proteasome subunit beta type 1, putative
PF3D7_1328100	99.1	15	6	proteasome subunit beta type 7 precursor, putative
PF3D7_1011400	99	17	5	proteasome subunit beta type-5
PF3D7_1353900	99.2	27	6	proteasome subunit, putative
PF3D7_1353800	98.8	14	4	proteasome subunit, putative
PF3D7_1474800	98.9	24	5	proteosome subunit alpha type 1, putative
PF3D7_0418200	99	11	5	golgi organization and biogenesis factor, putative
PF3D7_1454400	99.1	8	7	aminopeptidase P (APP)
PF3D7_1446200	99.2	24	15	M17 leucyl aminopeptidase (LAP)
PF3D7_1311800	99.1	6	9	M1-family alanyl aminopeptidase (M1AAP)
Digestive Vacuole				
PF3D7_1407900	99.2	16	6	plasmepsin I (PMI)
PF3D7_1408000	99	10	4	plasmepsin II
PF3D7_1408100	99.2	26	13	plasmepsin III,histo-aspartic protease (HAP)
PF3D7_1407800	99.1	13	5	plasmepsin IV (PM4)
PF3D7_1115700	98.4	5	3	cysteine proteinase falcipain 2a
PF3D7_1115300	98.3	5	3	cysteine proteinase falcipain 2b (FP2B)
PF3D7_1115400	99.2	16	10	cysteine proteinase falcipain 3

Translation				
PF3D7_1447000	98.7	12	4	40S ribosomal protein S2, putative
PF3D7_1105400	98.5	10	3	40S ribosomal protein S4, putative
PF3D7_0517000	99.1	32	6	60S ribosomal protein L12, putative
PF3D7_1004000	99	20	5	60S ribosomal protein L13, putative
PF3D7_1431700	99.1	30	5	60S ribosomal protein L14, putative
PF3D7_1341200	98.8	24	5	60S ribosomal protein L18, putative
PF3D7_1460700	95.2	15	3	60S ribosomal protein L27, putative
PF3D7_1323100	98.6	12	3	60S ribosomal protein L6, putative
PF3D7_1424400	99.1	16	5	60S ribosomal protein L7-3, putative
PF3D7_1130200	99.2	41	16	60S ribosomal protein P0
PF3D7_0211800	99	8	5	asparagine-tRNA ligase, putative
PF3D7_0102900	99	5	3	aspartyl-tRNA synthetase
PF3D7_1350100	98.7	6	3	lysine-tRNA ligase, putative
PF3D7_1034900	99.2	9	9	methionine-tRNA ligase, putative
PF3D7_1468700	99.1	15	7	eukaryotic initiation factor 4A (eIF4A)
PF3D7_1212700	99.1	6	10	eukaryotic translation initiation factor 3 subunit 10, putative

PF3D7_0918300	98.5	9	3	eukaryotic translation initiation factor 3 subunit 5, putative
PF3D7_1206200	99.1	4	5	eukaryotic translation initiation factor 3 subunit 8, putative
PF3D7_0212300	98.9	7	3	peptide chain release factor subunit 1, putative
PF3D7_1357000	99.2	34	16	elongation factor 1-alpha
PF3D7_1357100	99.2	34	16	elongation factor 1-alpha
PF3D7_1338300	99.1	20	10	elongation factor 1-gamma, putative
PF3D7_1451100	99.2	15	13	elongation factor 2
PF3D7_0607000	98.2	3	3	translation initiation factor IF-2, putative
PF3D7_1442300	99.1	14	7	tRNA binding protein, putative
PF3D7_0612100	98.7	5	4	eukaryotic translation initiation factor 3 subunit L, putative
PF3D7_0528200	98.6	6	4	eukaryotic translation initiation factor 3, subunit 6, putative
Rhoptry				
PF3D7_0929400	99.2	13	20	high molecular weight rhoptry protein 2 (RhopH2)
PF3D7_0905400	99.2	9	8	high molecular weight rhoptry protein 3 (RhopH3)
PF3D7_1252100	97.9	2	4	rhoptry neck protein 3 (RON3)
PF3D7_1116000	97.7	1	1	rhoptry neck protein 4 (RON4)
PF3D7_1410400	99	9	8	rhoptry-associated protein 1 (RAP1)
PF3D7_0501600	98.5	6	3	rhoptry-associated protein 2 (RAP2)

Biosynthetic/Metabolic Processes				
Glycolysis				
PF3D7_1015900	99.2	45	22	enolase (ENO)
PF3D7_1439900	99.2	37	9	triosephosphate isomerase (TIM)
PF3D7_1462800	99.2	37	15	glyceraldehyde-3-phosphate dehydrogenase (GAPDH)
PF3D7_1436000	99.1	12	7	glucose-6-phosphate isomerase (GPI)
PF3D7_0915400	99.2	11	16	6-phosphofructokinase (PFK9)
PF3D7_1444800	99.2	44	26	fructose-bisphosphate aldolase
PF3D7_0624000	99.2	32	16	hexokinase (HK)
PF3D7_1324900	99.2	38	19	L-lactate dehydrogenase (LDH)
PF3D7_0922500	99.2	37	18	phosphoglycerate kinase (PGK)
PF3D7_1120100	99.2	45	14	phosphoglycerate mutase, putative (PGM1)
PF3D7_0626800	99.2	29	18	pyruvate kinase (PyrK)
Biosynthetic				
PF3D7_1366500	96.8	11	1	nucleoside diphosphate kinase (NDK)
PF3D7_1308200	95	0	1	carbamoyl phosphate synthetase (cpsSII)
PF3D7_0922600	99.1	12	6	glutamine synthetase, putative
PF3D7_0511800	98.7	7	4	myo-inositol 1-phosphate synthase, putative
PF3D7_1124600	99.2	22	13	ethanolamine kinase, putative

PF3D7_1343000	99.2	38	11	phosphoethanolamine N-methyltransferase (PMT)
PF3D7_1029600	99	12	5	adenosine deaminase, putative
PF3D7_0621200	99.2	49	25	pyridoxine biosynthesis protein PDX1 (PDX1)
PF3D7_0922200	99.2	24	11	S-adenosylmethionine synthetase (SAMS)
PF3D7_1129000	99.2	22	8	spermidine synthase (SpdSyn)
PF3D7_0627500	99.2	71	17	4-methyl-5(B-hydroxyethyl)-thiazol monophosphate biosynthesis enzyme
PF3D7_1239600	99	13	4	hydroxyethylthiazole kinase, putative
Metabolic				
PF3D7_0627800	98.7	3	3	acetyl-CoA synthetase, putative
PF3D7_1008900	96.6	8	3	adenylate kinase (AK1)
PF3D7_0802000	99	4	4	glutamate dehydrogenase, putative (GDHc)
PF3D7_1416500	99	11	5	NADP-specific glutamate dehydrogenase (GDHa)
PF3D7_1235600	98.4	7	3	serine hydroxymethyltransferase (SHMT)
PF3D7_1226300	98.7	11	3	cof-like hydrolase, had-superfamily, subfamily iib
PF3D7_0513300	98.8	17	5	purine nucleoside phosphorylase (PNP)
PF3D7_0520900	99.2	11	5	S-adenosyl-L-homocysteine hydrolase (SAHH)
PF3D7_0608800	99.2	37	17	ornithine aminotransferase (OAT)
PF3D7_1454700	98.7	7	4	6-phosphogluconate dehydrogenase, decarboxylating, putative

PF3D7_0814900	97.2	7	1	Fe-superoxide dismutase (FeSOD)
PF3D7_0816600	98.2	2	2	ClpB protein, putative (ClpB1)
Nucleic Acid Binding				
PF3D7_1105100	95.6	14	2	histone H2B (H2B)
PF3D7_0705400	95.3	2	3	minchromosome maintenance (MCM) complex subunit, putative (MCM7)
PF3D7_1347500	99.1	18	7	DNA/RNA-binding protein Alba 4 (ALBA4)
PF3D7_1226600	98.6	8	3	proliferating cell nuclear antigen 2 (PCNA2)
PF3D7_1361900	99.2	31	8	proliferating cell nuclear antigen (PCNA)
PF3D7_0209800	97.6	2	1	ATP-dependent RNA helicase UAP56 (UAP56)
PF3D7_1302100	96.1	8	2	gamete antigen 27/25 (Pfg27)
PF3D7_1011800	99.2	9	11	QF122 antigen
PF3D7_0906000	95.5	1	2	RNB-like protein, putative
Other Protein Transport/Modification				
PF3D7_0914700	97.5	4	2	transporter, putative
PF3D7_0302900	98.1	3	3	exportin 1, putative
PF3D7_1352500	98.7	15	4	thioredoxin-related protein, putative

PF3D7_0802200	98.5	12	4	1-cys peroxiredoxin (1-cyspxn)
PF3D7_1021600	96.9	8	2	deoxyribose-phosphate aldolase, putative
PF3D7_1127000	98.3	8	3	protein phosphatase, putative
PF3D7_1438900	98	7	2	thioredoxin peroxidase 1 (Trx-Px1)
PF3D7_0818200	99.2	58	15	14-3-3 protein, putative
PF3D7_0720800	96.4	8	2	Ham1-like protein, putative
PF3D7_0826700	98.9	11	3	receptor for activated c kinase (RACK)
PF3D7_0812400	98.1	4	2	karyopherin alpha (KARalpha)
PF3D7_0524000	99.2	6	7	karyopherin beta (KASbeta)
PF3D7_0516700	98.2	2	2	ubiquitin carboxyl-terminal hydrolase 2, putative
PF3D7_1225800	98.7	3	3	ubiquitin-activating enzyme e1, putative (Uba1)
PF3D7_1010700	98.3	15	3	dolichyl-phosphate-mannose protein mannosyltransferase, putative
PF3D7_1346100	98.1	5	2	Sec61 alpha subunit, PfSec61 (SEC61)
PF3D7_1456800	98.7	4	4	V-type H( )-translocating pyrophosphatase, putative
PF3D7_1012400	99.1	25	9	hypoxanthine-guanine phosphoribosyltransferase (HGPRT)
PF3D7_1223100	99	10	5	cAMP-dependent protein kinase regulatory subunit (PKAr)
PF3D7_1129100	99	10	5	parasitophorous vacuolar protein 1 (PV1)
PF3D7_1127600	97.6	6	2	CRAL/TRIO domain-containing protein, putative

PfCYP19B				
Biosynthetic Processes				
PF3D7_0511800	98.7	2	1	myo-inositol 1-phosphate synthase, putative
Protein Folding				
PF3D7_0708400	99.2	13	9	heat shock protein 90 (Hsp90)
PF3D7_0818900	99.2	30	19	heat shock protein 70 (Hsp70)
PF3D7_0831700	99	6	4	heat shock protein 70, putative (Hsp70-x)
PF3D7_0917900	99.2	31	17	heat shock protein 70 (Hsp70-2)
PF3D7_1134000	99.2	26	13	heat shock protein 70 (Hsp70-3)
PF3D7_1115600	98.5	26	4	peptidyl-prolyl cis-trans isomerase (CYP19B)
Structure				
PF3D7_1246200	99.1	18	5	actin I (ACT1)
Translation				
PF3D7_1357000	99.2	19	8	elongation factor 1-alpha
PF3D7_1357100	99.2	19	8	elongation factor 1-alpha

Rhoptry				
PF3D7_1410400	99	6	4	rhoptry-associated protein 1 (RAP1)

PfFKBP35				
Unsorted				
PF3D7_0619400	99.1	8	7	cell division cycle protein 48 homologue, putative
PF3D7_1471100	97.7	7	2	exported protein 2 (EXP2)
PF3D7_1229400	99.1	53	6	macrophage migration inhibitory factor (MIF)
PF3D7_0930300	96	2	3	merozoite surface protein 1 (MSP1)
PF3D7_1129100	98.4	6	3	parasitophorous vacuolar protein 1 (PV1)
PF3D7_1011800	99.1	6	6	QF122 antigen
PF3D7_0511000	95.9	12	3	translationally controlled tumor protein homolog, putative
PF3D7_1140100	97.8	14	2	vacuolar ATP synthase subunit f, putative
Unknown Function				
PF3D7_0721100	98.9	16	3	conserved *Plasmodium* protein, unknown function
PF3D7_1459400	98.6	8	3	conserved *Plasmodium* protein, unknown function
PF3D7_1104400	99.2	19	9	conserved protein, unknown function

PF3D7_1333400	99.1	24	5	conserved protein, unknown function
Protein Folding				
PF3D7_0818900	99.2	24	17	heat shock protein 70 (Hsp70)
PF3D7_0917900	99.2	42	33	heat shock protein 70 (Hsp70-2)
PF3D7_1134000	99.2	23	16	heat shock protein 70 (Hsp70-3)
PF3D7_0708800	95.1	2	2	heat shock protein 70 (Hsp70-z)
PF3D7_0831700	99.2	9	7	heat shock protein 70, putative (Hsp70-x)
PF3D7_0708400	99.2	18	13	heat shock protein 90 (Hsp90)
PF3D7_1118200	97	1	1	heat shock protein 90, putative
PF3D7_1434300	97.6	5	3	Hsp70/Hsp90 organizing protein (HOP)
PF3D7_1473200	98.2	3	2	DnaJ protein, putative
PF3D7_1222300	98.5	5	5	endoplasmin homolog precursor, putative
PF3D7_1247400	99.2	60	37	FK506-binding protein (FKBP)-type peptidyl-prolyl isomerase (FKBP35)
PF3D7_0322000	99	22	4	peptidyl-prolyl cis-trans isomerase (CYP19A)
PF3D7_1115600	98.3	14	3	peptidyl-prolyl cis-trans isomerase (CYP19B)
Proteolysis				

PF3D7_1446200	99.1	8	4	M17 leucyl aminopeptidase (LAP)
PF3D7_1311800	98.8	3	4	M1-family alanyl aminopeptidase (M1AAP)
Digestive Vacuole				
PF3D7_1115700	99.1	13	7	cysteine proteinase falcipain 2a
PF3D7_1115300	99.1	13	7	cysteine proteinase falcipain 2b (FP2B)
PF3D7_1115400	98.8	7	4	cysteine proteinase falcipain 3
PF3D7_1407900	99.2	24	9	plasmepsin I (PMI)
PF3D7_1408000	99.2	25	9	plasmepsin II
PF3D7_1408100	99.2	16	10	plasmepsin III,histo-aspartic protease (HAP)
PF3D7_1407800	99.1	12	5	plasmepsin IV (PM4)
Translation				
PF3D7_0719700	98.3	23	4	40S ribosomal protein S10, putative
PF3D7_1358800	98.5	16	6	40S ribosomal protein S13, putative
PF3D7_0516200	99.2	40	7	40S ribosomal protein S14, putative
PF3D7_0316800	99.1	38	6	40S ribosomal protein S15A, putative
PF3D7_0813900	99	30	4	40S ribosomal protein S16, putative
PF3D7_1242700	97.2	15	2	40S ribosomal protein S17, putative
PF3D7_0519400	98.7	23	3	40S ribosomal protein S24, putative

PF3D7_1026800	99	23	7	40S ribosomal protein S2B, putative
PF3D7_1465900	98.4	14	3	40S ribosomal protein S3, putative
PF3D7_1105400	99.2	52	19	40S ribosomal protein S4, putative
PF3D7_1302800	99.1	17	7	40S ribosomal protein S7, putative
PF3D7_1408600	98.6	19	3	40S ribosomal protein S8e, putative
PF3D7_0821700	98.1	14	2	60S ribosomal protein L22, putative
PF3D7_1365900	99.1	34	4	60S ribosomal protein L40/UBI, putative
PF3D7_1424100	98.9	10	3	60S ribosomal protein L5, putative
PF3D7_1130200	99.2	21	6	60S ribosomal protein P0
PF3D7_1468700	99.2	24	10	eukaryotic initiation factor 4A (eIF4A)
PF3D7_1357000	99.2	43	22	elongation factor 1-alpha
PF3D7_1357100	99.2	43	22	elongation factor 1-alpha
PF3D7_1451100	99.2	8	7	elongation factor 2
Rhoptry				
PF3D7_1410400	99.2	8	7	rhoptry-associated protein 1 (RAP1)
PF3D7_0501600	98.3	7	3	rhoptry-associated protein 2 (RAP2)

Biosynthetic/Metabolic Processes				
Glycolysis				
PF3D7_1015900	99.2	52	24	enolase (ENO)
PF3D7_1444800	99.2	26	11	fructose-bisphosphate aldolase
PF3D7_1462800	99.2	44	18	glyceraldehyde-3-phosphate dehydrogenase (GAPDH)
PF3D7_0624000	99.2	15	6	hexokinase (HK)
PF3D7_1324900	99.2	38	14	L-lactate dehydrogenase (LDH)
PF3D7_0922500	99.2	25	10	phosphoglycerate kinase (PGK)
PF3D7_1120100	99.2	42	12	phosphoglycerate mutase, putative (PGM1)
PF3D7_1439900	99.2	47	12	triosephosphate isomerase (TIM)
PF3D7_0626800	99.2	13	7	pyruvate kinase (PyrK)
Biosynthetic				
PF3D7_0627500	99.1	33	5	4-methyl-5(B-hydroxyethyl)-thiazol monophosphate biosynthesis enzyme
PF3D7_1029600	99.2	19	9	adenosine deaminase, putative
PF3D7_1343000	99.2	37	11	phosphoethanolamine N-methyltransferase (PMT
PF3D7_0621200	99	18	5	pyridoxine biosynthesis protein PDX1 (PDX1)
PF3D7_0922200	99.2	23	9	S-adenosylmethionine synthetase (SAMS)
PF3D7_1129000	98.1	10	3	spermidine synthase (SpdSyn)

Metabolic				
PF3D7_0525100	99	7	4	acyl-CoA synthetase (ACS10)
PF3D7_1008900	99.2	48	11	adenylate kinase (AK1)
PF3D7_1226300	99.2	29	8	cof-like hydrolase, had-superfamily, subfamily iib
PF3D7_1033400	95.1	7	2	haloacid dehalogenase-like hydrolase, putative
PF3D7_1416500	98.2	7	3	NADP-specific glutamate dehydrogenase (GDHa)
PF3D7_0608800	99.2	29	12	ornithine aminotransferase (OAT)
Nucleic Acid Binding				
PF3D7_0823200	99.2	28	8	RNA binding protein, putative
PF3D7_0605100	98.9	5	4	RNA binding protein, putative
PF3D7_0814200	98.6	11	3	DNA/RNA-binding protein Alba 1 (ALBA1)
PF3D7_1346300	95	9	2	DNA/RNA-binding protein Alba 2 (ALBA2)
PF3D7_1006200	99	45	5	DNA/RNA-binding protein Alba 3 (ALBA3)
PF3D7_1347500	99.1	17	6	DNA/RNA-binding protein Alba 4 (ALBA4)
PF3D7_0817900	98.7	36	4	high mobility group protein (HMGB2)
PF3D7_0617800	98.9	32	5	histone H2A (H2A)
PF3D7_0320900	98.6	16	3	histone H2A variant, putative (H2A.Z)
PF3D7_1105100	99.2	57	8	histone H2B (H2B)
PF3D7_0714000	95.6	0	0	histone H2B variant, putative (H2Bv)

PF3D7_0610400	96.2	5	1	histone H3 (H3)
PF3D7_0617900	96.2	5	1	histone H3 variant, putative (H3.3)
PF3D7_1105000	98.9	39	4	histone H4 (H4)
PF3D7_0919000	99	14	4	nucleosome assembly protein (NAPS)
PF3D7_1361900	99.2	25	8	proliferating cell nuclear antigen (PCNA)
PF3D7_1224300	99.1	7	5	polyadenylate-binding protein, putative (PABP)
Other Protein Transport/Modification				
PF3D7_0818200	99.2	29	8	14-3-3 protein, putative
PF3D7_1419300	99.1	22	4	glutathione S-transferase (GST)
PF3D7_1211800	99.1	11	4	polyubiquitin (PfpUB)
PF3D7_1223100	99.1	12	6	cAMP-dependent protein kinase regulatory subunit (PKAr)
PF3D7_1010700	98.9	24	4	dolichyl-phosphate-mannose protein mannosyltransferase, putative
PF3D7_1134800	97.6	5	3	coatomer delta subunit, putative
PF3D7_1117700	98.9	19	4	GTP-binding nuclear protein ran/tc4 (RAN)
PF3D7_1012400	99.2	33	9	hypoxanthine-guanine phosphoribosyltransferase (HGPRT)
PF3D7_0812400	99.1	8	4	karyopherin alpha (KARalpha)
PF3D7_0621800	97.9	14	2	nascent polypeptide associated complex alpha chain, putative

PF3D7_0827900	99.2	32	18	protein disulfide isomerase (PDI8)
PF3D7_1242800	95.5	5	2	rab specific GDP dissociation inhibitor (rabGDI)
PF3D7_0826700	99.1	21	7	receptor for activated c kinase (RACK)
PF3D7_0416800	99	24	4	small GTP-binding protein sar1 (SAR1)
PF3D7_1027300	98.6	8	4	peroxiredoxin (nPrx)
Structure				
PF3D7_1246200	97.7	6	2	actin I (ACT1)
PF3D7_0503400	96.3	30	2	actin-depolymerizing factor 1 (ADF1)
PF3D7_0903700	98.9	11	4	alpha tubulin 1
PF3D7_1008700	99.1	10	4	tubulin beta chain

BIBLIOGRAPHY

[1] Acharya P, Kumar R, Tatu U. Chaperoning a cellular upheaval in malaria: heat shock proteins in *Plasmodium falciparum*. *Mol Biochem Parasitol.*, 153(2):85–94, Jun 2007. (Cited on pages 93, 94, and 147.)

[2] Adams B, Musiyenko A, Kumar R, Barik S. A novel class of dual–family immunophilins. *J Biol Chem.*, 280(26):24301–24314, Jul 2005. (Cited on page 19.)

[3] Aiken C. Mechanistic independence of Nef and cyclophilin A enhancement of human immunodeficiency virus type 1 infectivity. *Virology*, 248(1):139–147, Aug 1998. (Cited on page 30.)

[4] Alag R, Bharatham N, Dong A, Hills T, Harikishore A, Widjaja AA, Shochat SG, Hui R, Yoon HS. Crystallographic structure of the tetratricopeptide repeat domain of *Plasmodium falciparum* FKBP35 and its molecular interaction with Hsp90 C-terminal pentapeptide. *Protein Sci.*, 18(10):2115–2124, Oct 2009. (Cited on page 119.)

[5] Aliberti J, Valenzuela JG, Carruthers VB, Hieny S, Andersen J, Charest H, Reis e Sousa C, Fairlamb A, Ribeiro JM, Sher A. Molecular mimicry of a CCR5 binding-domain in the microbial activation of dendritic cells. *Nat Immunol*, 4(5):485–490, May 2003. (Cited on page 68.)

[6] Alifrangis M, Enosse S, Khalil IF, Tarimo DS, Lemnge MM, Thompson R, Bygbjerg IC, Ronn AM. Prediction of *Plasmodium falciparum* resistance to sulfadoxine/pyrimethamine in vivo by mutations in the dihydrofolate reductase and dihydropteroate synthetase genes: a comparative study between sites of differing endemicity. *Am J Trop Med Hyg.*, 69(6):601–606, Dec 2003. (Cited on page 17.)

[7] An P, Wang LH, Hutcheson-Dilks H, Nelson G, Donfield S, Goedert JJ, Rinaldo CR, Buchbinder S, Kirk GD, O'Brien SJ, Winkler CA. Regulatory polymorphisms in the cyclophilin A gene, PPIA, accelerate progression to AIDS. *PLoS Pathog.*, 3(6): e88, Jun 2007. (Cited on page 30.)

[8] Andrews KT, Tran TN, Fairlie DP. Towards histone deacetylase inhibitors as new antimalarial drugs. *Curr Pharm Des.*, 18(24): 3467–3479, 2012. (Cited on page 94.)

[9] Ardeshir F, Flint JE, Richman SJ, Reese RT. A 75 kDa merozoite surface protein of *Plasmodium falciparum* which is related to the 70 kDa heat–shock proteins. *EMBO J*, 6(2):493–499, Feb 1987. (Cited on page 93.)

[10] Arora K, Gwinn WM, Bower MA, Watson A, Okwumabua I, MacDonald HR, Bukrinsky MI, Constant SL. Extracellular cyclophilins contribute to the regulation of inflammatory responses. *J Immunol.*, 175(1):517–522, Jul 2005. (Cited on page 27.)

[11] Aultman KS, Gottlieb M, Giovanni MY, Fauci AS. *Anopheles gambiae* genome: completing the malaria triad. *Science*, 298 (5591):13, Oct 2002. (Cited on page 17.)

[12] Avellino R, Romano S, Parasole R, Bisogni R, Lamberti A, Poggi V, Venuta S, Romano MF. Rapamycin stimulates apoptosis of childhood acute lymphoblastic leukemia cells. *Blood*, 106(4): 1400–1406, Aug 2005. (Cited on page 30.)

[13] Baldi DL, Andrews KT, Waller RF, Roos DS, Howard RF, Crabb BS, Cowman A. RAP1 controls rhoptry targeting of RAP2 in the malaria parasite *Plasmodium falciparum*. *EMBO J.*, 19(11): 2435–2443, Jun 2000. (Cited on page 95.)

[14] Bannister LH, Hopkins JM, Fowler RE, Krishna S, Mitchell GH. Ultrastructure of rhoptry development in *Plasmodium falciparum* erythrocytic schizonts. *Parasitology.*, 1212(3):273–287, Sep 2000. (Cited on page 9.)

[15] Bannister LH, Mitchell GH, Butcher GA, Dennis ED, Cohen S. Structure and development of the surface coat of erythrocytic merozoites of *Plasmodium knowlesi*. *Cell Tissue Res.*, 245(2):281–290, 1986. (Cited on page 9.)

[16] Banumathy G, Singh V, Pavithra SR, Tatu U. Heat shock protein 90 function is essential for *Plasmodium falciparum* growth in human erythrocytes. *J Biol Chem.*, 278(20):18336–18345, May 2003. (Cited on pages 93 and 111.)

[17] Barik S. Immunophilins: for the love of proteins. *Cell Mol Life Sci.*, 63(24):2889–2900, Dec 2006. (Cited on page 20.)

[18] Bell A. Antimalarial peptides: the long and the short of it. *Curr Pharm Des.*, 17(25):2719–2731, 2011. (Cited on page 36.)

[19] Bell A, Monaghan P, Page AP. Peptidyl-prolyl cis-trans isomerases (immunophilins) and their roles in parasite biochem-

istry, host-parasite interaction and antiparasitic drug action. *Int J Parasitol*, 36(3):261–76, March 2006. (Cited on page 25.)

[20] Bell A, Wernli B, Franklin RM. Roles of peptidyl-prolyl *cis-trans* isomerase and calcineurin in the mechanisms of antimalarial action of cyclosporin A, FK506, and rapamycin. *Biochem Pharmacol*, 48(3):495–503, Aug 1994. (Cited on pages 36 and 67.)

[21] Blackman MJ, Scott-Finnigan TJ, Shai S, Holder AA. Antibodies inhibit the protease-mediated processing of a malaria merozoite surface protein. *J Exp Med.*, 180(1):389–393, Jul 1994. (Cited on page 11.)

[22] Bosco DA, Eisenmesser EZ, Pochapsky S, Sundquist WI, Kern D. Catalysis of cis/trans isomerization in native HIV–1 capsid by human cyclophilin A. *Proc Natl Acad Sci U S A.*, 99(8):5247–5252, Apr 2002. (Cited on page 30.)

[23] Bose S, Mathur M, Bates P, Joshi N, Banerjee AK. Requirement for cyclophilin A for the replication of vesicular stomatitis virus New Jersey serotype. *J Gen Virol.*, 84(7):1687–1699, Jul 2003. (Cited on page 31.)

[24] Braaten D, Luban J. Cyclophilin A regulates HIV–1 infectivity, as demonstrated by gene targeting in human T cells. *EMBO J*, 20(6):1300–1309, Mar 2001. (Cited on page 30.)

[25] Brandts JF, Halvorson HR, Brennan M. Consideration of the possibility that the slow step in protein denaturation reactions is due to *cis–trans* isomerism of proline residues. *Biochemistry.*, 14(22):4953–4963, Nov 1975. (Cited on page 19.)

[26] Braun PD, Barglow KT, Lin YM, Akompong T, Briesewitz R, Ray GT, Haldar K, Wandless TJ. A bifunctional molecule that displays context–dependent cellular activity. *J Am Chem Soc.*, 125(25):7575–7580, Jun 2003. (Cited on page 32.)

[27] Brent, R., Ptashne, M. A bacterial repressor protein or a yeast transcriptional terminator can block upstream activation of a yeast gene. *Nature*, 312(5995):612–5, Dec 1984. (Cited on page 58.)

[28] Bruce-Chwatt LJ. Classification of antimalarial drugs in relation to different stages in the life–cycle of the parasite: commentary on a diagram. *Bull World Health Organ.*, 27(2):287–290, 1962. (Cited on page 14.)

[29] Cantin R, Methot S, Tremblay MJ. Plunder and stowaways: incorporation of cellular proteins by enveloped viruses. *J Virol.*, 79(11):6577–6587, Jun 2005. (Cited on page 30.)

[30] Cao W, Konsolaki M. FKBP immunophilins and Alzheimer's disease: a chaperoned affair. *J Biosci.*, 36(3):493–498, Aug 2011. (Cited on page 29.)

[31] Capanna E. Grassi versus Ross: who solved the riddle of malaria? *Int Microbiol.*, 9(1):69–74, Mar 2006. (Cited on page 2.)

[32] Carrello A, Allan RK, Morgan SL, Owen BA, Mok D, Ward BK, Minchin RF, Toft DO, Ratajczak T. Interaction of the Hsp90 cochaperone cyclophilin 40 with Hsc70. *Cell Stress Chaperones*, 9(2):167–181, Apr 2004. (Cited on pages 27, 88, and 111.)

[33] Castro AP, Carvalho TM, MoussatchÃ© N, Damaso CR. Redistribution of cyclophilin A to viral factories during vaccinia

virus infection and its incorporation into mature particles. *J Virol.*, 77(16):9052–9068, Jun 2003. (Cited on page 31.)

[34] Chambraud B, Sardin E, Giustiniani J, Dounane O, Schumacher M, Goedert M, Baulieu EE. A role for FKBP52 in Tau protein function. *Proc Natl Acad Sci U S A.*, 107(6):2658–2663, Feb 2010. (Cited on page 29.)

[35] Chatterji U, Bobardt M, Selvarajah S, Yang F, Tang H, Sakamoto N, Vuagniaux G, Parkinson T, Gallay P. The isomerase active site of cyclophilin A is critical for hepatitis C virus replication. *J Biol Chem.*, 284(25):16998–17005, Jun 2009. (Cited on page 31.)

[36] Chen H, Zhang W, Sun X, Yoshimoto M, Chen Z, Zhu W, Liu J, Shen Y, Yong W, Li D, *et al*. Fkbp1a controls ventricular myocardium trabeculation and compaction by regulating endocardial Notch1 activity. *Development*, 140(9):1946–1957, May 2012. (Cited on page 27.)

[37] Chung CT, Miller RH. Preparation and storage of competent *Escherichia coli* cells. *Methods Enzymol.*, 218:621–627, 1 1993. (Cited on page 46.)

[38] Cockburn IL, Pesce ER, Pryzborski JM, Davies-Coleman MT, Clark PG, Keyzers RA, Stephens LL, Blatch GL. Screening for small molecule modulators of Hsp70 chaperone activity using protein aggregation suppression assays: inhibition of the *Plasmodial* chaperone PfHsp70-1. *Biol Chem*, 392(5):431–438, May 2011. (Cited on page 111.)

[39] Colgan J, Asmal M, Neagu M, Yu B, Schneidkraut J, Lee Y, Sokolskaja E, Andreotti A, Luban J. Cyclophilin A regulates

TCR signal strength in CD4+ T cells via a proline–directed conformational switch in Itk. *Immunity.*, 21(2):189–201, Aug 2004. (Cited on page 26.)

[40] Counihan NA, Kalanon M, Coppel RL, de Koning-Ward TF. *Plasmodium* rhoptry proteins: why order is important. *Trends Parasitol.*, 29(5):228–236, May 2013. (Cited on pages 94 and 113.)

[41] Cowman AF, Berry D, Baum J. The cellular and molecular basis for malaria parasite invasion of the human red blood cell. *J Cell Biol.*, 198(6):961–971, Sep 2012. (Cited on pages 10, 11, and 147.)

[42] Cox FE. History of human parasitology. *Clin Microbiol Rev.*, 15 (4):595–612, Oct 2002. (Cited on page 2.)

[43] Cox FE. History of the discovery of the malaria parasites and their vectors. *Parasit Vectors.*, 3(1):5, Feb 2010. (Cited on page 2.)

[44] Crowther GJ, He P, Rodenbough PP, Thomas AP, Kovzun KV, Leibly DJ, Bhandari J, Castaneda LJ, Hol WG, Gelb MH, Napuli AJ, Van Voorhis WC. Use of thermal melt curves to assess the quality of enzyme preparations. *Anal Biochem*, 399(2):268–275, Apr 2010. (Cited on pages 125, 126, and 127.)

[45] Curtidor H, Ocampo M, Tovar D, Lopez R, Garcia J, Valbuena J, Vera R, Suarez J, Rodriguez LE, Puentes A, Guzman F, Torres E, Patarroyo ME. Specific erythrocyte binding capacity and biological activity of *Plasmodium falciparum*–derived rhoptry–associated protein 1 peptides. *Vaccine.*, 22(8):1054–1062, Feb 2004. (Cited on page 95.)

[46] Czar MJ, Lyons RH, Welsh MJ, Renoir JM, Pratt WB. Evidence that the FK506-binding immunophilin heat shock protein 56 is

required for trafficking of the glucocorticoid receptor from the cytoplasm to the nucleus. *Mol Endocrinol*, 9(11):1549–1560, Nov 1995. (Cited on page 89.)

[47] Deleersnijder A, Van Rompuy AS, Desender L, Pottel H, BuÃ©e L, Debyser Z, Baekelandt V, Gerard M. Comparative analysis of different peptidyl–prolyl isomerases reveals FK506-binding protein 12 as the most potent enhancer of alpha–synuclein aggregation. *J Biol Chem.*, 286(30):26687–26701, Jul 2011. (Cited on page 29.)

[48] Dobson MJ. Malaria in England: a geographical and historical perspective. *Parassitologia.*, 36(1–2):35–60, Aug 1994. (Cited on page 2.)

[49] Dobson S, Kar B, Kumar R, Adams B, Barik S. A novel tetratricopeptide repeat (TPR) containing PP5 serine/threonine protein phosphatase in the malaria parasite, *Plasmodium falciparum*. *BMC Microbiol.*, 31(1):epub, Nov 2001. (Cited on page 93.)

[50] Dolinski K, Muir S, Cardenas M, Heitman J. All cyclophilins and FK506 binding proteins are, individually and collectively, dispensable for viability in *Saccharomyces cerevisiae*. *Proc Natl Acad Sci U S A.*, 94(24):13093–13098, Nov 1997. (Cited on page 26.)

[51] Dubois P, Druilhe P, Arriat D, Jendoubi M, Jouin H. Changes in recognition of *Plasmodium falciparum* antigens by human sera depending on previous malaria exposure. *Ann Inst Pasteur Immunol.*, 138(3):383–396, May–Jun 1987. (Cited on page 93.)

[52] Ecker A, Lehane AM, Clain J, Fidock DA. PfCRT and its role in antimalarial drug resistance. *Trends Parasitol.*, 28(11):504–514, Nov 2012. (Cited on page 17.)

[53] Egan AF, Morris J, Barnish G, Allen S, Greenwood BM, Kaslow DC, Holder AA, Riley EM. Clinical immunity to *Plasmodium falciparum* malaria is associated with serum antibodies to the 19–kDa C–terminal fragment of the merozoite surface antigen, PfMSP–1. *J Infect Dis.*, 173(3):765–769, Mar 1996. (Cited on page 11.)

[54] Faust EC. The history of malaria in the united states. *American Scientist*, 39(1):121–130, Aug 1951. (Cited on page 2.)

[55] Fedosov DA, Lei H, Caswell B, Suresh S, Karniadakis GE. Multiscale modeling of red blood cell mechanics and blood flow in malaria. *PLoS Comput Biol.*, 7(12):e1002270, Dec 2011. (Cited on page 13.)

[56] Fellerer C, Schweiger R, Schongruber K, Soll J, Schwenkert S. Cytosolic HSP90 cochaperones HOP and FKBP interact with freshly synthesized chloroplast preproteins of *Arabidopsis*. *Mol Plant*, 4(6):1133–1145, Nov 2011. (Cited on page 88.)

[57] Fischer G, Bang H. The refolding of urea–denatured ribonuclease A is catalyzed by peptidyl–prolyl *cis–trans* isomerase. *Biomed Biochim Acta.*, 828(1):39–42, Mar 1985. (Cited on page 18.)

[58] Fischer G, Bang H, Mech C. [determination of enzymatic catalysis for the *cis–trans*–isomerization of peptide binding in proline–containing peptides]. *Biomed Biochim Acta.*, 43(10):1101–1111, 1984. (Cited on page 18.)

[59] Fischer G, Schmid FX. The mechanism of protein folding. implications of *in vitro* refolding models for de novo protein folding and translocation in the cell. *Biochemistry.*, 29(9):2205–2212, Mar 1990. (Cited on page 19.)

[60] Fischer G, Wittmann-Liebold B, Lang K, Kiefhaber T, Schmid FX. Cyclophilin and peptidyl–prolyl *cis–trans* isomerase are probably identical proteins. *Nature*, 337(6206):476–478, Feb 1989. (Cited on page 18.)

[61] Francis SE, Sullivan DJ Jr, Goldberg DE. Hemoglobin metabolism in the malaria parasite *Plasmodium falciparum*. *Annu Rev Microbiol.*, 51:97–123, 1997. (Cited on page 12.)

[62] Freeman BC, Toft DO, Morimoto RI. Molecular chaperone machines: chaperone activities of the cyclophilin Cyp–40 and the steroid aporeceptor–associated protein p23. *Science*, 6274(5293): 1718–1720, Dec 1996. (Cited on page 25.)

[63] Galat A. Peptidylprolyl *cis–trans* isomerases (immunophilins): biological diversity–targets–functions. *Curr Top Med Chem.*, 3 (12):1315–1347, 2003. (Cited on pages 19, 20, 22, 25, and 149.)

[64] Gardner MJ, Hall N, Fung E, White O, Berriman M, Hyman RW, Carlton JM, Pain A, Nelson KE, Bowman S, *et al*. Genome sequence of the human malaria parasite *Plasmodium falciparum*. *Nature*, 419(6906):498–511, Oct 2003. (Cited on page 17.)

[65] Gavigan CS, Kiely S, Hirtzlin J, Bell A. Cyclosporin-binding proteins of *Plasmodium falciparum*. *Int J Parasitol*, 33(9):987–96, Aug 2004. (Cited on pages 31, 33, 55, 67, 69, 70, 93, 104, 114, and 145.)

[66] Gerard M, Deleersnijder A, DaniÃ«ls V, Schreurs S, Munck S, Reumers V, Pottel H, Engelborghs Y, Van den Haute C, Taymans JM, Debyser Z, Baekelandt V. Inhibition of FK506 binding proteins reduces alpha–synuclein aggregation and Parkinson's disease–like pathology. *J Neurosci.*, 30(7):2454–2463, Feb 2010. (Cited on page 29.)

[67] Gietz RD, Woods, RA. Genetic Transformation of Yeast. *Biotechniques*, 30:816–830, 2001. (Cited on page 59.)

[68] Ginsburg H, Krugliak M, Eidelman O, Cabantchik ZI. New permeability pathways induced in membranes of *Plasmodium falciparum* infected erythrocytes. *Mol Biochem Parasitol.*, 8(2):177–190, Jun 1983. (Cited on page 12.)

[69] Gitau GW, Mandal P, Blatch GL, Przyborski J, Shonhai A. Characterisation of the *Plasmodium falciparum* Hsp70-Hsp90 organising protein (PfHop). *Cell Stress Chaperones*, 17(2):191–202, Mar 2012. (Cited on page 87.)

[70] Gothel SF, Scholz C, Schmid FX, Marahiel MA. Cyclophilin and trigger factor from *Bacillus subtilis* catalyze *in vitro* protein folding and are necessary for viability under starvation conditions. *Biochemistry.*, 37(38):13392–13399, Sep 1998. (Cited on page 26.)

[71] Gramiccia G. Ledger's *cinchona* seeds: a composite of field experience, chance, and intuition. *Parassitologia.*, 1987, volume = 29, pages = 207–220, number = 2–3, month = May–Dec,. (Cited on page 14.)

[72] Griffith JP, Kim JL, Kim E, Sintchak M, Thomson J, Fitzgibbon M, Fleming M, Caron P, Hsiao K, Navia M. X-ray structure of calcineurin inhibited by the immunophilin-

immunosuppressant FKBP12-FK506 complex. *Cell*, 82(3):507–522, Aug 1995. (Cited on page 119.)

[73] Gysin J, Dubois P, Pereira da Silva L. Protective antibodies against stages of *Plasmodium falciparum* in experimental infection in the squirrel monkey *Saoemiri scirueus*. *Parasite Immunol*, 4(6):421–430, Nov 1982. (Cited on page 93.)

[74] Handschumacher RE, Harding MW, Rice J, Drugge RJ, Speicher DW. Cyclophilin: a specific cytosolic binding protein for cyclosporin A. *Science*, 226(4674):544–547, Nov 1984. (Cited on page 18.)

[75] Hanssen E, Knoechel C, Dearnley M, Dixon MW, Le Gros M, Larabell C, Tilley L. Soft X–ray microscopy analysis of cell volume and hemoglobin content in erythrocytes infected with asexual and sexual stages of *Plasmodium falciparum*. *J Struct Biol.*, 177(2):224–232, Feb 2012. (Cited on page 12.)

[76] Harding MW, Galat A, Uehling DE, Schreiber SL. A receptor for the immunosuppressant FK506 is a *cis–trans* peptidyl–prolyl isomerase. *Nature*, 341(6244):758–760, Oct 1989. (Cited on page 19.)

[77] Harlow, E. and Lane, D. *Antibodies: A Laboratory Manual.* Cold Spring Harbor Laboratory Press, Cold Spring Harbor, New York., 1st edition, 1988. (Cited on page 54.)

[78] Harnyuttanakorn P, McBride JS, Donachie S, Heidrich HG, Ridley RG. Inhibitory monoclonal antibodies recognise epitopes adjacent to a proteolytic cleavage site on the RAP–1 protein of *Plasmodium falciparum*. *Mol Biochem Parasitol.*, 55(1–2):177–186, Oct 1992. (Cited on page 94.)

[79] Hayakawa T, Culleton R, Otani H, Horii T, Tanabe K. Big bang in the evolution of extant malaria parasites. *Mol Biol Evol.*, 25 (10):2233–2239, Oct 2008. (Cited on page 1.)

[80] Ho S, Clipstone N, Timmermann L, Northrop J, Graef I, Fiorentino D, Nourse J, Crabtree GR. The mechanism of action of cyclosporin A and FK506. *Clin Immunol Immunopathol.*, 80(3):40–45, Sep 1996. (Cited on page 22.)

[81] Holder AA. The precursor to major merozoite surface antigens: structure and role in immunity. *Prog Allergy*, 41(1):72–97, 1988. (Cited on page 11.)

[82] Howard RF, Peterson C. Limited RAP–1 sequence diversity in field isolates of *Plasmodium falciparum*. *Mol Biochem Parasitol.*, 77 (1):95–98, Apr 1996. (Cited on page 94.)

[83] Jiang L, Mu J, Zhang Q, Ni T, Srinivasan P, Rayavara K, Yang W, Turner L, Lavstsen T, Theander TG, *et al.* PfSETvs methylation of histone H3K36 represses virulence genes in *Plasmodium falciparum*. *Nature*, 399(7457):223–227, Jul 2013. (Cited on page 113.)

[84] Jinwal UK, Koren J 3rd, Borysov SI, Schmid AB, Abisambra JF, Blair LJ, Johnson AG, Jones JR, Shults CL, O'Leary JC 3rd, Jin Y, Buchner J, Cox MB, Dickey CA. The Hsp90 cochaperone, FKBP51, increases Tau stability and polymerizes microtubules. *J Neurosci*, 30(2):591–599, Jan 2010. (Cited on page 29.)

[85] Justice SS, Hunstad DA, Harper JR, Duguay AR, Pinkner JS, Bann J, Frieden C, Silhavy TJ, Hultgren SJ. Periplasmic peptidyl prolyl *cis–trans* isomerases are not essential for viability, but SurA is required for pilus biogenesis in *Escherichia coli*. *J Bacteriol.*, 187(22):7680–7686, Nov 2005. (Cited on page 26.)

[86] Kang CB, Ye H, Yoon HR, Yoon HS. Solution structure of FK506 binding domain (FKBD) of *Plasmodium falciparum* FK506 binding protein 35 (PfFKBP35). *Proteins*, 70(1):300–302, Jan 2008. (Cited on pages 65, 119, 121, 138, and 139.)

[87] Kofron JL, Kuzmic P, Kishore V, Colon-Bonilla E, Rich DH. Determination of kinetic constants for peptidyl prolyl *cis-trans* isomerases by an improved spectrophotometric assay. *Biochemistry*, 30(25):6127–6234, Jun 1991. (Cited on page 62.)

[88] Krucken J, Greif G, von Samson–Himmelstjerna G. In silico analysis of the cyclophilin repertoire of apicomplexan parasites. *Parasit Vectors*, 2(1):27, Jun 2009. (Cited on pages 32 and 33.)

[89] Krugliak M, Zhang J, Ginsburg H. Intraerythrocytic *Plasmodium falciparum* utilizes only a fraction of the amino acids derived from the digestion of host cell cytosol for the biosynthesis of its proteins. *Mol Biochem Parasitol.*, 119(2):249–256, Feb 2002. (Cited on page 12.)

[90] Kumar, R., Adams, B., Musiyenko, A., Shulyayeva, O., Barik, S. The FK506-binding protein of the malaria parasite, *Plasmodium falciparum*, is a FK506-sensitive chaperone with FK506-independent calcineurin-inhibitory activity. *Mol Biochem Parasitol*, 141(2):163–73, Jun 2005. (Cited on pages 32, 33, 34, 68, 85, 87, 89, 117, 138, and 143.)

[91] Kuzuhara T, Horikoshi M. A nuclear FK506-binding protein is a histone chaperone regulating rDNA silencing. *Nat Struct Mol Biol.*, 11(3):275–283, Mar 2004. (Cited on pages 89, 99, 100, 112, and 147.)

[92] LaCount DJ, Vignali M, Chettier R, Phansalkar A, Bell R, Hesselberth JR, Schoenfeld LW, Ota I, Sahasrabudhe S, Kurschner C, Fields S, Hughes RE. A protein interaction network of the malaria parasite *Plasmodium falciparum*. *Nature*, 438(7064):103–7, Nov 2005. (Cited on pages 68 and 87.)

[93] Laemmli UK. Cleavage of structural proteins during the assembly of the head of bacteriophage T4. *Nature*, 5259(227):680–5, Aug 1970. (Cited on page 51.)

[94] Lalremruata A, Ball M, BianucciR , Welte R, Nerlich AG, Kun J, Pusch CM. Molecular Identification of *Falciparum* Malaria and Human Tuberculosis Co-Infections in Mummies from the Fayum Depression (Lower Egypt). *PLoS One*, 8(4):e60307, 2013. (Cited on page 2.)

[95] Lamarque, M., S. Besteiro, J. Papoin, M. Roques, B. Vulliez-Le Normand, J. Morlon-Guyot, J.F. Dubremetz, S. Fauquenoy, S. Tomavo, B.W. Faber, et al. The RON2-AMA1 interaction is a critical step in moving junction–dependent invasion by apicomplexan parasites. *PLoS Pathog*, epub:e1001276, 2011. (Cited on page 9.)

[96] Le Roch KG, Zhou Y, Blair PL, Grainger M, Moch JK, Haynes JD, De La Vega P, Holder AA, Batalov S, Carucci DJ, Winzeler EA. Discovery of gene function by expression profiling of the malaria parasite life cycle. *Science.*, 301(5639):1503–1508, Sep 2003. (Cited on page 32.)

[97] Li J, Soroka J, Buchner J. The Hsp90 chaperone machinery: conformational dynamics and regulation by co–chaperones.

Biochim Biophys Acta., 1823(3):624–635, Mar 2012. (Cited on page 111.)

[98] Liao F. Discovery of Artemisinin (Qinghaosu). *Molecules*, 14 (12):5362–5366, 2009. (Cited on page 15.)

[99] Lindner J, Meissner KA, Schettert I, Wrenger C. Trafficked Proteins-Druggable in *Plasmodium falciparum*? *Int J Cell Biol.*, 10(1155):435981, Apr 2013. (Cited on page 90.)

[100] Liu N, Song W, Wang P, Lee K, Chan W, Chen H, Cai Z. Proteomics analysis of differential expression of cellular proteins in response to avian H9N2 virus infection in human cells. *Proteomics*, 8(9):1851–1859, May 2008. (Cited on page 31.)

[101] Liu W, Li Y, Learn GH, Rudicell RS, Robertson JD, Keele BF, Ndjango JB, Sanz CM, Morgan DB, Locatelli S, et al. Origin of the human malaria parasite *Plasmodium falciparum* in gorillas. *Nature*, 467(7314):420–425, Sep 2010. (Cited on page 1.)

[102] Longhurst HJ, Holder AA. The histones of *Plasmodium falciparum*: identification, purification and a possible role in the pathology of malaria. *Parasitology.*, 114(5):413–419, May 1997. (Cited on pages 60, 99, and 100.)

[103] Luo C, Luo H, Zheng S, Gui C, Yue L, Yu C, Sun T, He P, Chen J, Shen J, *et al*. Nucleocapsid protein of SARS coronavirus tightly binds to human cyclophilin A. *Biochem Biophys Res Commun.*, 321(3):557–565, Aug 2004. (Cited on page 31.)

[104] Lyons WE, George EB, Dawson TM, Steiner JP, Snyder SH. Immunosuppressant FK506 promotes neurite outgrowth in cul-

tures of PC12 cells and sensory ganglia. *Proc Natl Acad Sci U S A.*, 91(8):3191–3195, Apr 1994. (Cited on page 29.)

[105] Malmquist NA, Moss TA, Mecheri S, Scherf A, Fuchter MJ. Small–molecule histone methyltransferase inhibitors display rapid antimalarial activity against all blood stage forms in *Plasmodium falciparum*. *Mol Biochem Parasitol.*, 109(41):16708–16743, Oct 2012. (Cited on page 94.)

[106] Maniatis T, Fritsch EF, and Sambrook J. *Molecular Cloning: A Laboratory Manual*. Cold Spring Harbour, New York, 1982. (Cited on page 47.)

[107] Marin-Menendez, A, Monaghan P, Bell A. A family of cyclophilin-like molecular chaperones in *Plasmodium falciparum*. *Mol Biochem Parasitol*, 184(1):44–7, July 2012. (Cited on pages 25, 31, 33, 34, 35, 54, 67, 68, and 70.)

[108] Mattei D,Scherf A,Bensaude O, Pereira da Silva L. A heat shock–like protein from the human malaria parasite *Plasmodium falciparum* induces autoantibodies. *Eur J Immunol,*, 19(10): 1823–1828, Oct 1989. (Cited on page 93.)

[109] McFadden GI, Reith ME, Munholland J, Lang-Unnasch N. Plastid in human parasites. *Nature*, 381(6582):482, Jun 1992. (Cited on page 9.)

[110] Medana IM, Turner GD. Human cerebral malaria and the blood–brain barrier. *Int J Parasitol.*, 36(5):555–568, May 2006. (Cited on page 13.)

[111] Menard R, Tavares J, Cockburn I, Markus M, Zavala F, Amino R. Looking under the skin: the first steps in malarial infection and

immunity. *Nat Rev Microbiol*, 11(10):701–712, Sep 2013. (Cited on pages 7 and 8.)

[112] Mok D, Allan RK, Carrello A, Wangoo K, Walkinshaw MD, Ratajczak T. The chaperone function of cyclophilin 40 maps to a cleft between the prolyl isomerase and tetratricopeptide repeat domains. *FEBS Lett.*, 580(11):2761–2768, May 2006. (Cited on page 25.)

[113] Monaghan P, Bell A. A *Plasmodium falciparum* FK506-binding protein (FKBP) with peptidyl-prolyl cis-trans isomerase and chaperone activities. *Mol Biochem Parasitol*, 139:185–195, Feb 2005. (Cited on pages 31, 33, 34, 35, 43, 54, 67, 68, 70, 87, 117, 123, 130, 138, 140, and 145.)

[114] Monaghan P, Fardis M, Revill WP, Bell A. Antimalarial effects of macrolactones related to FK520 (ascomycin) are independent of the immunosuppressive properties of the compounds. *J Infect Dis*, 191(8):1342–1349, Apr 2005. (Cited on pages 36, 67, and 153.)

[115] Moreno R, Poltl-Frank F, Stuber D, Matile H, Mutz M, Weiss NA, Pluschke G. Rhoptry-associated protein 1-binding monoclonal antibody raised against a heterologous peptide sequence inhibits *Plasmodium falciparum* growth *in vitro*. *Infect Immun*, 69(4):2558–2568, Apr 2001. (Cited on pages 90, 94, 104, 114, and 149.)

[116] Morot-Gaudry-Talarmain Y. Physical and functional interactions of cyclophilin B with neuronal actin and peroxiredoxin-1 are modified by oxidative stress. *Free Radic Biol Med.*, 47(12):1715–1730, Dec 2009. (Cited on page 89.)

[117] Mukaide H, Adachi Y, Taketani S, Iwasaki M, Koike-Kiriyama N, Shigematsu A, Shi M, Yanai S, Yoshioka K, Kamiyama Y, Ikehara S. FKBP51 expressed by both normal epithelial cells and adenocarcinoma of colon suppresses proliferation of colorectal adenocarcinoma. *Cancer Invest*, 26(4):385–390, May 2008. (Cited on page 30.)

[118] Muregi FW, Kirira PG, Ishih A. Novel rational drug design strategies with potential to revolutionize malaria chemotherapy. *Curr Med Chem.*, 18(1):113–143, 2011. (Cited on page 18.)

[119] Nelson CJ, Santos-Rosa H, Kouzarides T. Proline isomerization of histone H3 regulates lysine methylation and gene expression. *Cell*, 126(5):905–916, Sep 2006. (Cited on pages 89, 99, 102, 113, and 147.)

[120] O'Donnell RA, Saul A, Cowman AF, Crabb BS. Functional conservation of the malaria vaccine antigen MSP–119across distantly related *Plasmodium* species. *Nat Med.*, 6(1):91–95, Jan 2000. (Cited on page 11.)

[121] Oeuvray C, Bouharoun-Tayoun H, Gras-Masse H, Bottius E, Kaidoh T, Aikawa M, Filgueira MC, Tartar A, Druilhe P. Merozoite surface protein-3: a malaria protein inducing antibodies that promote *Plasmodium falciparum* killing by cooperation with blood monocytes. *Blood*, 84(5):1594–1602, Sep 1994. (Cited on page 11.)

[122] O'Malley KJ, Dhir R, Nelson JB, Bost J, Lin Y, Wang Z. The expression of androgen–responsive genes is up–regulated in the epithelia of benign prostatic hyperplasia. *Prostate*, 69(16):1716–1723, Dec 2009. (Cited on page 30.)

[123] Owens-Grillo JK, Hoffmann K, Hutchinson KA, Yem AW, Deibel MR Jr, Handschumacher RE, Pratt WB. The cyclosporin A-binding immunophilin CyP40 and the FK506-binding immunophilin Hsp56 bind to a common site on Hsp90 and exist in independent cytosolic heterocomplexes with the untransformed glucocorticoid receptor. *J Biol Chem.*, 270(35):20479–20484, Sep 1995. (Cited on pages 27, 88, and 111.)

[124] Parmakelis A, Russello MA, Caccone A, Marcondes CB, Costa J, Forattini OP, Sallum MA, Wilkerson RC, Powell JR. Historical analysis of a near disaster: *Anopheles gambiae* in Brazil. *Am J Trop Med Hyg.*, 78(1):176–178, Jan 2008. (Cited on page 2.)

[125] Periyasamy S, Warrier M, Tillekeratne MP, Shou W, Sanchez ER. The immunophilin ligands cyclosporin A and FK506 suppress prostate cancer cell growth by androgen receptor–dependent and –independent mechanisms. *Endocrinology*, 148(10):4716–4726, Oct 2007. (Cited on page 30.)

[126] Perrot-Applanat M, Cibert C, Geraud G, Renoir JM, Baulieu EE. The 59 kDa FK506-binding protein, a 90 kDa heat shock protein binding immunophilin (FKBP59-HBI), is associated with the nucleus, the cytoskeleton and mitotic apparatus. *J Cell Sci*, 108(5):2037–2051, May 1995. (Cited on page 89.)

[127] Pirkl F, Fischer E, Modrow S, Buchner J. Localization of the chaperone domain of FKBP52. *J Biol Chem.*, 276(40):37034–37041, Oct 2001. (Cited on page 25.)

[128] Plowe CV. Monitoring antimalarial drug resistance: making the most of the tools at hand. *J Exp Biol.*, 206(21):3745–3752, Nov 2003. (Cited on page 17.)

[129] Poinar G Jr. *Plasmodium dominicana* n. sp. (*Plasmodiidae: Haemosporida*) from Tertiary Dominican amber. *Syst Parasitol.*, 61(1): 47–52, May 2005. (Cited on page 1.)

[130] Quinta HR, Galigniana MD. The neuroregenerative mechanism mediated by the Hsp90–binding immunophilin FKBP52 resembles the early steps of neuronal differentiation. *Br J Pharmacol.*, 166(2):637–649, May 2012. (Cited on page 29.)

[131] Quinta HR, Maschi D, Gomez-Sanchez C, Piwien-Pilipuk G, Galigniana MD. Subcellular rearrangement of Hsp90-binding immunophilins accompanies neuronal differentiation and neurite outgrowth. *J Neurochem*, 115(3):716–734, Nov 2010. (Cited on pages 27 and 89.)

[132] Ramm K, Pluckthun A. High enzymatic activity and chaperone function are mechanistically related features of the dimeric *E. coli* peptidyl–prolyl–isomerase FkpA. *J Mol Biol.*, 310(2):485–498, Jul 2001. (Cited on page 25.)

[133] Ratajczak T, Carrello A. Cyclophilin 40 (CyP-40), mapping of its Hsp90 binding domain and evidence that FKBP52 competes with CyP-40 for Hsp90 binding. *J Biol Chem.*, 271(6):2961–2965, Feb 1996. (Cited on pages 27, 88, and 111.)

[134] Ratajczak T, Ward BK, Minchin RF. Immunophilin chaperones in steroid receptor signalling. *Curr Top Med Chem.*, 3(12):1348–1357, 2003. (Cited on pages 27 and 147.)

[135] Renia L, Mattei D, Goma J, Pied S, Dubois P, Miltgen F, Nussler A, Matile H, Menegaux F, Gentilini M, *et al.* A malaria heat–shock-like determinant expressed on the infected hepatocyte surface is the target of antibody–dependent cell–mediated

cytotoxic mechanisms by nonparenchymal liver cells. *Eur J Immunol.*, 20(7):1445–1449, Jul 1990. (Cited on page 93.)

[136] Richardson JS. beta-Sheet topology and the relatedness of proteins. *Nature*, 268(5620):495–500, Aug 1977. (Cited on page 142.)

[137] Riggs DL, Cox MB, Cheung-Flynn J, Prapapanich V, Carrigan PE, Smith DF. Functional specificity of co–chaperone interactions with Hsp90 client proteins. *Crit Rev Biochem Mol Biol.*, 39 (5–6):279–295, Sep–Dec 2004. (Cited on page 27.)

[138] Rits MA, van Dort KA, Kootstra NA. Polymorphisms in the regulatory region of the Cyclophilin A gene influence the susceptibility for HIV–1 infection. *PLoS One*, 3(12):e3975, Dec 2008. (Cited on page 30.)

[139] Roberts DR, Laughlin LL, Hsheih P, Legters LJ. DDT, global strategies, and a malaria control crisis in South America. *Emerg Infect Dis.*, 3(3):295–302, Aug 1997. (Cited on page 3.)

[140] Romano S, Di Pace A, Sorrentino A, Bisogni R, Sivero L, Romano MF. FK506 binding proteins as targets in anticancer therapy. *Anticancer Agents Med Chem.*, 10(9):651–656, Nov 2010. (Cited on page 30.)

[141] Roos DS, Crawford MJ, Donald RG, Kissinger JC, Klimczak LJ, Striepen B. Origin, targeting, and function of the apicomplexan plastid. *Curr Opin Microbiol.*, 2(4):526–432, Aug 1999. (Cited on page 9.)

[142] Sam-Yellowe TY, Banks TL, Fujioka H, Drazba JA, Yadav SP. *Plasmodium yoelii*: novel rhoptry proteins identified within the

body of merozoite rhoptries in rodent *Plasmodium* malaria. *Exp Parasitol.*, 120(1):113–117, Sep 2008. (Cited on page 94.)

[143] Shaw ML, Stone KL, Colangelo CM, Gulcicek EE, Palese P. Cellular proteins in influenza virus particles. *PLoS Pathog.*, 4(6): e1000085, Jun 2008. (Cited on page 31.)

[144] Siegel RE, Poynter FN. Robert Talbor, Charles ii, and *cinchona* a contemporary document. *Med Hist.*, 1962, volume = 6, pages = 82–85, number = 1, month = Jan,. (Cited on page 14.)

[145] Siekierka JJ, Hung SH, Poe M, Lin CS, Sigal NH. A cytosolic binding protein for the immunosuppressant FK506 has peptidyl–prolyl isomerase activity but is distinct from cyclophilin. *Nature*, 341(6244):755–757, Oct 1989. (Cited on page 19.)

[146] Singh S, Alam MM, Pal-Bhowmick I, Brzostowski JA, Chitnis CE. Distinct external signals trigger sequential release of apical organelles during erythrocyte invasion by malaria parasites. *PLoS Pathog*, 6(2):e1000746, Feb 2010. (Cited on page 11.)

[147] Singh S, More KR, Chitnis CE. Role of calcineurin and actin dynamics in regulated secretion of microneme proteins in *Plasmodium falciparum* merozoites during erythrocyte invasion. *Cell Microbiol*, 2013. (Cited on page 68.)

[148] Sivils JC, Storer CL, Galigniana MD, Cox MB. Regulation of steroid hormone receptor function by the 52–kDa FK506–binding protein (FKBP52). *Curr Opin Pharmacol.*, 11(4):314–319, Aug 2011. (Cited on page 30.)

[149] Smith DC, Sanford LB. Laveran's germ: the reception and use of a medical discovery. *Am J Trop Med Hyg.*, 34(1):2–20, Jan 1985. (Cited on page 2.)

[150] Staalsoe T, Giha HA, Dodoo D, Theander TG, Hviid L. Detection of antibodies to variant antigens on *Plasmodium falciparum*-infected erythrocytes by flow cytometry. (Cited on page 41.)

[151] Steiner JP, Dawson TM, Fotuhi M, Glatt CE, Snowman AM, Cohen N, Snyder SH. High brain densities of the immunophilin FKBP colocalized with calcineurin. *Nature*, 358(6387):584–587, Aug 1992. (Cited on page 29.)

[152] Suchanek M, Radzikowska A, Thiele C. Photo–leucine and photo–methionine allow identification of protein–protein interactions in living cells. *Nature Methods*, 2(4):261–267, Apr 2005. (Cited on page 135.)

[153] Sugata H, Matsuo K, Nakagawa T, Takahashi M, Mukai H, Ono Y, Maeda K, Akiyama H, Kawamata T. A peptidyl–prolyl isomerase, FKBP12, accumulates in Alzheimer neurofibrillary tangles. *Neurosci Lett.*, 459(2):96–99, Aug 2009. (Cited on page 29.)

[154] Sullivan DJ Jr, Gluzman IY, Goldberg DE. *Plasmodium* hemozoin formation mediated by histidine–rich proteins. *Science*, 271 (5246):219–222, Jan 1996. (Cited on page 12.)

[155] Sumanadasa SD, Goodman CD, Lucke AJ, Skinner-Adams T, Sahama I, Haque A, Do TA, McFadden GI, Fairlie DP, Andrews KT. Antimalarial activity of the anticancer histone deacetylase inhibitor SB939. *Antimicrob Agents Chemother.*, 56(7):3849–3856, Jul 2012. (Cited on page 94.)

[156] Sutherland CJ, Tanomsing N, Nolder D, Oguike M, Jennison C, Pukrittayakamee S, Dolecek C, Hien TT, do Rosario VE, Arez AP, *et al.* Two nonrecombining sympatric forms of the human malaria parasite *Plasmodium ovale* occur globally. *J Infect Dis*, 201(10):1544–1550, May 2010. (Cited on page 6.)

[157] Takahashi N, Hayano T, Suzuki M. Peptidyl–prolyl *cis–trans) isomerase is the cyclosporin a–binding protein cyclophilin.*, journal = Nature, year = 1989, volume = 337, pages = 473–475, number = 6206, month = Feb,. (Cited on page 18.)

[158] Takeuchi H. Contribution of Cyclophilin A to determination of simian immunodeficiency virus tropism: a progress update. *Vaccine.*, 28(Suppl. 2):51–54, May 2010. (Cited on page 30.)

[159] Thera MA, Doumbo OK, Coulibaly D, Laurens MB, Ouattara A, Kone AK, Guindo AB, Traore K, Traore I, Kouriba B, *et al.* A field trial to assess a blood–stage malaria vaccine. *N Engl J Med.*, 365(11):1004–1013, Sep 2011. (Cited on page 11.)

[160] Thiel P, Kaiser M, Ottmann C. Small-molecule stabilization of protein-protein interactions: an underestimated concept in drug discovery? *Angew Chem Int Ed Engl.*, 51(9):2012–2018, Feb 2012. (Cited on page 37.)

[161] Thommen-Scott K. Antimalarial activity of cyclosporin A. *Biochemistry*, 11(6-7):770–773, Dec 1981. (Cited on pages 36 and 67.)

[162] Tian X, Zhao C, Zhu H, She W, Zhang J, Liu J, Li L, Zheng S, Wen YM, Xie Y. Hepatitis B virus (HBV) surface antigen interacts with and promotes cyclophilin a secretion: possible link to pathogenesis of HBV infection. *J Virol*, 84(7):3373–3381, Apr 2010. (Cited on page 30.)

[163] Tilley L, Dixon MW, Kirk K. The *Plasmodium falciparum*–infected red blood cell. *Int J Biochem Cell Biol.*, 43(6):839–842, Jun 2011. (Cited on page 12.)

[164] Toovey S. The miraculous fever-tree. the cure that changed the world fiametta rocco; harper collins, san francisco, 2004, 348 pages, paperback, isbn 0-00-6532357. *Travel Med Infect Dis.*, 2004, volume = 2, pages = 109–110, number = 2, month = May,. (Cited on page 14.)

[165] Trager W, Jensen JB. Human malaria parasites in continuous culture. *Science.*, 193(4254):673–675, Aug 1976. (Cited on page 3.)

[166] Trager W, Jenson JB. Cultivation of malarial parasites. *Nature*, 273:621–2, June 1978. (Cited on page 39.)

[167] Venter JC, Adams MD, Myers EW, Li PW, Mural RJ, Sutton GG, Smith HO, Yandell M, Evans CA, Holt RA, *et al*. The sequence of the human genome. *Science*, 291(5507):1304–1351, Feb 2001. (Cited on page 17.)

[168] Vythilingam I, Noorazian YM, Huat TC, Jiram AI, Yusri YM, Azahari AH, Norparina I, Noorrain A, Lokmanhakim S. *Plasmodium knowlesi* in humans, macaques and mosquitoes in peninsular Malaysia. *Parasit Vectors*, 1(1):26, Aug 2008. (Cited on page 6.)

[169] Wang P, Heitman J. The cyclophilins. *Genome*, 6(7):226, Jun 2005. (Cited on page 22.)

[170] Watashi K, Ishii N, Hijikata M, Inoue D, Murata T, Miyanari Y, Shimotohno K. Cyclophilin B is a functional regulator of

hepatitis C virus RNA polymerase. *Mol Cell*, 19(1):111–122, Jul 2005. (Cited on page 31.)

[171] Wells JA, McClendon CL. Reaching for high–hanging fruit in drug discovery at protein–protein interfaces. *Nature*, 450(7172): 1001–1009, Dec 2007. (Cited on page 37.)

[172] White NJ. Antimalarial drug resistance. *J Clin Invest.*, 113(8): 1084–1092, Apr 2004. (Cited on pages 16 and 17.)

[173] WHO. *World Malaria Report*. http://www.who.int/malaria, 2012. (Cited on page 5.)

[174] Willcox ML, Bodeker G. Traditional herbal medicines for malaria. *BMJ*, 329(7475):1156–1159, Nov 2002. (Cited on page 14.)

[175] Wright CW, Linley PA, Brun R, Wittlin S, Hsu E. Ancient Chinese methods are remarkably effective for the preparation of artemisinin–rich extracts of Qing Hao with potent antimalarial activity. *Molecules*, 15(2):804–812, Feb 2010. (Cited on page 14.)

[176] Wu Y, Craig A. Comparative proteomic analysis of metabolically labelled proteins from *Plasmodium falciparum* isolates with different adhesion properties. *Malar J*, 3(5):67, Aug 2006. (Cited on page 33.)

[177] Wu Y, Li Q, Chen XZ. Detecting protein–protein interactions by Far western blotting. *Nat Protoc.*, 2(12):3278–3284, 2007. (Cited on page 63.)

[178] Yoon HR, Kang CB, Chia J, Tang K, Yoon HS. Expression, purification, and molecular characterization of *Plasmodium falciparum*

FK506-binding protein 35 (PfFKBP35). *Protein Expr Purif.*, 53(1): 179–185, May 2007. (Cited on pages 34 and 117.)

[179] Zander K, Sherman MP, Tessmer U, Bruns K, Wray V, Prechtel AT, Schubert E, Henklein P, Luban J, Neidleman J, Greene WC, Schubert U. Cyclophilin A interacts with HIV-1 Vpr and is required for its functional expression. *J Biol Chem.*, 278(44): 43202–43213, Oct 2003. (Cited on page 30.)

[180] Zuccala ES, Baum J. Cytoskeletal and membrane remodelling during malaria parasite invasion of the human erythrocyte. *Br J Haematol*, epub:j.1365–2141.2011.08766.x., 2011. (Cited on page 9.)

[181] Zuckerman A. Harvesting of *Plasmodium falciparum* with saponin. *Bull WHO*, 37:431–436, 1967. (Cited on page 41.)

COLOPHON

This document was typeset using the typographical look-and-feel `classicthesis` developed by André Miede. The style was inspired by Robert Bringhurst's seminal book on typography *"The Elements of Typographic Style"*. `classicthesis` is available for both LaTeX and LyX:

http://code.google.com/p/classicthesis/

Happy users of `classicthesis` usually send a real postcard to the author, a collection of postcards received so far is featured at:

http://postcards.miede.de/

Final Version as of April 28, 2014 (`classicthesis` version 4.1).